

NASA Technical Memorandum 78533

(NASA-TM-78533) INVESTIGATION OF THE
ASYMMETRIC AERODYNAMIC CHARACTERISTICS OF
CYLINDRICAL BODIES OF REVOLUTION WITH
VARIATIONS IN NOSE GEOMETRY AND ROTATIONAL
ORIENTATION AT ANGLES OF ATTACK TO 58°

N79-30146

63/02 Encl as
36294

**Investigation of the Asymmetric
Aerodynamic Characteristics of
Cylindrical Bodies of Revolution
With Variations in Nose Geometry
and Rotational Orientation
at Angles of Attack to 58°
and Mach Numbers to 2**

Robert L. Kruse, Earl R. Keener,
Gary T. Chapman, and Gary Claser

SEPTEMBER 1979

NASA



NASA Technical Memorandum 78533

**Investigation of the Asymmetric
Aerodynamic Characteristics of
Cylindrical Bodies of Revolution
With Variations in Nose Geometry
and Rotational Orientation
at Angles of Attack to 58°
and Mach Numbers to 2**

Robert L. Kruse, Earl R. Keener, and Gary T. Chapman
Ames Research Center
Moffett Field, California

Gary Claser
ARO, Inc.
Moffett Field, California

NASA

National Aeronautics
and Space Administration

**Scientific and Technical
Information Branch**

1979

NOMENCLATURE

All forces and moments are referred to the body axis coordinate system with the moment center at the model base. Because the data are computer-plotted, both the conventional symbol and the plot symbol are given.

Symbol	Plot symbol	Definition
A_b		exposed base area on which p_b acts
C_A		axial force coefficient, $\frac{\text{axial force}}{qS}$
C_{AF}	C_{AF}	axial force coefficient adjusted for base pressure equal to free-stream static pressure, $C_A + C_{pb} \frac{A_b}{S}$
C_m	C_m	pitching-moment coefficient, $\frac{\text{pitching moment}}{qSd}$
C_N	C_N	normal force coefficient, $\frac{\text{normal force}}{qS}$
C_n	C_n	yawing-moment coefficient, $\frac{\text{yawing moment}}{qSd}$
CP_R	CP_R	resultant center of pressure position forward of body base, in body diameters
C_{pb}		base pressure coefficient, $\frac{p_b - p}{q}$
C_R	C_R	resultant force coefficient, $\sqrt{C_N^2 + C_Y^2}$
C_Y	C_Y	side force coefficient, $\frac{\text{side force}}{qS}$
$ C_Y $	$ C_Y $	absolute value of C_Y
d		diameter at model base, 6.60 cm (2.6 in.)
l		model length
M	M ; MACH	free-stream Mach number

Symbol	Plot symbol	Definition
p		free-stream static pressure
p_b		base pressure
q		free-stream dynamic pressure
Re	Re	free-stream Reynolds number, based on d
R_n/R_b		ratio of blunted nose radius to model base radius
S		reference base area with diameter = d
α	α	angle of attack
ϕ_T	PHI-T	angle of rotation of tip, forebody, and afterbody, respectively, clockwise looking upstream, deg
ϕ_F	PHI-F	
ϕ_A	PHI-A	

Configuration Description:

$A_{\text{—}}$	$A_{\text{—}}$	afterbody with a fineness ratio given by —
$B_{\text{—}}$	$B_{\text{—}}$	bluntness ratio of tip given by —, $\frac{R_n}{R_b}$
$F_{\text{—}}$	$F_{\text{—}}$	forebody with a fineness ratio given by ___

**INVESTIGATION OF THE ASYMMETRIC AERODYNAMIC CHARACTERISTICS OF
CYLINDRICAL BODIES OF REVOLUTION WITH VARIATIONS IN NOSE
GEOMETRY AND ROTATIONAL ORIENTATION AT ANGLES OF
ATTACK TO 58° AND MACH NUMBERS TO 2**

Robert L. Kruse, Earl R. Keener, Gary T. Chapman, and Gary Claser*

Ames Research Center

SUMMARY

Wind-tunnel tests were conducted to investigate the side forces and yawing moments that can occur at high angles of attack and zero sideslip for cylindrical bodies of revolution. Two bodies having several tangent ogive forebodies with fineness ratios of 0.5, 1.5, 2.5, and 3.5 were tested. The forebodies with fineness ratios of 2.5 and 3.5 had several bluntnesses. The cylindrical afterbodies had fineness ratios of 7 and 13. The model components – tip, forebody, and afterbody – were tested in various rotational positions about their axes of symmetry.

Most of the tests were conducted at a Mach number of 0.25, a Reynolds number of 0.32×10^6 , and with the afterbody that had a fineness ratio of 7 and with selected forebodies. The effect of Mach number was determined with the afterbody that had a fineness ratio of 13 and with selected forebodies at Mach numbers from 0.25 to 2 at $Re = 0.32 \times 10^6$. Maximum angle of attack was 58°.

The configuration with the pointed forebody that had a fineness ratio of 3.5 developed an appreciable side force and yawing moment at high angles of attack, results similar to those of previous tests. The side force increases to a maximum as angle of attack increases to about 50° and then decreases with further increase in angle. For the lower fineness-ratio forebodies, the side force is much lower over the angle-of-attack range tested (up to 58°) and is nearly zero for the fineness-ratio-0.5 forebody. Tests with the longer afterbody (fineness ratio of 13) showed that the side force first occurs in the angle-of-attack range of 12° to 17°, regardless of forebody slenderness. For this afterbody with the fineness-ratio-3.5 forebody, the largest increase in side force occurs above 30°, which is close to the onset angle for the forebody-alone data of previous tests. This implies that the largest side force occurs when the flow asymmetry on the body moves forward onto the forebody with increasing angle of attack. With increasing Mach number, the side forces decrease to near zero at Mach numbers of 1.2 and 2.

Bluntness produces mixed effects on the side forces and yawing moments, depending on the forebody fineness ratio and angle of attack. For configurations with large side forces, bluntness can result in large reductions in side force. For configurations with small side forces, bluntness can increase the side force.

*ARO, Inc., Moffett Field, California.

Rotation of the complete model, of the forebody alone, of the forebody tip section, or of the afterbody section can have a large effect on the side force for both the pointed and the blunted configurations. Changes in direction of side force can occur as many as eight times during a complete revolution. Thus, the effect of rotational position is important in tests of bodies at high angles of attack.

INTRODUCTION

When a body of revolution is pitched to high angles of attack, a side force can occur at zero sideslip angle. This side force occurs when the separation-induced vortex flow field on the lee side of the body becomes asymmetric. Since the configuration of the body can play an important role in the stability and control characteristics of aircraft and missiles at high angles of attack, a comprehensive wind-tunnel investigation was undertaken at Ames Research Center to obtain static aerodynamic data for body models. The tests included a wide range of forebody shapes, afterbody lengths, Reynolds numbers, and Mach numbers. Reports thus far generated from this test program are listed in references 1 to 12.

Several previous experimental investigations have shown that small asymmetries in the nose-tip geometry have a strong influence on the asymmetric forces and moments at high angles of attack (e.g., see ref. 1). These results indicated that it is important to test body models in various rotational positions. Consequently, one objective of the present experimental program was to systematically investigate the effect of the rotational position of the body models. Circular bodies with removable tangent-ogive forebodies and nose tips were tested in several positions of rotation of the various body components.

The fineness ratios of the tangent-ogive forebodies varied from 0.5 to 3.5 and bluntness ratios varied from 8 to 50 percent of the maximum body radius. These forebodies were tested with a circular afterbody having a fineness ratio of 7, similar to previous tests (refs. 2 and 8). To investigate the effect of afterbody fineness ratio, several of the forebodies were tested with an afterbody having a fineness ratio of 13.

The investigation was conducted in the Ames 6- X 6-Foot Transonic/Supersonic Wind Tunnel. The tests for the effects of rotational position and of forebody configuration were conducted at a Mach number of 0.25 and a Reynolds number, based on base diameter, of 0.32×10^6 . The fineness-ratio 13 afterbody was tested with several forebodies at Mach numbers up to 2. The angle-of-attack range was 28° to 58° for most of the tests and -2° to 58° for tests with the fineness-ratio 13 afterbody.

This report presents the basic data that show the effects of body rotational position, forebody fineness ratio, and afterbody fineness ratio on the aerodynamic characteristics of the body models.

TEST FACILITY

The experimental investigation was conducted in the 6- by 6-Foot Transonic/Supersonic Wind Tunnel at Ames Research Center. The tunnel is a variable pressure, continuous-flow facility providing continuous Mach number variation from 0.6 to 2.2 and a low-speed test condition of $M = 0.25$. The test section has a perforated floor and ceiling for boundary layer removal at transonic speeds.

MODELS AND BALANCE

A sketch of the model components used in the investigation is presented in figure 1. Photographs of the model installation in the tunnel are shown in figure 2. The forebodies were circular-arc tangent ogives with fineness ratios of 0.5, 1.5, 2.5, and 3.5. The forebodies with fineness ratios of 2.5 and 3.5 were of two designs: one forebody was made in one piece and the other forebody had a removable pointed tip which could be replaced with a blunted one. The blunted tips for the forebody with a fineness ratio of 2.5 had bluntness ratios, R_n/R_b , of 8, 20, and 50 percent. The cylindrical afterbodies had fineness ratios of 7 and 13 and a diameter of 6.60 cm (2.6 in.). The afterbody could be rotated on the balance in 90° increments. The one-piece forebodies had fineness ratios of 0.5, 1.5, 2.5, and 3.5 and could be rotated in 90° increments. The two-piece forebodies with fineness ratios of 2.5 and 3.5 could be rotated in 45° increments. The tips were secured with a setscrew and could be set at any rotational position. The junctions between each model component were carefully made to be rearward-facing steps less than 0.003 cm in height and without gaps.

The zero rotation position ($\phi = 0$) for all of the components was arbitrarily selected. The configurations are referred to by a " B_F_A " or " F_A " identifier system where the numbers following B , F , and A are, respectively, the bluntness ratio, forebody fineness ratio, and afterbody fineness ratio.

The models were sting-mounted through the base on a six-component strain gage "Task" balance.

TEST CONDITIONS AND PROCEDURES

Two support systems were used in the tests. The low angle-of-attack system covered the 0° to 28° range (fig. 2(a)) and the high angle-of-attack system covered the 28° to 58° angle-of-attack range (fig. 2(b)). Most of the tests were conducted on the high angle-of-attack system at a Mach number of 0.25 and a Reynolds number of 0.32×10^6 (based on model base diameter), using the afterbody with a fineness ratio of 7. A few tests were made at a Mach number of 0.6 and at Reynolds numbers of 0.32×10^6 , 0.43×10^6 , and 0.65×10^6 . In these tests, the afterbody with a fineness ratio of 7 was used with both the one-piece and two-piece forebodies. Since a remotely rotatable sting was not available, the model was tested in 90° increments of roll angle by rotating the model on the balance. In addition, the nose tip, forebody, and afterbody sections were tested in 90°

increments of roll angle. Next, the two-piece forebodies were tested with the various blunt nose tips. Since the afterbody with a fineness ratio of 7 had previously been tested over the Mach number range of 0.25 to 2 (refs. 2 and 8), only the afterbody with a fineness ratio of 13 was tested with the one-piece forebodies (fineness ratios of 3.5, 2.5, and 1.5) at several Mach numbers up to 2.

DATA REDUCTION

Six-component aerodynamic force and moment data were measured at each test condition. Static (mean) values of the data were determined by electronic filtering of the force and moment measurements that were at times unsteady. All data were reduced to coefficient form and referred to the body axis coordinate system. The base pressure was taken at one point in the model base cavity and was used to compute the base drag. This was subtracted from the total axial force balance measurements so that the drag data presented are for forces ahead of the body base.

Data repeatability for the principal parameters was estimated by reviewing repeat points and was as follows:

$$\begin{array}{lll} \alpha = \pm 0.03^\circ & C_N = \pm 0.06 & C_m = \pm 0.06 \\ Re = \pm 0.02 \times 10^6 & C_Y = \pm 0.04 & C_n = \pm 0.04 \end{array}$$

RESULTS AND DISCUSSION

Experimental results, presented in figures 3 to 28, show the effects of rotational position of the model components about their axes of symmetry and the effects of Reynolds number, fineness ratio, Mach number, and bluntness on the side forces and yawing moments at zero sideslip. In figures 3 to 18 only the side force coefficient C_Y and yawing-moment coefficient C_n are presented because the asymmetric forces and moments are of primary interest in these tests. In figures 19 to 24 the results for C_Y , C_n , C_N , C_m , C_{AF} , C_{PR} , $C_R - C_N$, and $|C_Y|/C_N$ are presented for the tests with the afterbody with a fineness ratio of 13 at Mach numbers up to 2. The effect of blunting the nose tip is shown in figures 25 to 28. All data were machine plotted and faired.

Effects of Model Component Rotational Position, 2-Piece Fineness-Ratio 3.5 Forebody, (BOF3.5A7)

The pointed two-piece forebody of fineness ratio 3.5 (BOF3.5) was combined with the fineness-ratio-7 afterbody (A7) and tested on the high-angle support system ($\alpha = 28^\circ$ to 58°) in 90° increments of roll at a Mach number of 0.25. Some limited tests of rotational effects were made at a Mach number of 0.6.

Rotation of complete model— The effect of rotational position of the complete model at $M = 0.25$ and $Re = 0.32 \times 10^6$ is shown in figures 3. Before discussing the effects of rotation, note that an appreciable side force and yawing moment occur at high angles of attack at each roll

position. The side force and yawing moment increase to a maximum at $\alpha \approx 50^\circ$ and then decrease, which is similar to the results of references 2 and 8 for a similar model.

The effect of rotating the model is generally to change the sign (direction) of the side force and yawing moment for every 90° increment of rotation, except for an angle of 90° , where the force and moment values are intermediate between the maximum positive and negative values. At rotation angles of 0° , 180° , and 270° , the curves are generally similar in shape and magnitude. The data at a rotation angle of 90° indicate that the change from positive to negative values is sometimes progressive with roll angle, rather than instantaneous (i.e., occurring within a small increment in rotation angle). These data at various rotation angles show the usefulness of having a continuously variable rotation angle, preferably remotely controlled.

Rotation of tip alone and tip plus forebody together— The effect of tip rotational position at $M = 0.25$ and $Re = 0.32 \times 10^6$, and at $M = 0.6$ and $Re = 0.32 \times 10^6$, 0.43×10^6 , and 0.65×10^6 is shown in figures 4 to 7. Similar results, where the tip and forebody were rotated as a unit at $M = 0.25$ and $Re = 0.32 \times 10^6$, are shown in figure 8.

Comparing figures 4 and 8, the changes in side force and yawing moment obtained when rotating the tip only (figs. 4) are similar but not identical to the changes obtained when rotating the tip and forebody as a unit (figs. 8). There is also a similarity to the changes obtained when the model was rotated as a complete unit (fig. 3). For all these data, the side forces and yawing moments are positive at zero rotation angle and change sign (direction) every 90° increment in rotation. Even the magnitudes of the side forces and yawing moments are approximately the same. This supports the findings in previous tests that the direction of the forces and moments is governed primarily by asymmetries in the body geometry in the forebody section, especially the nose tip.

Results at a Mach number of 0.6 (figs. 5 to 7) are similar to those of figures 4, although the magnitudes of the side forces and yawing moments are less than at $M = 0.25$. The results of the variation of Reynolds number ($Re = 0.32 \times 10^6$, 0.43×10^6 , and 0.65×10^6) at $M = 0.6$, shown in figures 5 to 7, indicate that the magnitudes of side force and yawing moment vary with Reynolds number. The maximum measured¹ values of C_Y and C_n occur at $Re = 0.43 \times 10^6$.

Rotation of the afterbody— From the foregoing results, it was conjectured that the direction and magnitude of the side forces and yawing moments might not change much if the rotational angle of the tip section (or tip-and-forebody section) was held fixed (constant with respect to the balance axes) and the aft section was tested in four rotational positions on the balance in 90° increments. It was generally expected that small machining errors in a smooth, one-piece aftersection should not greatly affect the asymmetric forces and moments when rotated. Further, it was felt that it was more likely that the results would be affected by small discontinuities at the junction.

The effect of rotation of forebody and afterbody as a unit about their axes with tip fixed was determined from tests at $M = 0.25$. The tip was fixed at $\phi T = 0$, a value selected from the data of figures 4 because this angle gave a typical variation of side force and yawing moment with angle of attack. These results are shown in figures 9. Similar tests were conducted at $M = 0.6$ and $Re = 0.43 \times 10^6$ with $\phi T = 0$, and those results are shown in figures 10.

¹ The term "maximum measured" is used because higher values of side force and yawing moment might have occurred at other rotational positions that were not measured.

At both Mach numbers (figs. 9 and 10), the results of rotating the forebody and afterbody as a unit and holding the tip fixed are very different from the results of rotating the tip alone (figs. 4–7). With tip fixed, the signs of the side forces and yawing moments are the same for rotation angles of 0, 90°, and 180°, whereas, the signs for the data for rotating the tip (figs. 4 to 7) changed for every 90° increment. Hence, the effect of this kind of rotation with the tip fixed was less than the effect of rotating the tip alone. However, the changes were not as small as expected and a large change in side force and yawing moment occurred at a rotation angle of 270°.

The effect of rotating the afterbody with the rotational position of the tip and forebody held fixed as a unit is shown in figures 11 for $M = 0.25$. The changes with this kind of rotation with the forebody fixed are smaller than the changes from rotating the forebody alone (figs. 8). Again, the changes were not as small as expected and a large change in side force and yawing moment occurred at a rotation angle of 270°.

Effects of Model Component Rotational Position, One-Piece Forebodies

Since two one-piece forebodies (F2.5 and F3.5) were available from previous tests (refs. 2 and 8), the effect of rotating these forebodies as well as the afterbody was investigated for comparison with the results for two-piece forebodies, including the previous test results at zero roll angle. This comparison assesses the repeatability of the results for two forebodies having the same shape but one having a nose tip with possible junction effects on the local flow. Accordingly, the results of tests with configurations F3.5A7 and F2.5A7 at $M = 0.25$ and $Re = 0.32 \times 10^6$ are shown in figures 12 to 15.

Fineness-ratio-3.5 forebody (F3.5A7)— The forebody of configuration F3.5A7 was rotated in 45° increments, and C_Y and C_n are presented in figures 12. The variation of side force and yawing moment with angle of attack are similar to the results for the two-piece forebody. However, the side force and yawing moment are seen to change direction (sign) every 45° of rotation compared to every 90° of rotation for the two-piece forebody. Apparently, small asymmetries in the geometry and junctions can trigger the vortex asymmetry to change sense (direction) up to at least eight times in a 360° rotation.

These results show clearly that body models tested at high angles of attack should include several roll angles if the objective is to determine the maximum side forces and yawing moments.

Tests were also conducted with the afterbody rotated in 90° increments but with the forebody angle fixed at $\phi = 270^\circ$; the forebody angle was selected because it resulted in the maximum measured side force and yawing moment in figures 12. The results in figures 13 show that rotating the afterbody can induce large changes in the side force and yawing moment, similar to the effects with the two-piece forebody.

Fineness-ratio-2.5 forebody (F2.5A7)— The results of tests with the forebody with a fineness ratio of 2.5, positioned at 90° increments, are shown in figures 14. Note that the measured side force and yawing moment are less than for the forebody with fineness ratio of 3.5; however, the data give some indication that the maximum values might be larger at angles of attack greater than 58°, the maximum angle of the test.

The effect of rotating the afterbody in 90° increments with the forebody angle fixed at 180° is shown in figures 15. Note that the maximum side forces are larger when the afterbody is rotated than when the forebody is rotated (figs. 14). However, the side forces are smaller than for the forebody with fineness ratio of 3.5.

Fineness-ratio-1.5 and 0.5 forebodies (F1.5A7 and F0.5A7)— Results of tests of the forebodies with fineness ratios of 1.5 and 0.5, positioned at 90° increments in roll angle, are shown in figures 16 and 17, respectively. Both the side forces and the yawing moments are small for the fineness-ratio-1.5 forebody and nearly zero for the fineness-ratio-0.5 forebody.

Effect of Forebody Fineness Ratio

As mentioned in the previous sections, the magnitude of the measured side force and yawing moment for the angle-of-attack range tested of 0° to 58° is much lower for the lower fineness ratios and are nearly zero for the fineness-ratio-0.5 forebody. These data agree with previous findings (refs. 2, 3, and 8), namely, that forebody fineness ratio can have a large effect on the magnitudes of the side forces and yawing moments.

Tests with the Fineness-Ratio-13 Afterbody

References 2 and 8 present the results of tests with the fineness-ratio-7 afterbody at Mach numbers from 0.25 to 2 with the F2.5 and F3.5 one-piece forebodies. Consequently, the present tests were conducted at Mach numbers up to 2 with the fineness-ratio-13 afterbody (A13) attached to the forebodies with fineness ratios of 1.5, 2.5, and 3.5 (F1.5, F2.5, and F3.5, respectively).

M = 0.25— Configurations F3.5A13 and F2.5A13 were tested first with the forebodies in two rotational positions of 0° and 180° at $M = 0.25$. These results are shown in figures 18. Comparing these data with those for configurations with the shorter fineness-ratio-7 afterbody (F3.5A7 and F2.5A7, figs. 12 and 14), the variations of side force and yawing moment with angle of attack are similar. Also, the magnitudes are much larger with the fineness-ratio-3.5 forebody (F3.5A13) than with the fineness-ratio-2.5 forebody (F2.5A13), which is similar to the results for the fineness-ratio-7 afterbody configuration for the angle of attack and Reynolds number ranges tested. The side force did not change sign for these two roll angles.

Effect of Mach number— Tests with configurations F3.5A13, F2.5A13, and F1.5A13 were conducted at several Mach numbers up to 2.0 at angles of attack from -2° to 58° . The forebody rotational position, selected from the data of figures 18 for the maximum side force, was $\phi_F = 180^\circ$ for configuration F3.5A13, and $\phi_F = 0$ for configuration F2.5A13. Since no forebody rotation tests were conducted with configuration F1.5A13, it was arbitrarily set at $\phi_F = 0$. The data are presented in figures 19 to 24. In addition to C_Y and C_n , several other coefficients are presented (C_N , C_m , C_{AF} , C_{PR} , $(C_R - C_N)$, and $|C_Y|/C_N$).

Note in figures 19 that the side force at $M = 0.25$ is much smaller than that for the same test condition in figures 18. Evidently, these data were not repeatable, probably for some reason associated with the particular roll position of the forebody. Because of limited time, the tests were not repeated at other forebody roll positions.

The results show that the side forces and yawing moments decrease to nearly zero with increasing Mach number, which is similar to the previously reported results for the fineness-ratio-7 afterbody models.

Angle of onset— Figures 19 to 24 include data at angles from -2° to 28° , obtained on the low-angle support system for the purpose of determining the onset angle of attack at which the side force and yawing moment first occur. For the F3.5A13 configuration (figs. 19), the onset angle is about 12° for both side force and yawing moment. However, note that the force and moment are not large until angles above about 32° . The latter angle is approximately the onset angle for the forebody alone side force and yawing moment determined in previous tests (ref. 1). These data indicate that the side force and yawing moment occur from asymmetric flow over the afterbody but that they do not get large until the asymmetric flow reaches the forebody.

For the configuration with the fineness-ratio-2.5 forebody (F2.5A13), the onset angle is in the range of 12° to 17° (figs. 22). This range encompasses the onset angle for the F3.5A13 configuration. For this fineness-ratio-2.5 forebody the onset angle for the forebody alone is about 42° (ref. 4); however, above 42° the side force and yawing moment do not increase prominently, as they do for the F3.5A13 configuration at angles of attack above its forebody onset angle of 32° .

For the configuration with the fineness-ratio-1.5 forebody (F1.5A13, figs. 23 and 24) the onset angle is also about 12° , similar to the F2.5A13 and F3.5A13 configurations. The side force and yawing moment are small until angles of attack above 45° where a moderate asymmetric force and moment occur at $M = 0.25$.

The foregoing results indicate that the forebody fineness ratio does not influence the onset angle of attack when the afterbody fineness ratio is large.

Effects of Bluntness

The two-piece forebodies (fineness ratios 3.5 and 2.5) were tested with blunt tips having bluntness ratios from 4 to 50 percent of the base radius. Tests were conducted at $M = 0.25$ and at $Re = 0.32 \times 10^6$ using the fineness-ratio-7 afterbody and the results are presented in figures 25 to 28. Again, C_Y and C_N are presented to show the effects of bluntness on the asymmetric forces and moments.

Fineness-ratio-3.5 forebody— The effect of bluntness on the fineness-ratio-3.5 forebody is shown in figures 25. The asymmetric forces and moments are much smaller for the blunted configurations. The largest incremental decrease in force and moment (about 50 percent in the peak value) occurs between the data for the pointed tip and the smallest blunted tip having only 4 percent bluntness. As the bluntness increases, the asymmetric force and moment generally decrease at angles of attack below about 45° . Above 45° the results are mixed and the most blunt configuration does not have the smallest asymmetric force and moment.

Configuration B8F3.5A7 was tested with the 8-percent blunt tip in four rotational positions and these data are presented in figures 26. There is a significant effect of rotation on the asymmetric force and moment.

Fineness-ratio-2.5 forebody— The effect of bluntness for the fineness-ratio-2.5 forebody is shown in figures 27. When compared to the pointed configuration in figures 14, the side force and yawing moment are small for the pointed configuration and bluntness does not reduce the magnitude further. In fact, at $\alpha = 55^\circ$ the side force and yawing moment are increased by bluntness.

Configuration E8F2.5A7, which had the 8-percent blunt tip, was tested in four rotational positions and these data are presented in figures 28. At angles of attack above 48° there is a small effect of rotation on the side force and yawing moment.

CONCLUSIONS

The following conclusions have been determined from a wind-tunnel investigation of the asymmetric forces and moments that occurred at high angles of attack and zero sideslip on two cylindrical bodies of revolution of different lengths having several tangent ogive forebodies of different fineness ratios and bluntnesses.

The configuration with the pointed forebody having a fineness ratio of 3.5 develops an appreciable side force and yawing moment at high angles of attack similar to those found in previous tests. The side force increases to a maximum as angle of attack increases to about 50° and then decreases with further increase in angle. For the lower fineness-ratio forebodies, the side force is much lower over the angle-of-attack range tested up to 58° and is nearly zero for the fineness-ratio-0.5 forebody. Tests with the longer afterbody having a fineness ratio of 13 showed that the side force first occurs in the angle-of-attack range of 12° to 17° , regardless of forebody slenderness. For this afterbody with the fineness-ratio-3.5 forebody, the largest increase in side force occurs above 30° , which is close to the onset angle for the forebody-alone data in previous tests. This implies that the largest side force occurs when the flow asymmetry on the body moves forward onto the forebody with increasing angle of attack. With increasing Mach number the side forces decrease to near zero at Mach numbers of 1.5 and 2. Bluntness produces mixed effects on the side forces and yawing moments, depending on the forebody fineness ratio, angle of attack, and the degree of bluntness. For the large side force on the forebody having a fineness ratio 3.5 even the smallest bluntness of 4 percent reduced the side force by as much as 50 percent; larger bluntness reduced the side force further at angles of attack below 45° . However, for the smaller side force on the fineness-ratio-2.5 forebody, the side force can be increased by bluntness for some test conditions.

Rotation of the complete model, of the forebody alone or of the forebody tip section, or of the afterbody section can have a large effect on the side force for both the pointed and the blunted configurations. Changes in direction of side force can occur as many as eight times during a complete revolution. Thus, the effect of rotational position is important in tests of bodies at high angles of attack.

Ames Research Center
National Aeronautics and Space Administration
Moffett Field, California 94035, October 10, 1978

REFERENCES

1. Keener, Earl R.; and Chapman, Gary T.: Onset of Aerodynamic Side Forces at Zero Sideslip on Symmetric Forebodies at High Angles of Attack. AIAA Paper 74-770, Aug. 1974.
2. Keener, Earl R.; Chapman, Gary T.; and Kruse, Robert L.: Effects of Mach Number and Afterbody Length on Onset of Asymmetric Forces on Bodies at Zero Sideslip and High Angles of Attack. AIAA Paper 76-66, Jan. 1976.
3. Keener, Earl R.; and Chapman, Gary T.: Similarity in Vortex Asymmetries over Slender Bodies and Wings. AIAA J., vol. 15, no. 9, Sept. 1977, pp. 1370-1372.
4. Keener, Earl R.; and Taleghani, Jamshid: Wind Tunnel Investigation of the Aerodynamic Characteristics of Five Forebody Models at High Angles of Attack at Mach Numbers From 0.25 to 2. NASA TM X-73,076, 1975.
5. Keener, Earl R.; Chapman, Gary T.; Cohen, Lee; and Taleghani, Jamshid: Side Forces on a Tangent Ogive Forebody With a Fineness Ratio of 3.5 at High Angles of Attack and Mach Numbers from 0.1 to 0.7. NASA TM X-3437, 1977.
6. Keener, Earl R.; Chapman, Gary T.; Cohen, Lee; and Taleghani, Jamshid: Side Forces on Forebodies at High Angles of Attack and Mach Numbers From 0.1 to 0.7: Two Tangent Ogives, Paraboloid and Cone. NASA TM X-3438, 1977.
7. Keener, Earl R.; and Valdez, Jose: Side Forces on a Tangent Ogive Forebody With a Fineness Ratio of 2.5 at High Angles of Attack and Low Speed. NASA TM X-73,176, 1976.
8. Jorgensen, Leland H.; and Nelson, Edgar R.: Experimental Aerodynamic Characteristics for a Cylindrical Body of Revolution With Various Noses at Angles of Attack From 0° to 58° and Mach Numbers from 0.6 to 2.0. NASA TM X-3128, 1974.
9. Jorgensen, Leland H.; and Nelson, Edgar R.: Experimental Aerodynamic Characteristics for a Cylindrical Body of Revolution With Side Strakes and Various Noses at Angles of Attack From 0° to 58° and Mach Numbers From 0.6 to 2.0. NASA TM X-3130, 1975.
10. Jorgensen, Leland H.; and Nelson, Edgar R.: Experimental Aerodynamic Characteristics for Bodies of Elliptic Cross Section at Angles of Attack From 0° to 58° and Mach Numbers From 0.6 to 2.0. NASA TM X-3129, 1975.
11. Jorgensen, Leland H.: Prediction of Static Aerodynamic Characteristics for Slender Bodies Alone and with Lifting Surfaces to Very High Angles of Attack. NASA TR R-474, Sept. 1977.
12. Chapman, Gary T.; Keener, Earl R.; and Malcolm, Gerald N.: Asymmetric Aerodynamic Forces on Aircraft Forebodies at High Angles of Attack - Some Design Guides. AGARD CP-199: Stall/Spin Problems of Military Aircraft, 12-1-12-9, Nov. 1976.

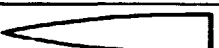
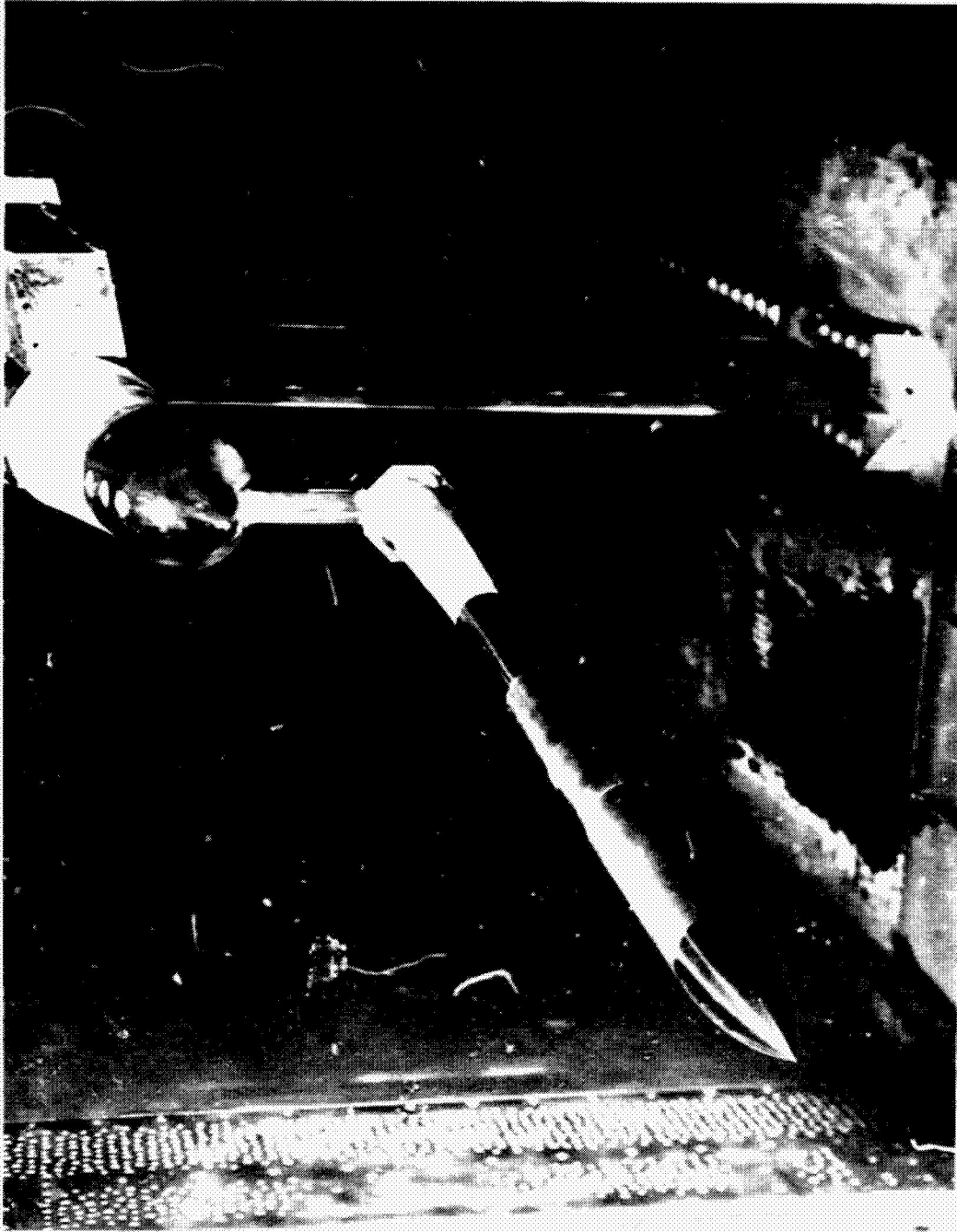
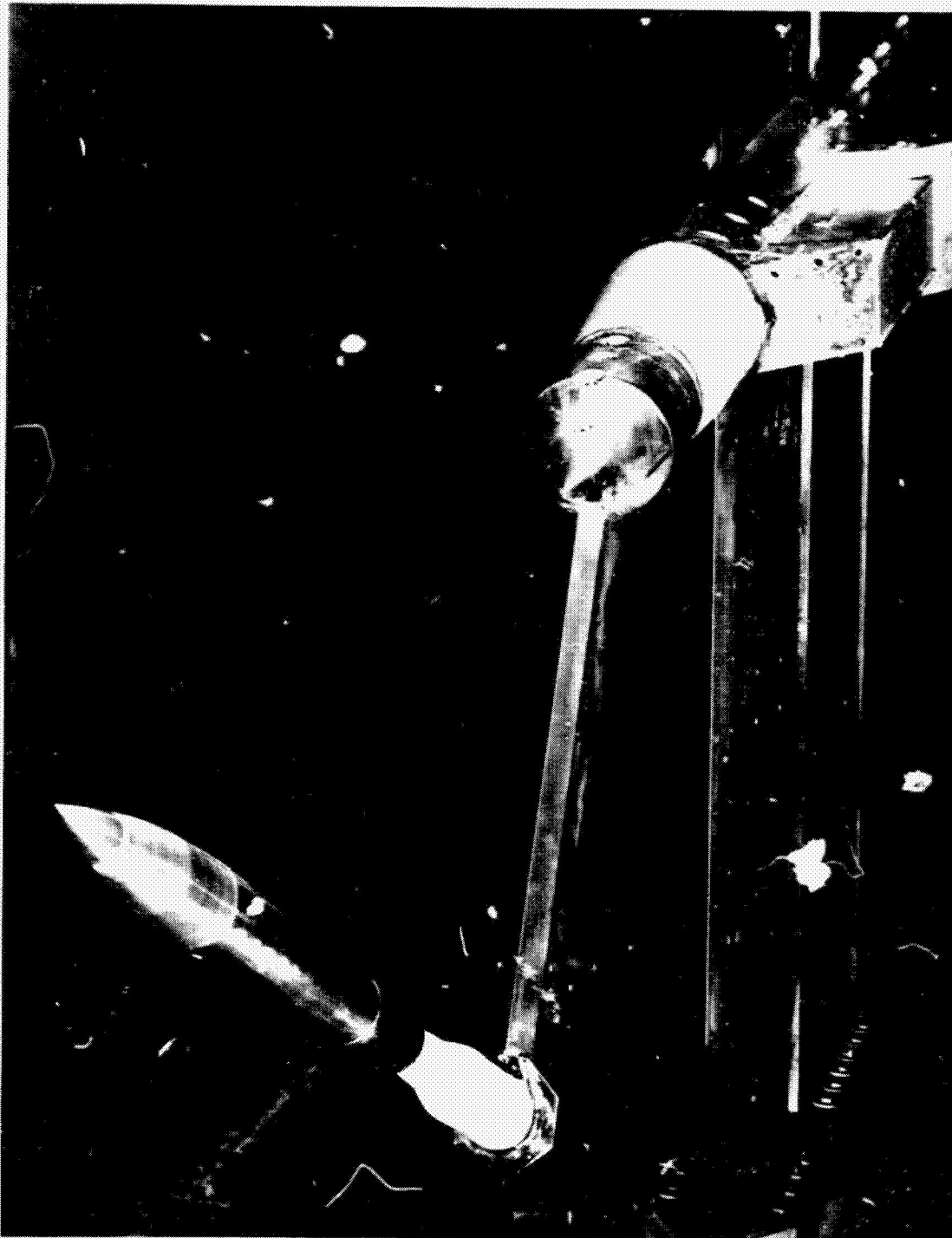
FOREBODY FINENESS RATIO	$R_N/R_B, \%$	SYMBOL	PLANFORM	
0.5	0	F0.5		
1.5	0	F1.5		
2.5	0 (1 PIECE)	F2.5		
	8 20 50	B8F2.5 B20F2.5 B50F2.5		
	0 (1 PIECE)	F3.5		
3.5	0 (REMOVABLE POINTED TIP)	B0F3.5		
	4 8 20 50	B4F3.5 B8F3.5 B20F3.5 B50F3.5		
AFTERBODY FINENESS RATIO	SYMBOL	PLANFORM		
7	A7			
13	A13			

Figure 1. Model components.



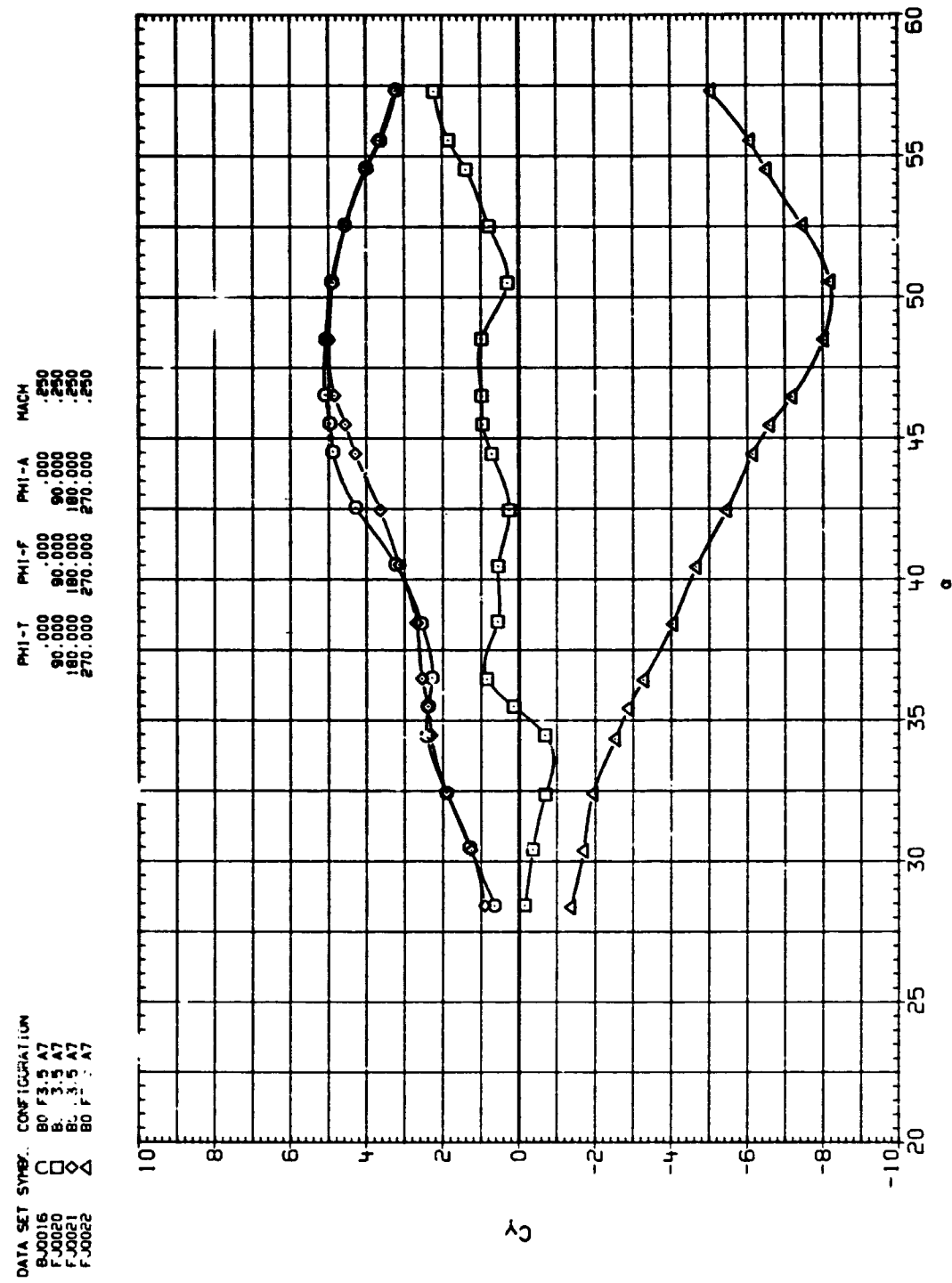
(a) Three-quarter front view, configuration F-2.5A13, low angle-of-attack support system, $\alpha = 0^\circ$ to 27° .

Figure 2. Typical model installation in the Ames 6- by 6-foot Wind Tunnel.



(b) Three-quarter front view, configuration BOF 3.5A7, high angle-of-attack support system, $\alpha = 28^\circ$ to 57° .

Figure 2. Concluded.

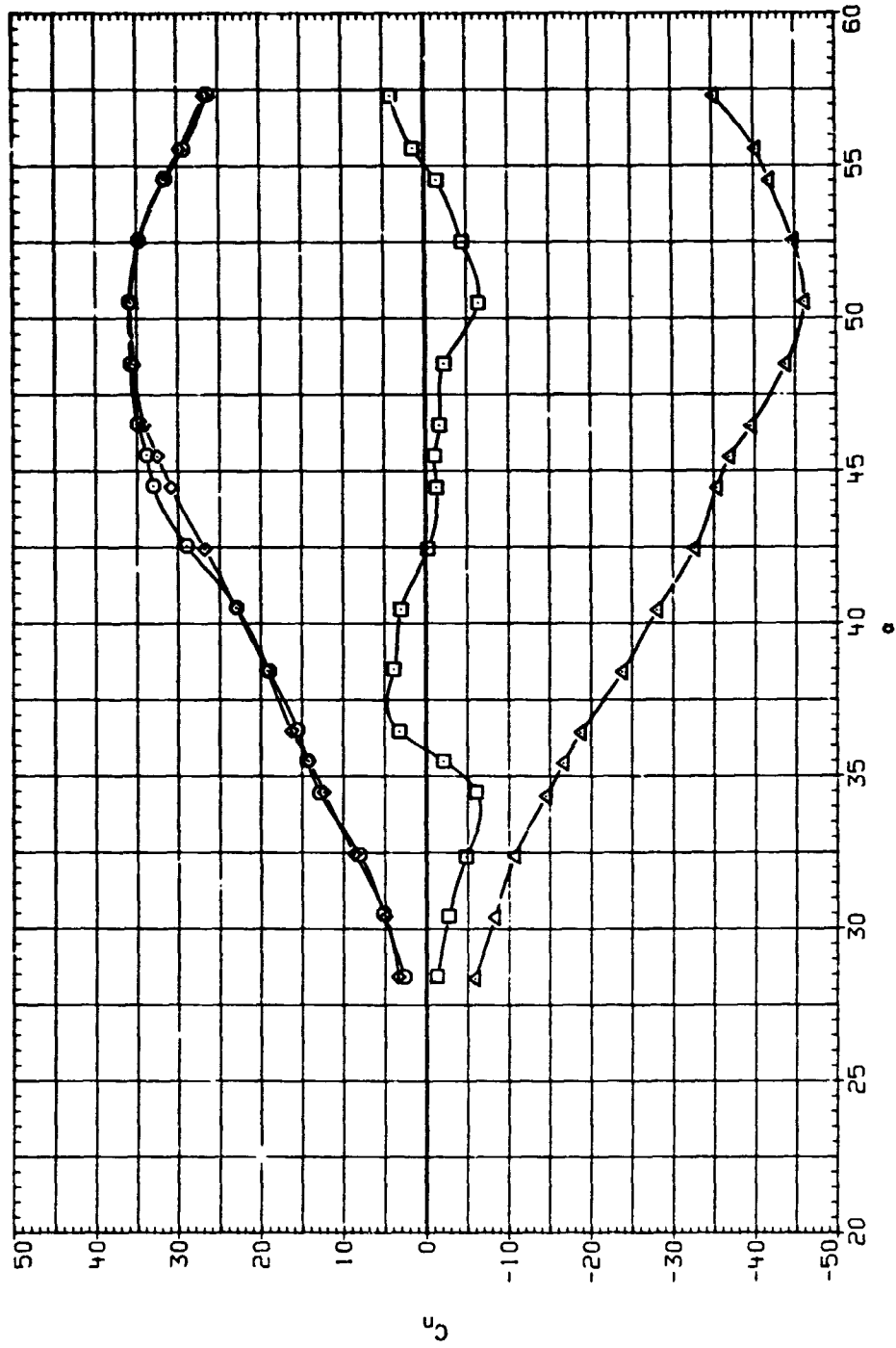


(a) C_y vs α .

Figure 3.— Effect of tip, forebody, and afterbody, rotated as a unit, BOF3.5A7, $Re = 0.32 \times 10^6$.

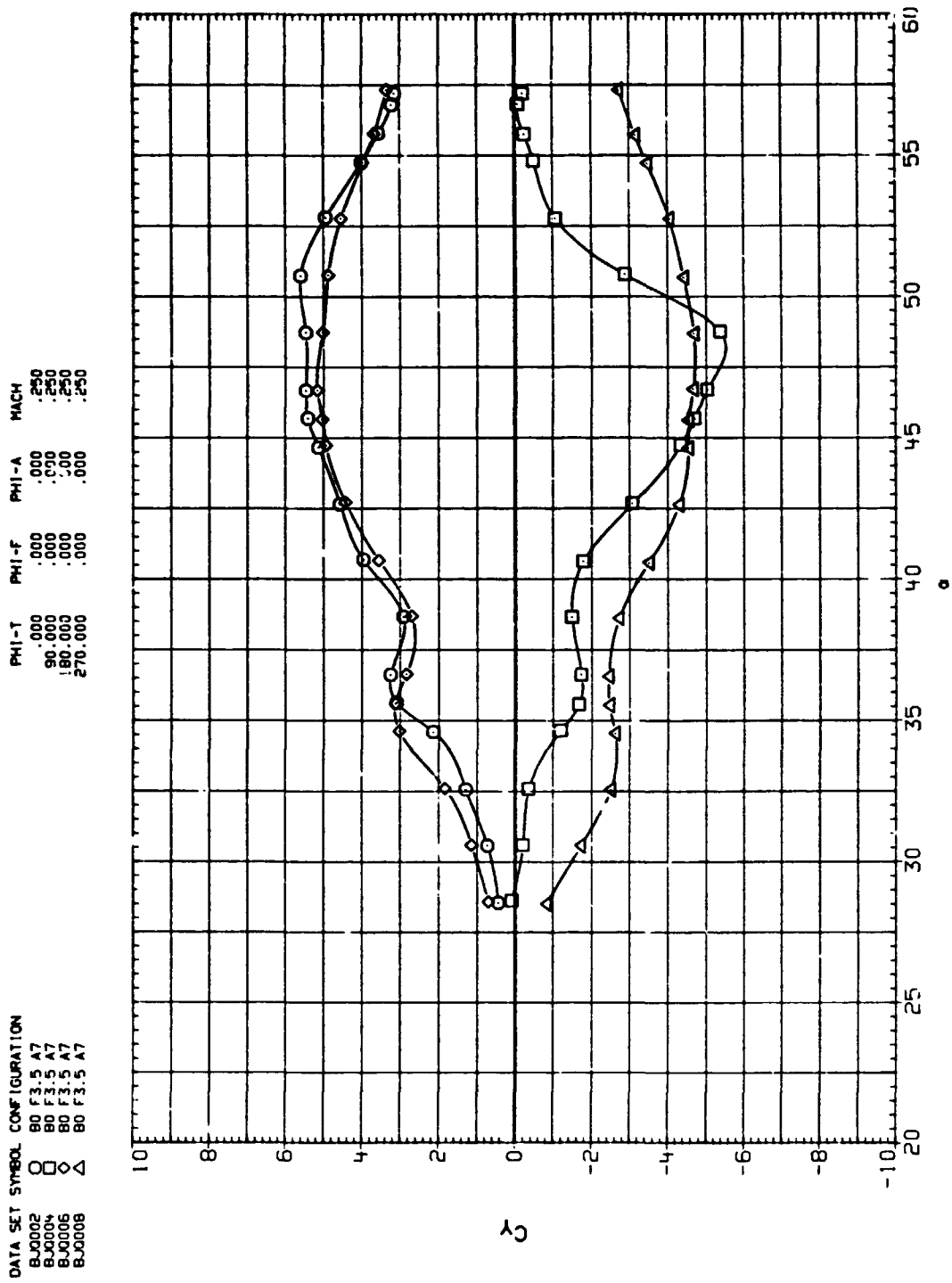
DATA SET SYMBOL CONFIGURATION:
 B-J0016 80 F3.5 A7
 F-J0020 80 F3.5 A7
 F-J0021 80 F3.5 A7
 F-J0022 80 F3.5 A7

PHI-T PHI-F PHI-A MACH
 .000 .000 .000 .250
 90.000 90.000 90.000 .250
 180.000 180.000 180.000 .250
 270.000 270.000 270.000 .250



(b) C_{l1} vs α .

Figure 3.-- Concluded.

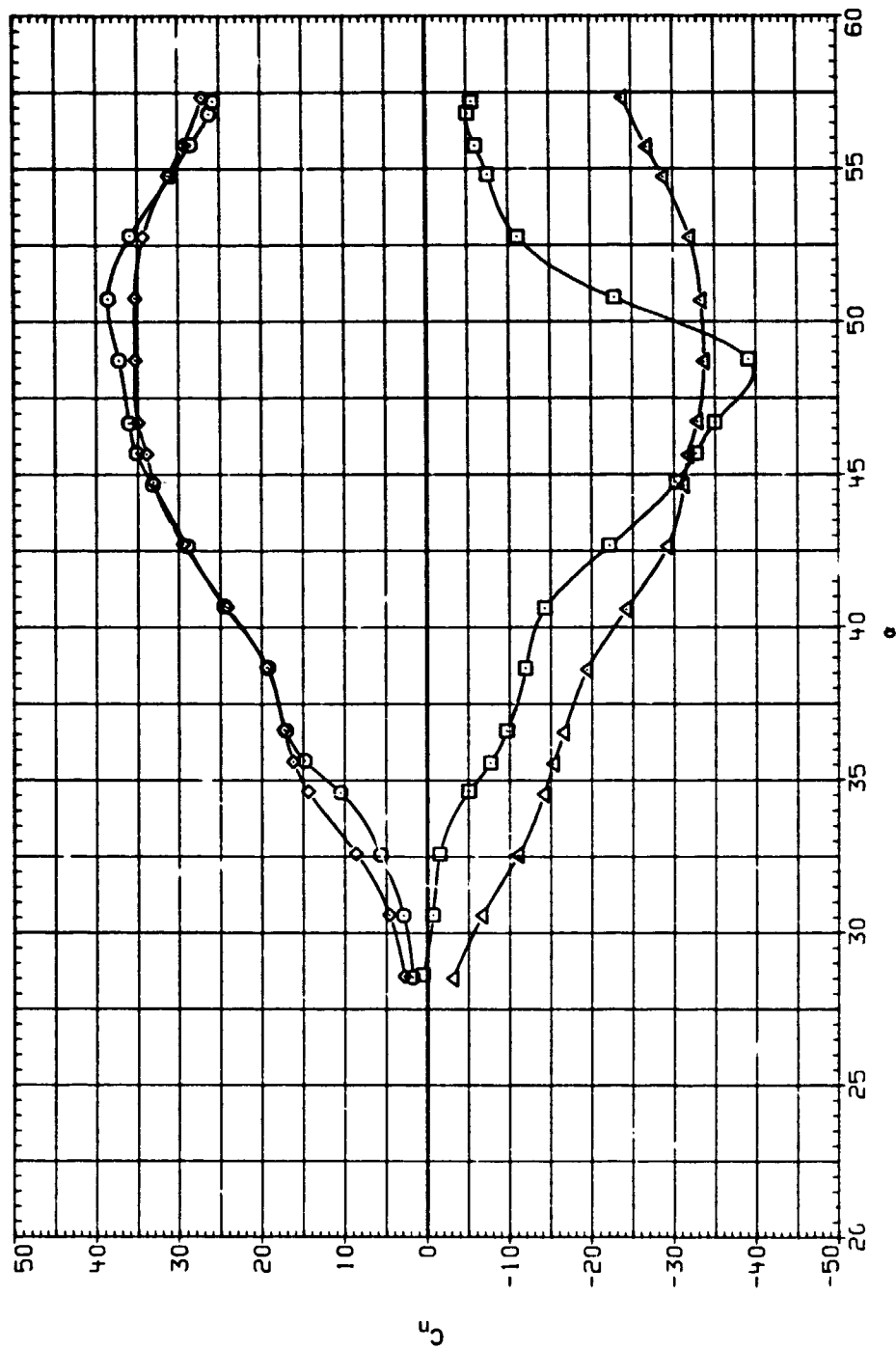


(a) C_y vs α .

Figure 4.— Effect of tip rotation, BOF3.5A7, forebody and afterbody fixed, $Re = 0.32 \times 10^6$.

DATA SET SYMBOL CONFIGURATION
 8AJ0002 ○ 80 F3.5 A7
 8AJ0004 □ 80 F3.5 A7
 8AJ0006 ◇ 80 F3.5 A7
 8AJ0008 △ 80 F3.5 A7

PHI-T PHI-F PHI-A MACH
 .000 .000 .000 .250
 90.000 .000 .000 .250
 180.000 .000 .000 .250
 270.000 .000 .000 .250



(b) C_H vs α .

Figure 4.- Concluded.

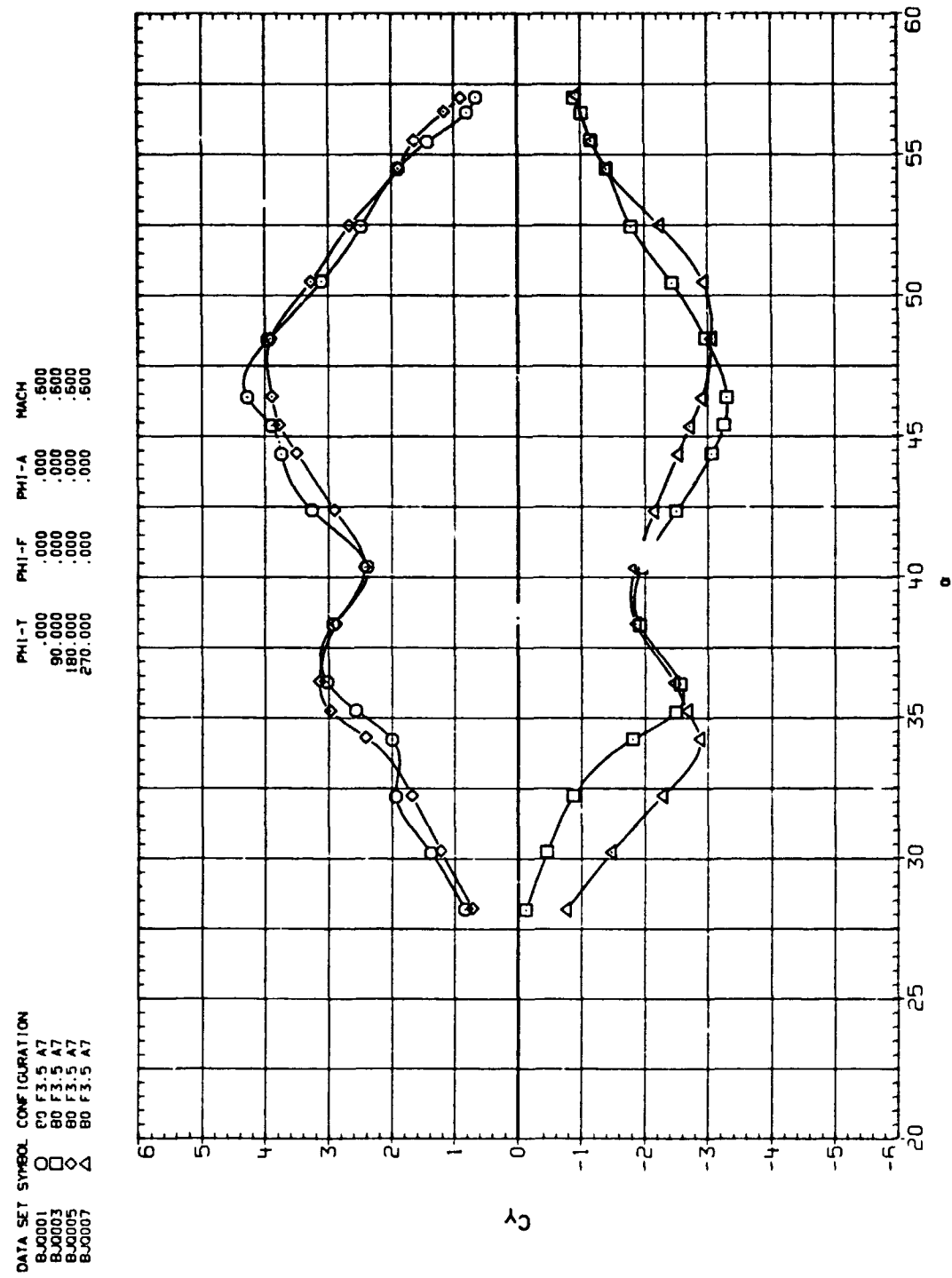
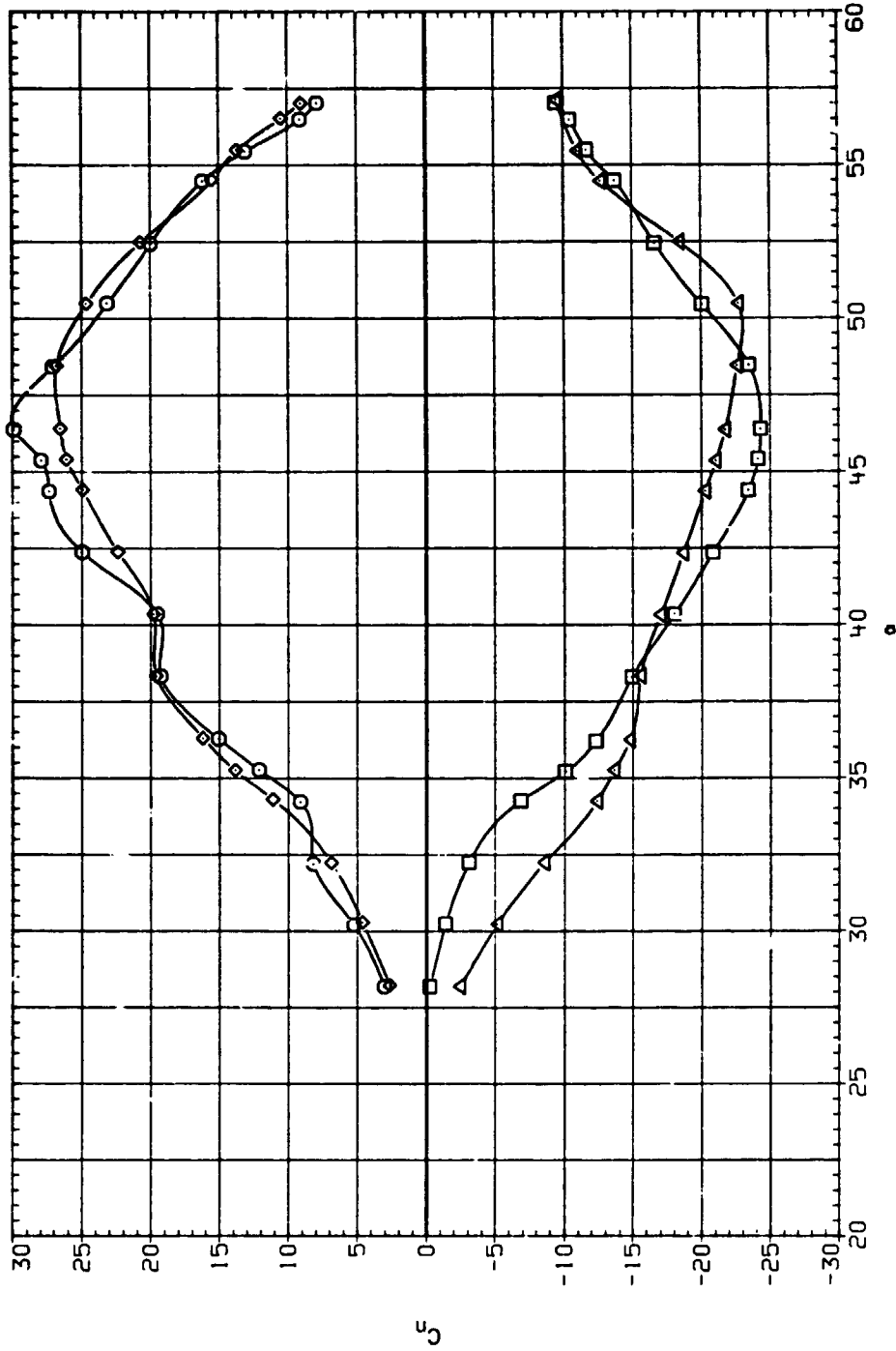


Figure 5.— Effect of tip rotation, BOF3.5A7, forebody and afterbody fixed, $Re = 0.32 \times 10^6$.

DATA SET SYMBOL CONFIGURATION
 B-J0001 ○ 80 F3.5 A7
 B-J0003 □ 80 F3.5 A7
 B-J0005 △ 80 F3.5 A7
 B-J0007

PHI-T PHI-F PHI-A MACH
 .000 .000 .000 .500
 90.000 .000 .000 .500
 180.000 .000 .000 .500
 270.000 .000 .000 .500

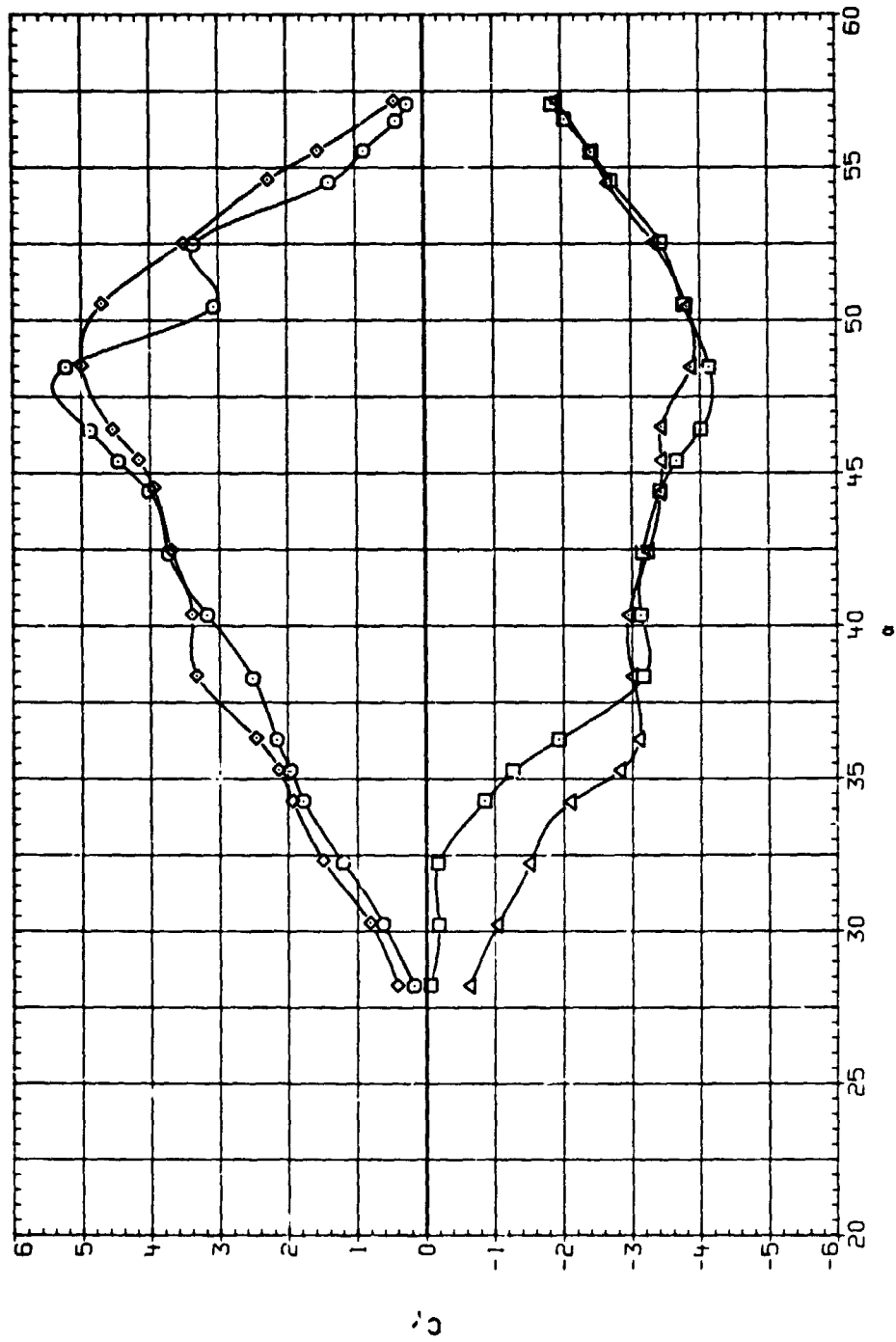


(b) C_{l} vs α .

Figure 5. Concluded.

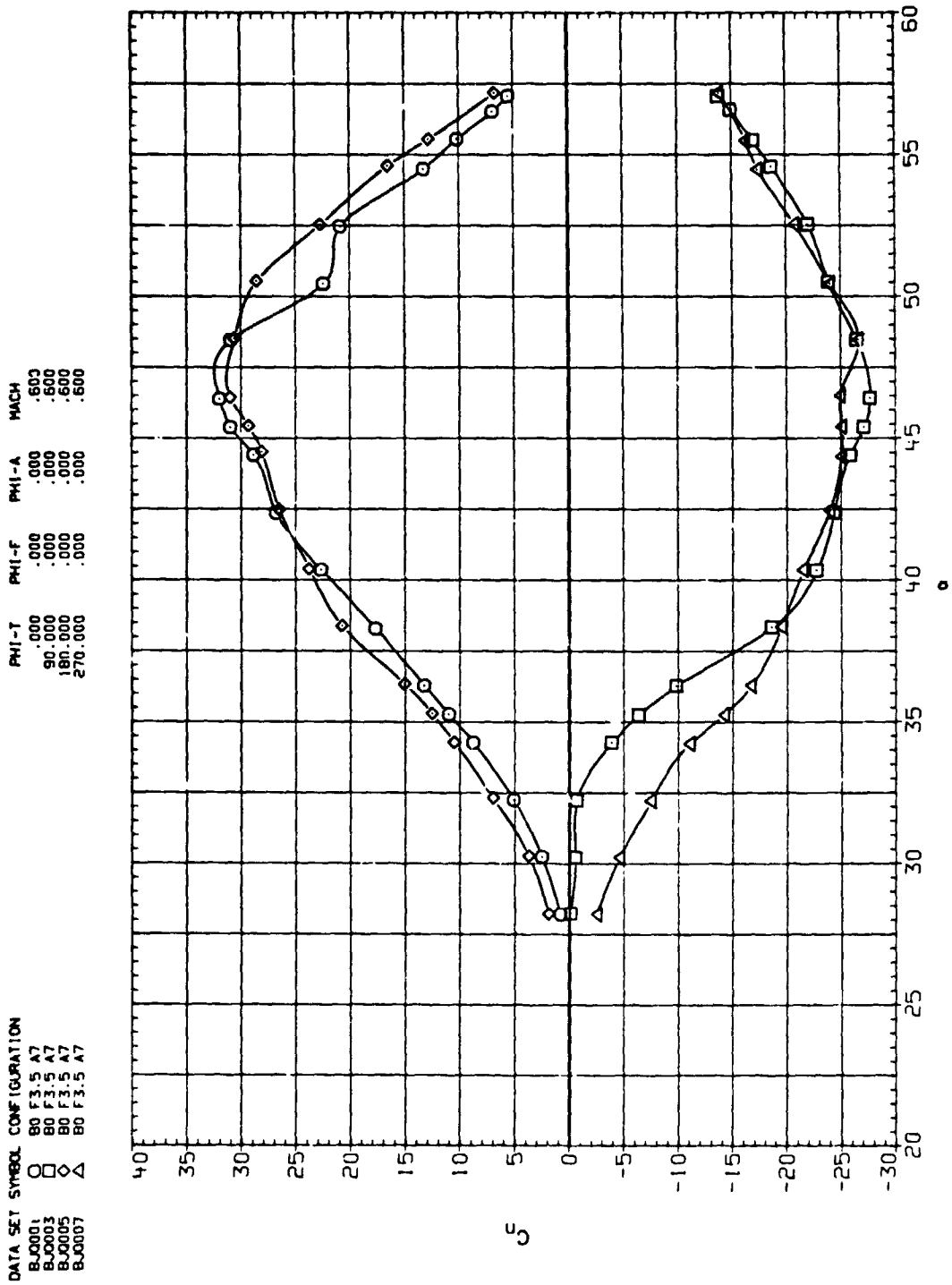
DATA SET SYMBOL: CONFIGURATION
 BJO001 80 F3.5 A7
 BJO003 80 F3.5 A7
 BJO005 80 F3.5 A7
 BJO007 80 F3.5 A7

PHI-T PHI-F PHI-A MACH
 .000 .000 .000 .600
 90.000 .000 .000 .600
 180.000 .000 .000 .600
 270.000 .000 .000 .600



(a) C_L vs α .

Figure 6. - Effect of tip rotation, BOF3.5A7, forebody and afterbody fixed, $Re = 0.43 \times 10^6$.

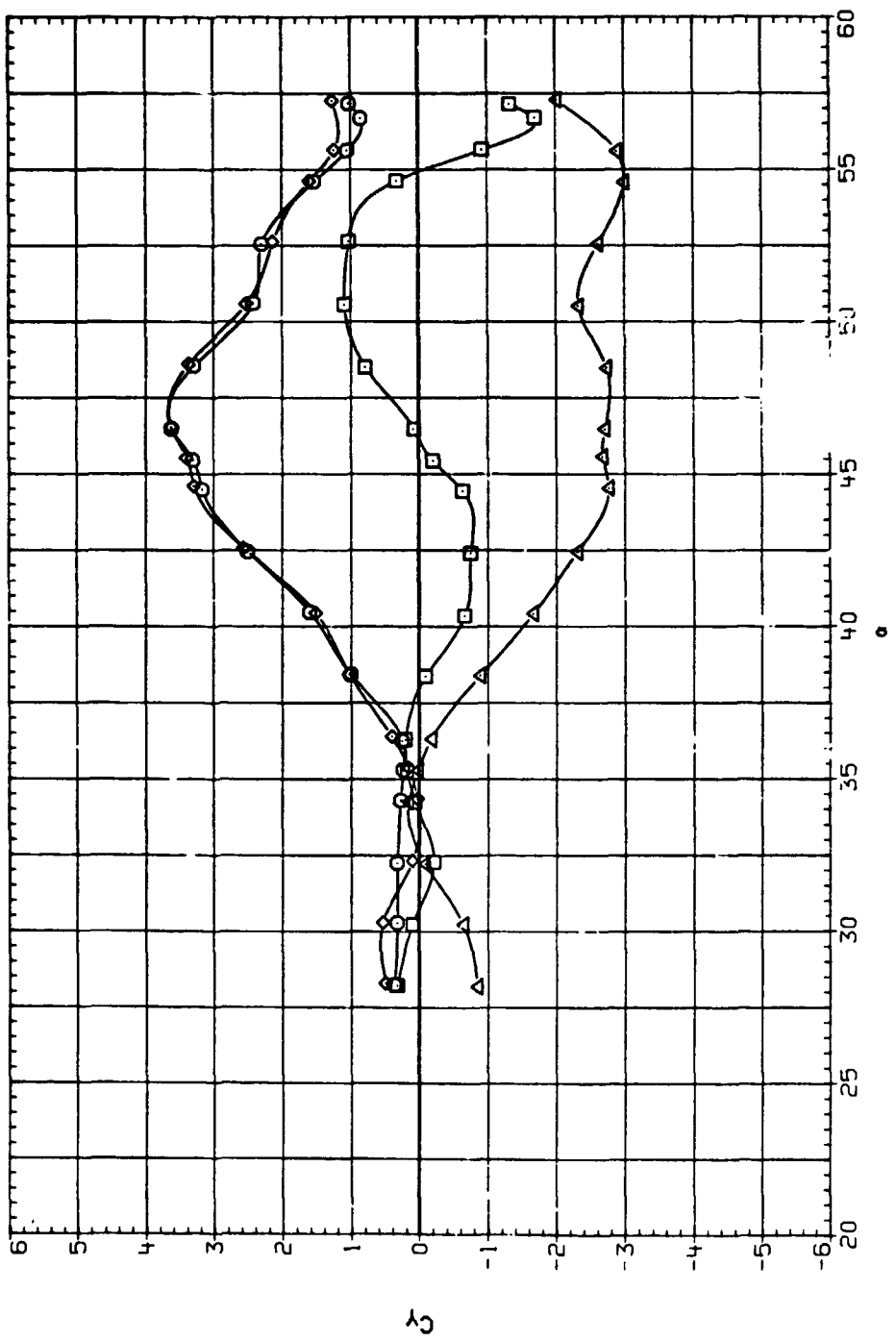


(b) C_H vs α .

Figure 6. Concluded.

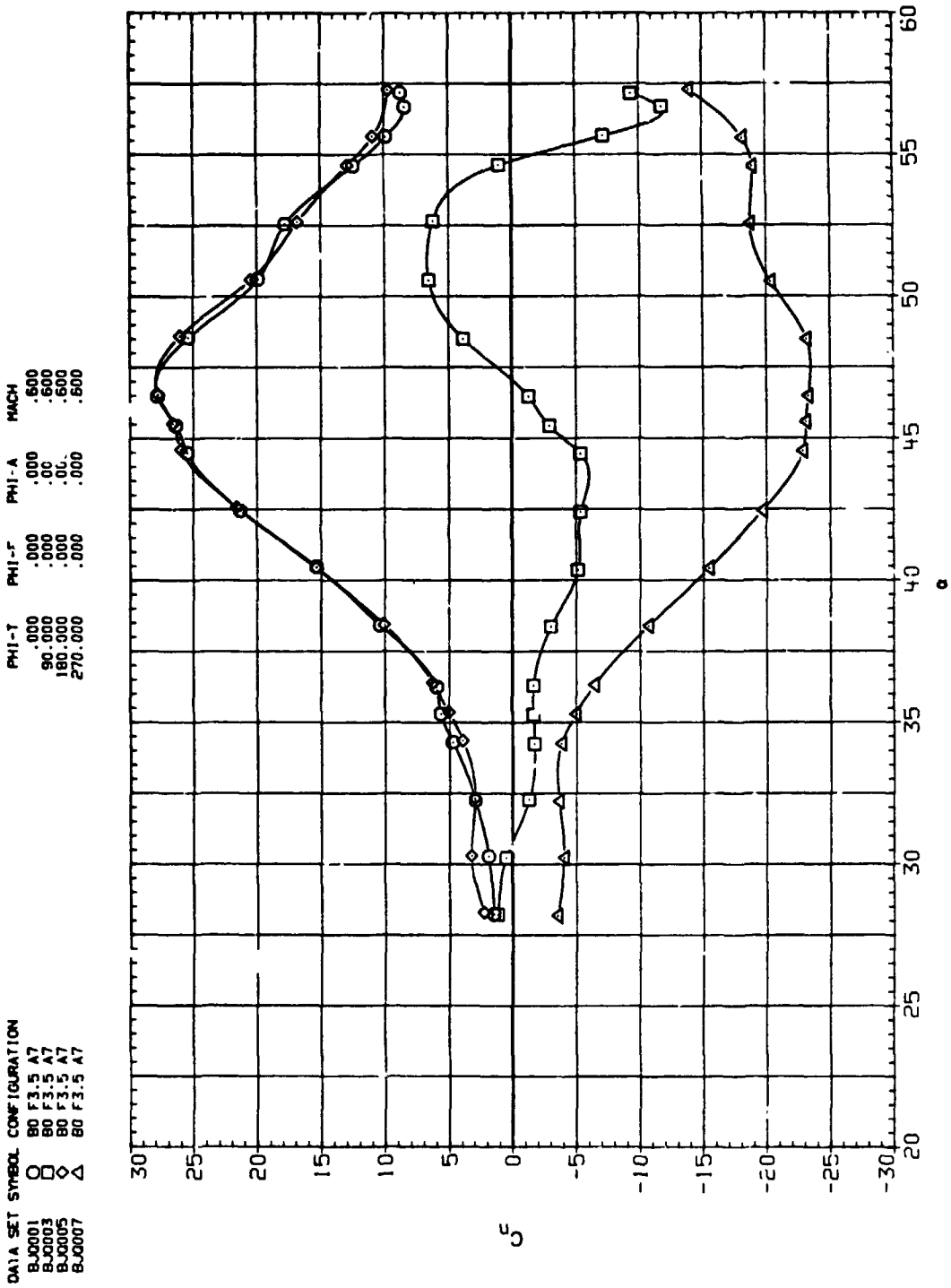
DATA SET SYMBOL CONFIGURATION
 B.0001 O 80 F3.5 A7
 B.0003 □ 80 F3.5 A7
 B.0005 △ 80 F3.5 A7
 B.0007 △ 80 F3.5 A7

PHI-T PHI-F PHI-A MACH
 .000 .000 .000 .600
 90.000 .000 .000 .600
 180.000 .000 .000 .600
 270.000 .000 .000 .600



(a) C_L vs α .

Figure 7.— Effect of tip rotation, BOF3.5A7, forebody and afterbody fixed, $Re = 0.65 \times 10^6$.

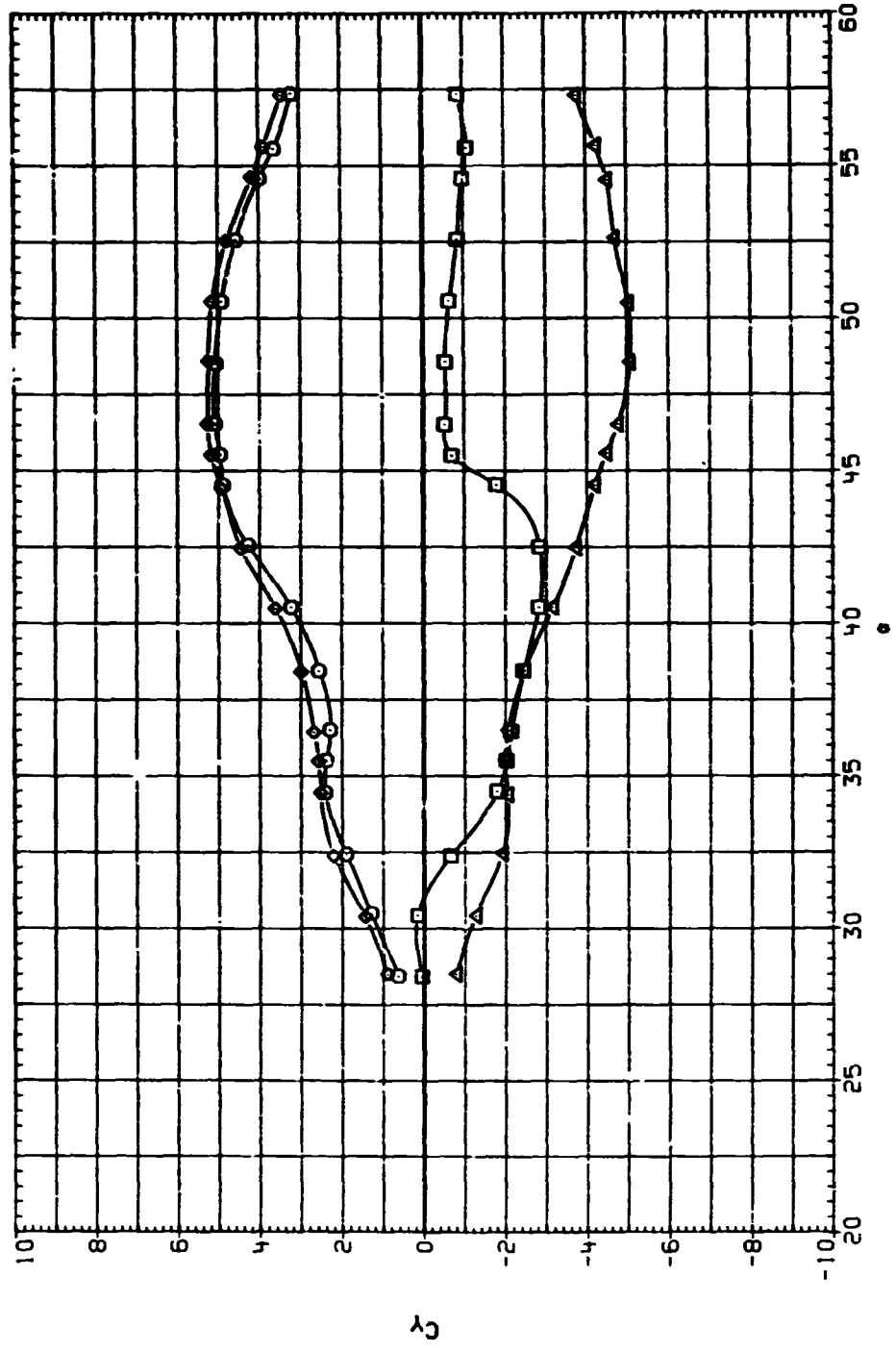


(b) C_H vs α .

Figure 7.- Concluded.

DATA SET SYMBOL CONFIGURATION
 B-0016 80 F3.5 A7
 F-0017 80 F3.5 A7
 F-0018 80 F3.5 A7
 F-0019 80 F3.5 A7

PHI-T PHI-F PHI-A MACH
 .000 .000 .000 .250
 90.000 90.000 .000 .250
 180.000 180.000 .000 .250
 270.000 270.000 .000 .250



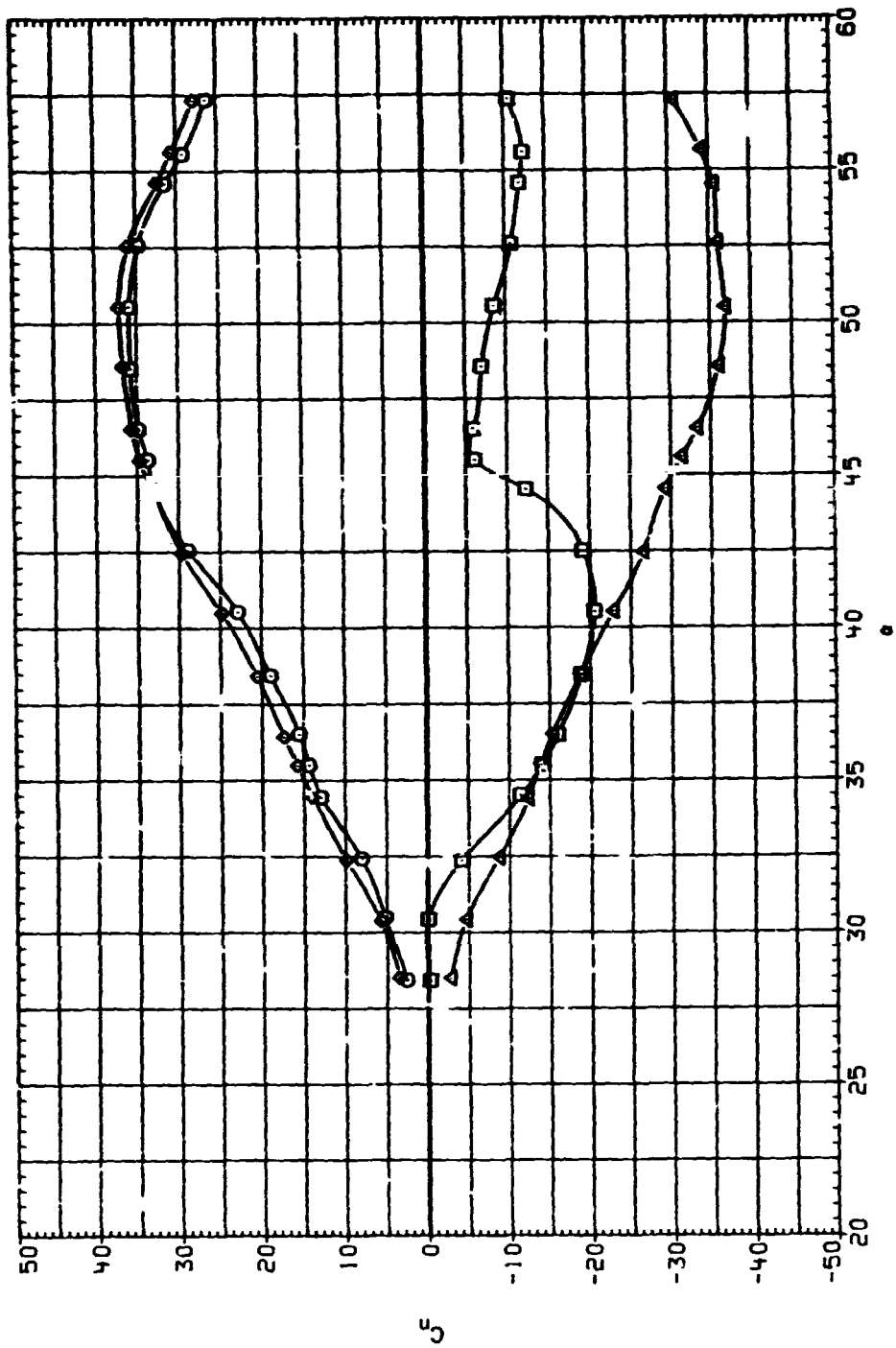
(a) C_y vs α .

Figure 8. Effect of tip and forebody rotation, BOF3.5A7, afterbody fixed, $Re = 0.32 \times 10^6$.

DATA SET SYMBOL CONFIGURATION

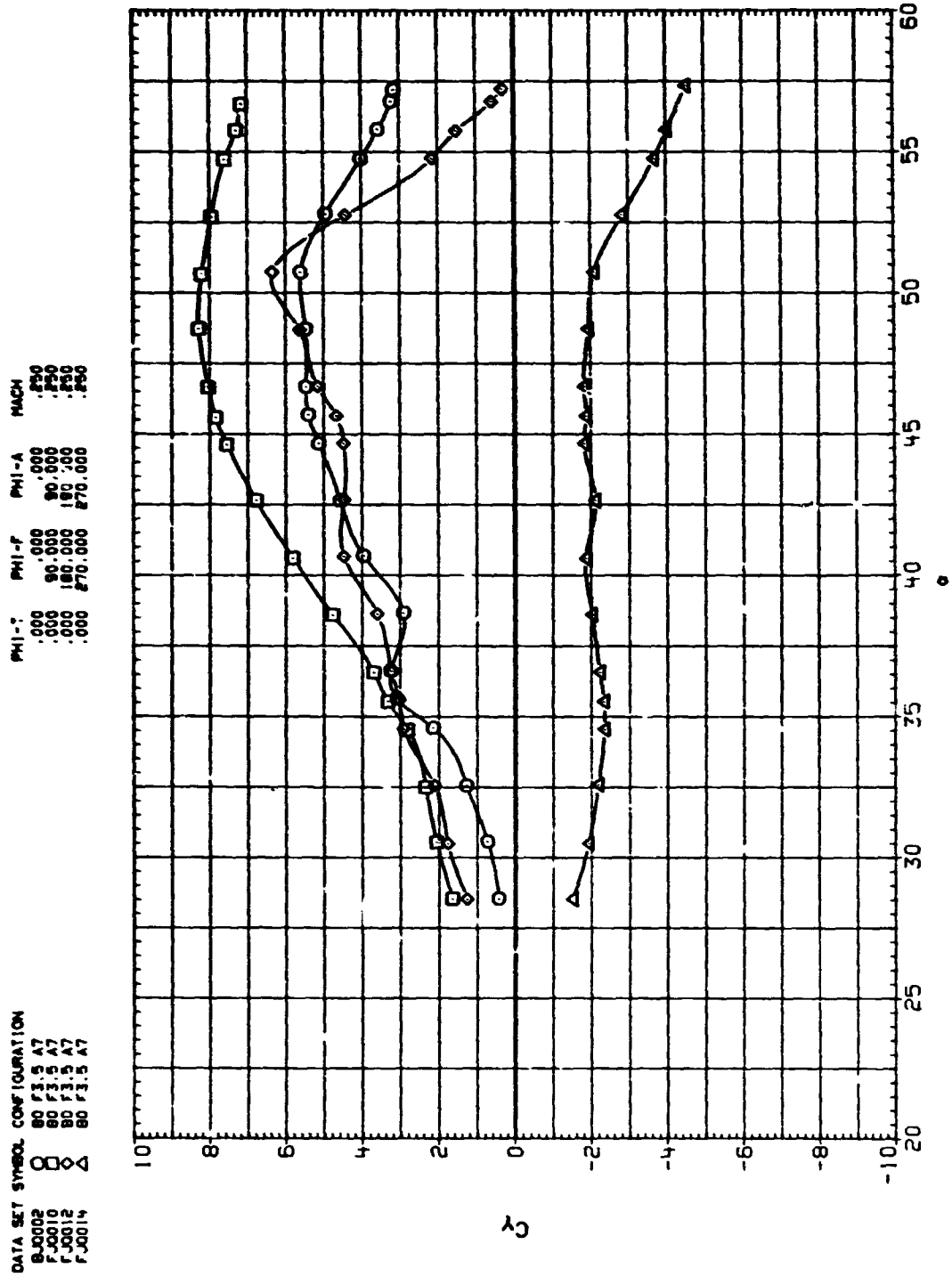
8J0015	○	80 F3.5 A7
8J0017	⊗	80 F3.5 A7
8J0018	⊙	80 F3.5 A7
8J0019	△	80 F3.5 A7

PHI-T	PHI-F	PHI-A	MACH
.000	.000	.000	.250
90.000	90.000	.000	.250
180.000	180.000	.000	.250
270.000	270.000	.000	.250



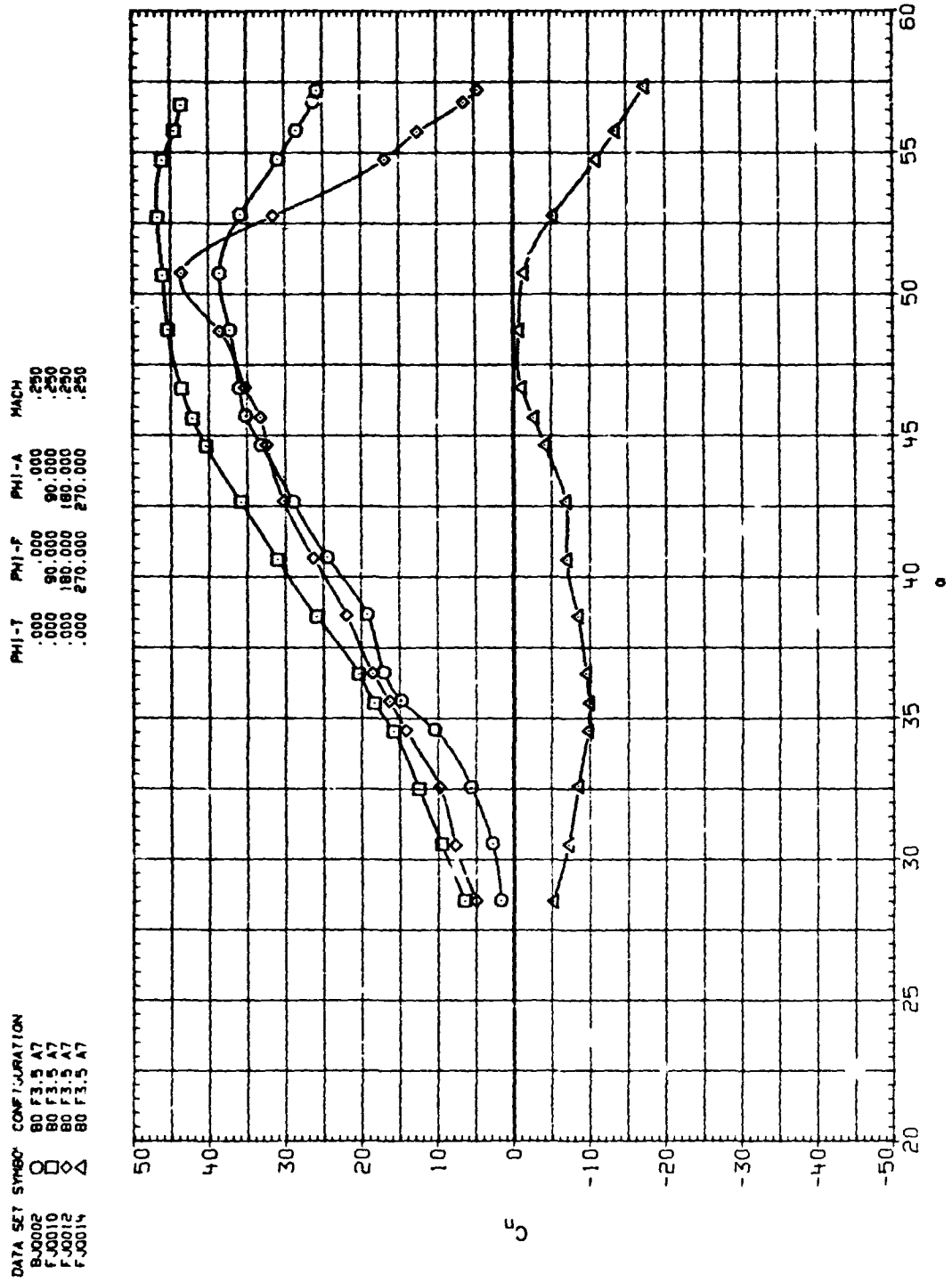
(b) C_H vs α .

Figure 8. Concluded.



(a) C_y vs α

Figure 9. - Effect of forebody and afterbody rotation, BOF3.SA7, tip fixed, $Re = 0.32 \times 10^6$.

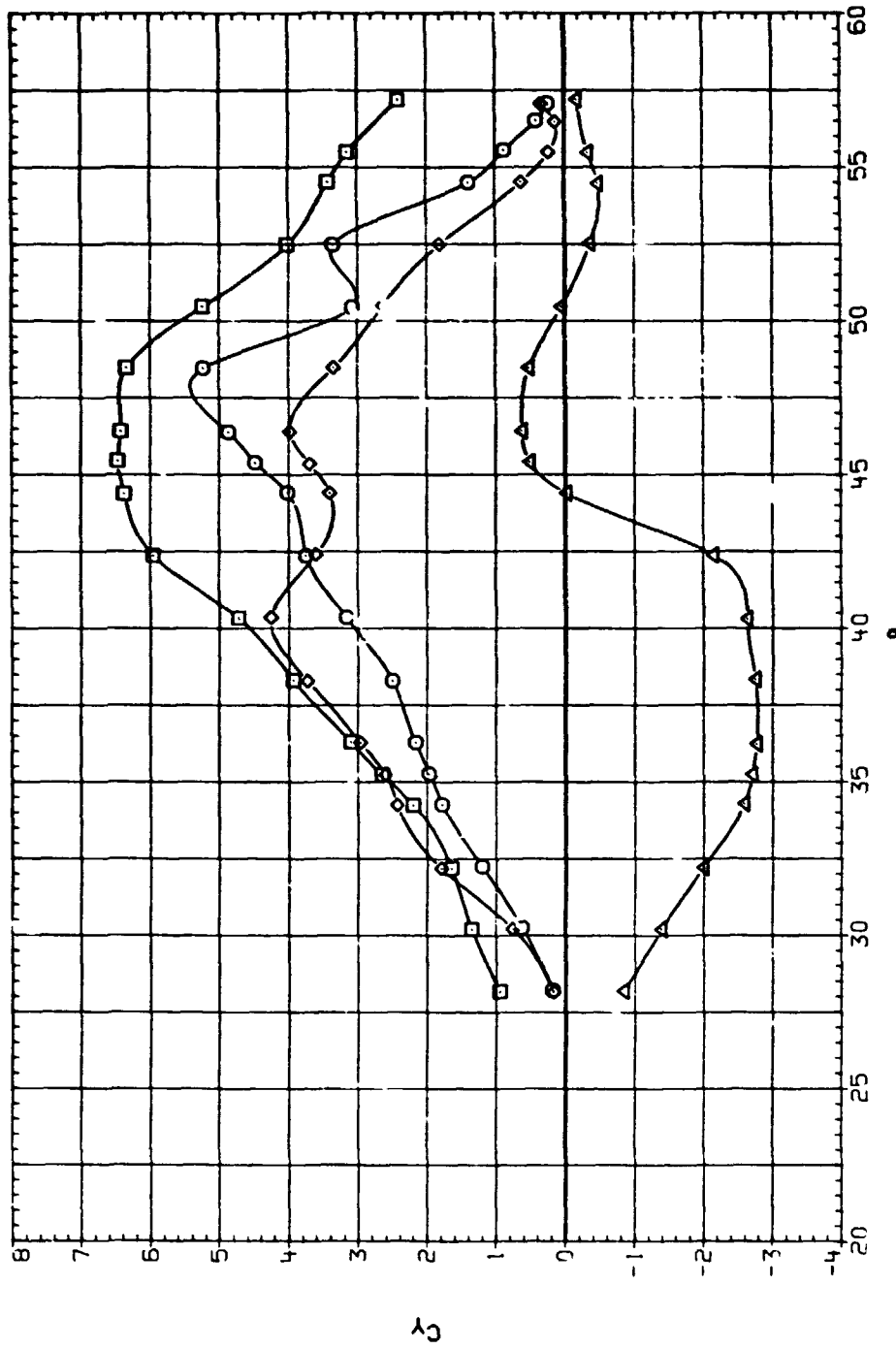


(b) C_l vs α .

Figure 9. Concluded.

DATA SET SYMBOL CONFIGURATION
 B.0001 B0 F3.5 A7
 F.0009 F0 F3.5 A7
 F.0011 B0 F3.5 A7
 F.0013 B0 F3.5 A7

PHI-T PHI-F PHI-A MACH
 .000 .000 .000 .60
 .000 90.000 90.000 .60
 .000 180.000 180.000 .60
 .000 270.000 270.000 .60

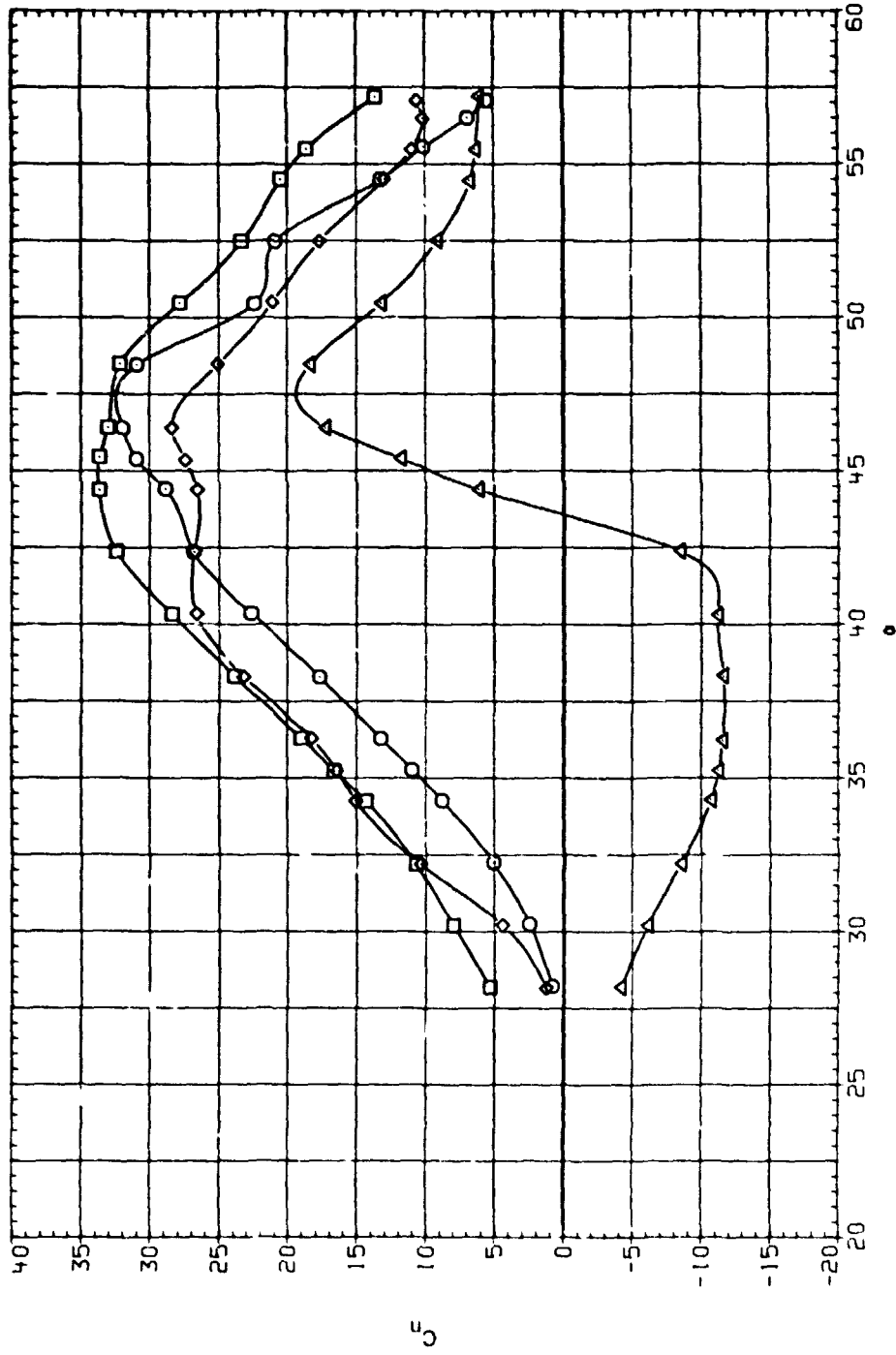


(a) C_y vs α .

Figure 10. — Effect of forebody and afterbody rotation, BOF3.5A7, tip fixed, $Re = 1.43 \times 10^6$.

DATA SET SYMBOL CONFIGURATION
 BU0001 O 80 F3.5 A7
 FU0009 □ 80 F3.5 A7
 FU0011 ◇ 80 F3.5 A7
 FU0013 △ 80 F3.5 A7

PHI-T PHI-T PHI-A MACH
 .000 .000 .000 .600
 .000 90.000 90.000 .600
 .000 180.000 180.000 .600
 .000 270.000 270.000 .600

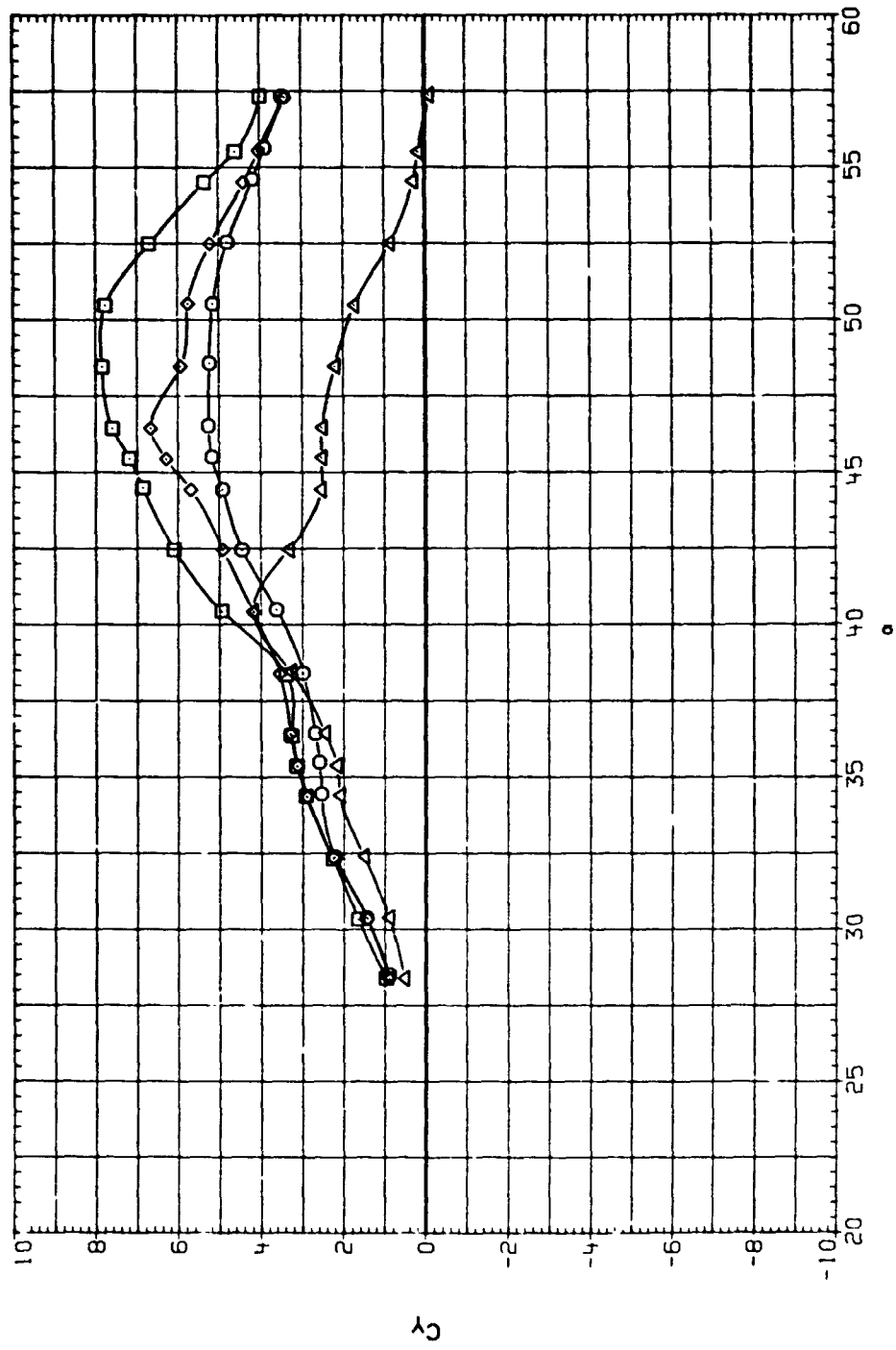


(b) C_l vs α .

Figure 10. ... Concluded.

DATA SET SYMBOL CONFIGURATION
 FJ0018 ○ 80 F3.5 A7
 FJ0024 □ 80 F3.5 A7
 FJ0A21 ◇ 80 F3.5 A7
 FJ0023 △ 80 F3.5 A7

PHI-T PHI-F PHI-A MACH
 180.000 180.000 .000 .250
 180.000 180.000 90.000 .250
 180.000 180.000 180.000 .250
 180.000 180.000 270.000 .250

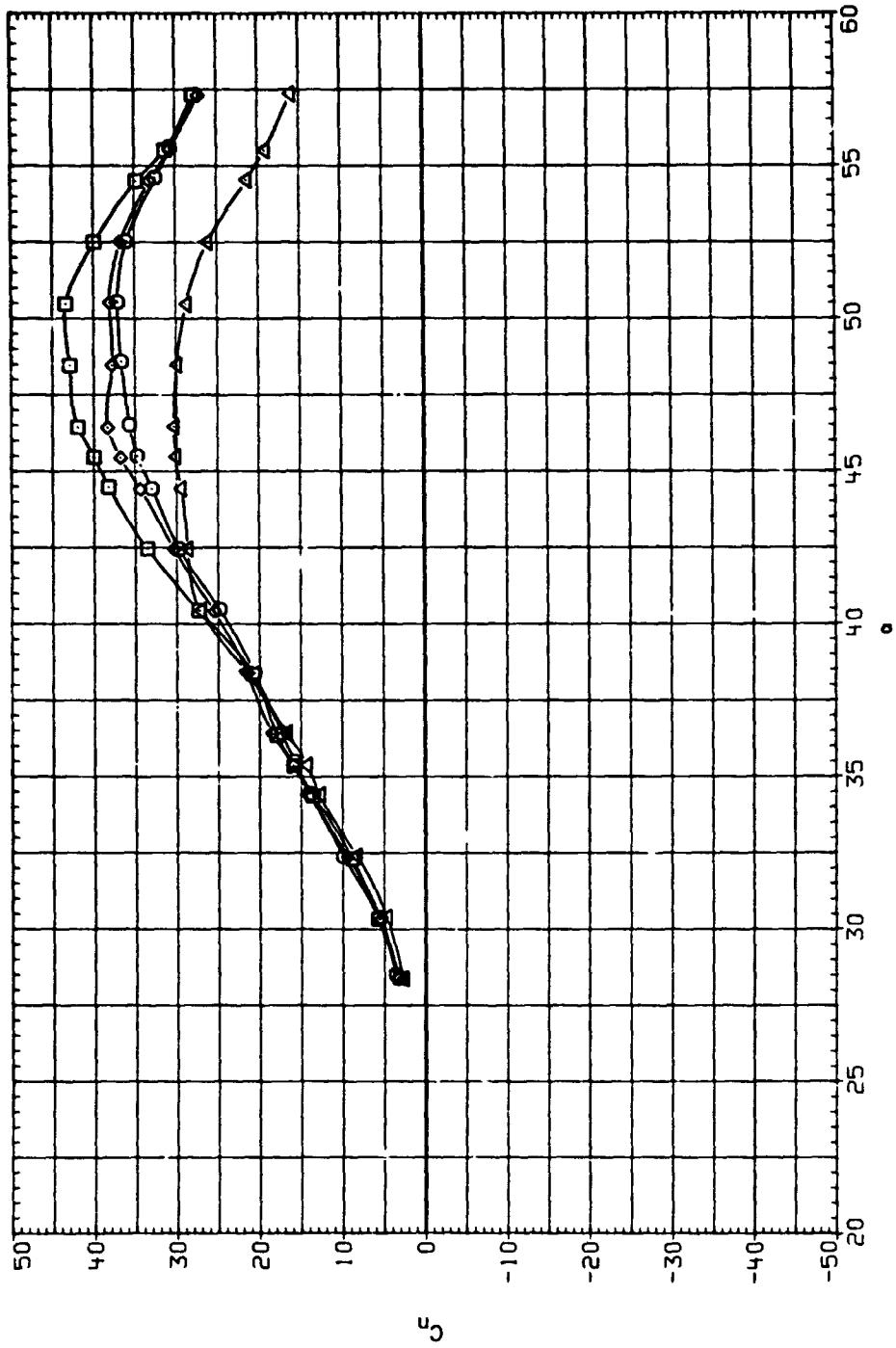


(a) C_y vs α .

Figure 11.- Effect of afterbody rotation, BOF3.5A7, tip and forebody fixed, $Re = 0.32 \times 10^6$.

DATA SET SYMBOL CONFIGURATION
 FJ0018 80 F3.5 A7
 FJ0024 80 F3.5 A7
 FJ0A21 80 F3.5 A7
 FJ023 80 F3.5 A7

PHI-7 PHI-F PHI-A MACH
 180.000 180.000 .000 .250
 180.000 180.000 90.000 .250
 180.000 180.000 180.000 .250
 180.000 180.000 270.000 .250

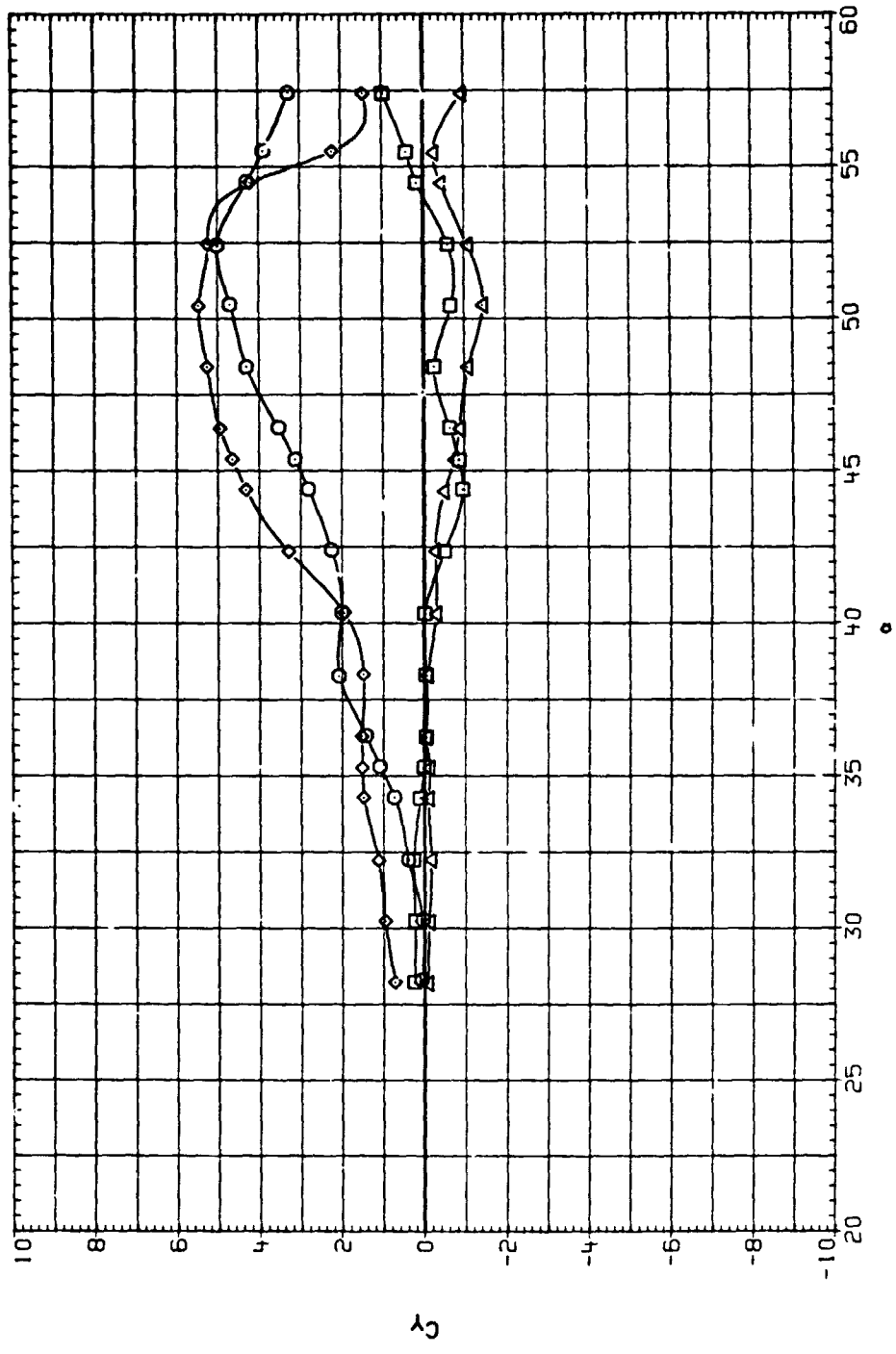


(b) C_{ll} vs α .

Figure 11. - Concluded.

DATA SET SYMBOL CONFIGURATION
 BJ0037 F3.5 A7
 BJ0039 F3.5 A7
 BJ0040 F3.5 A7
 BJ0041 F3.5 A7

PHI-F PHI-B MACH
 .000 .000 .250
 45.000 .000 .250
 90.000 .000 .250
 135.000 .000 .250

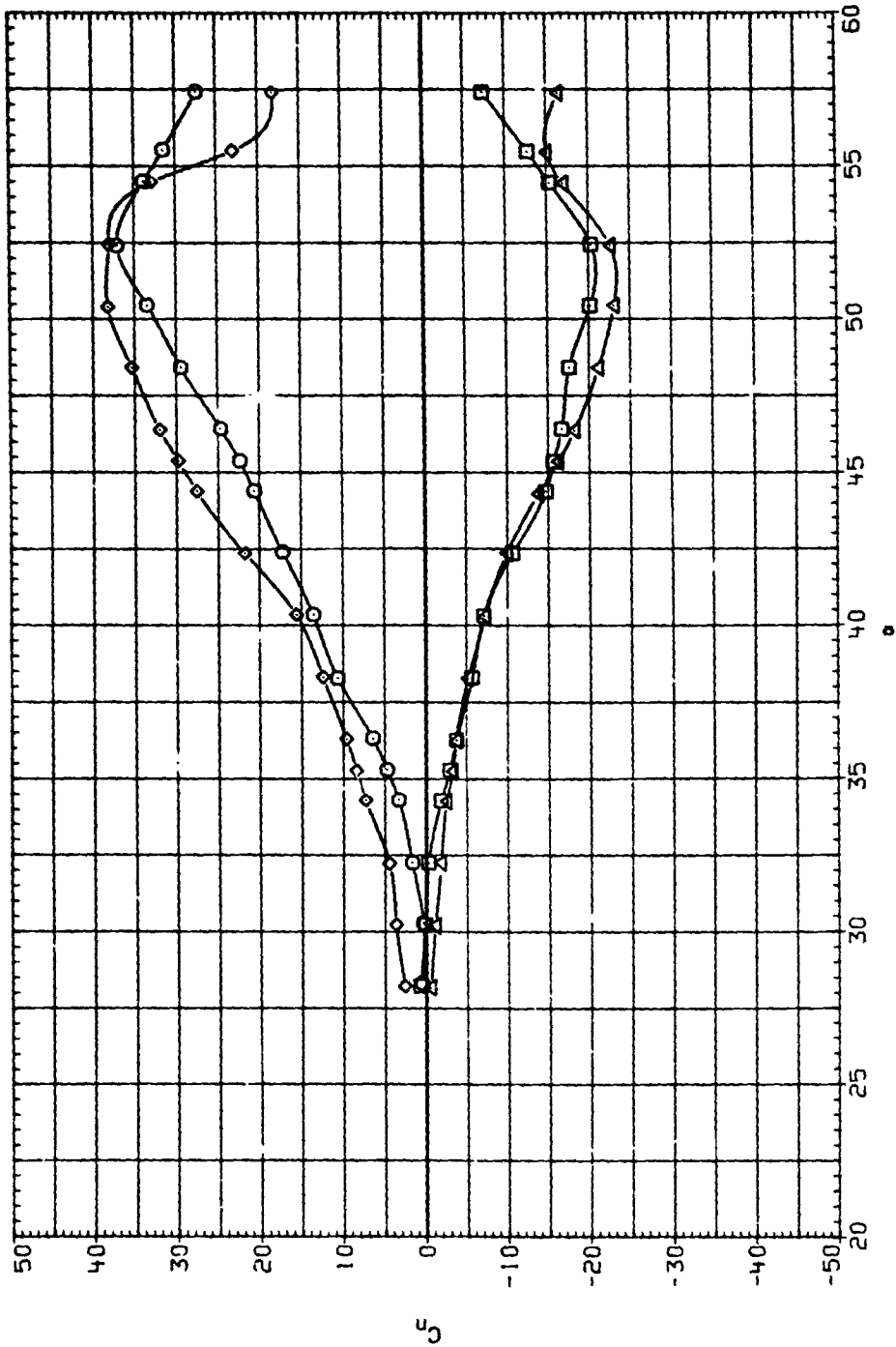


(a) C_l vs α , $0 \leq \phi \leq 135$.

Figure 12. Effect of forebody rotation, F3.5A7, afterbody fixed, $Re = 0.32 \times 10^6$.

DATA SET SYMBOL CONFIGURATION
 BJJ037 ○ F3.5 A7
 BJJ039 □ F3.5 A7
 BJJ040 ◇ F3.5 A7
 BJJ041 △ F3.5 A7

PHI-F PHI-A MACH
 .000 .50 .250
 .45.000 .500 .500
 .90.000 .500 .500
 135.000 .500 .500

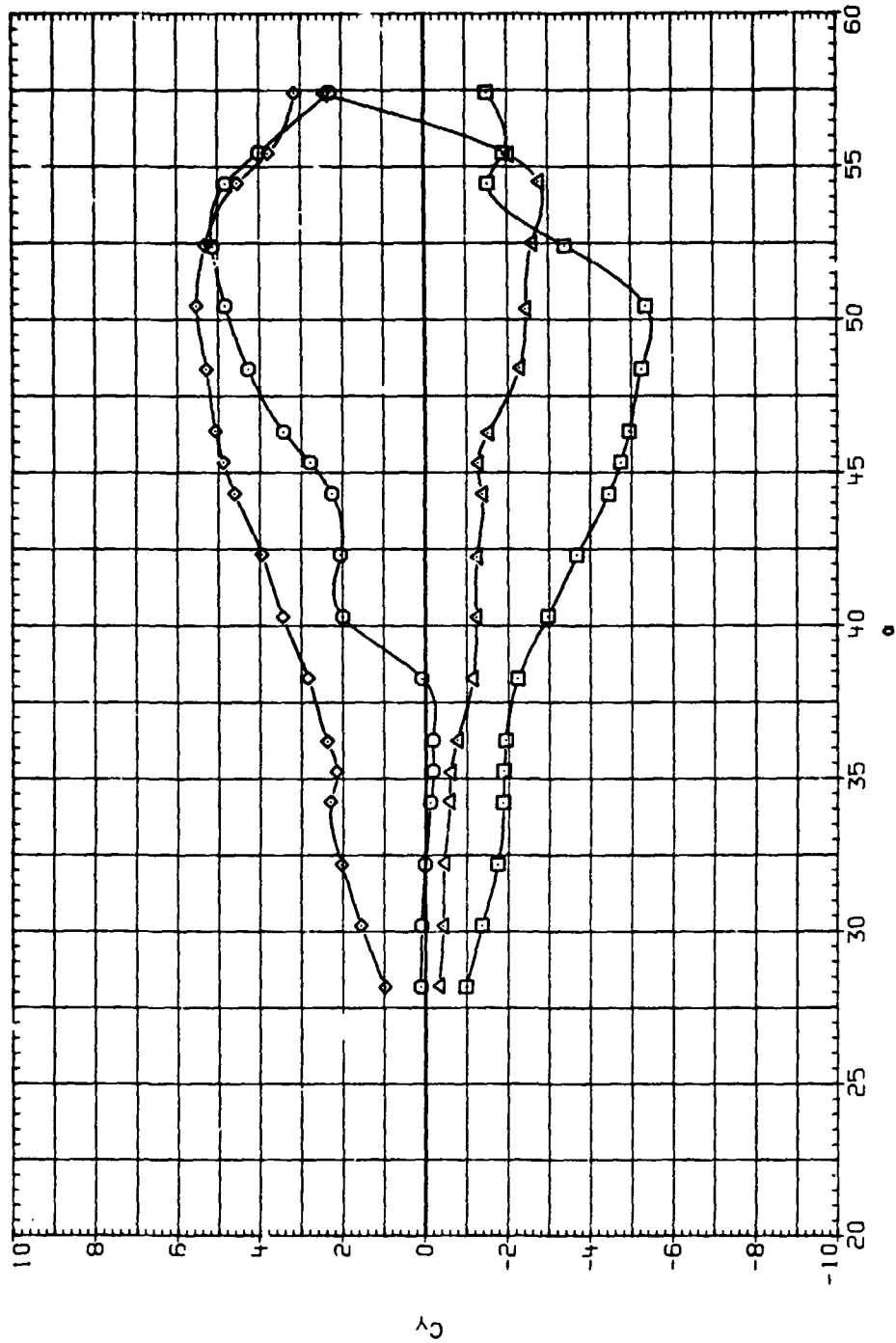


(b) C_L vs α , $0 \leq \phi \leq 135$.

Figure 12. - Continued.

DATA SET SYMBOL CONFIGURATION
 BU0042 □ F3.5 A7
 BU0043 ○ F3.5 A7
 BU0044 ◇ F3.5 A7
 BU0045 △ F3.5 A7

PHI-F PHI-A MACH
 180.000 .000 .250
 225.000 .000 .250
 270.000 .000 .250
 315.000 .000 .250

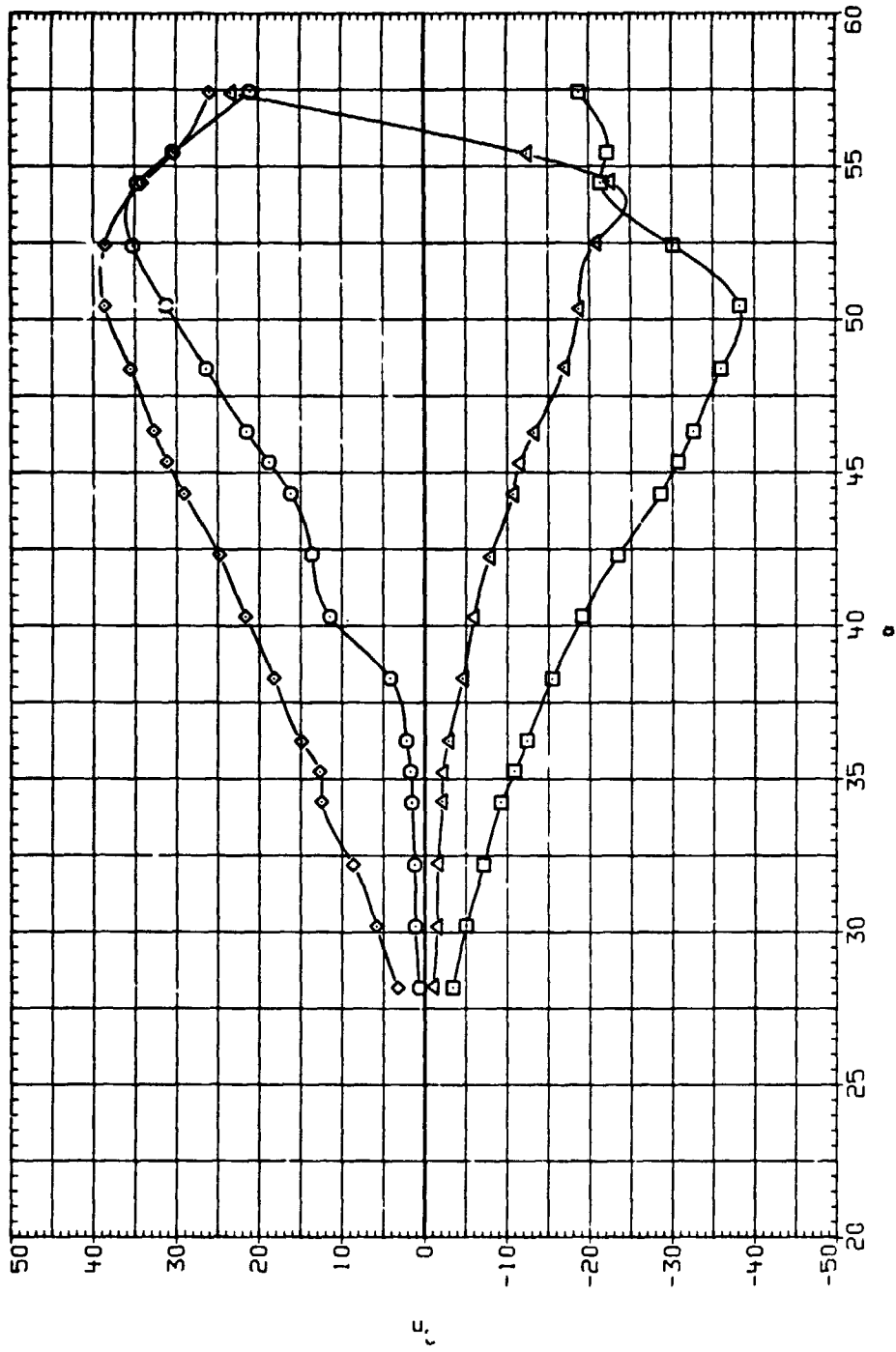


(c) C_L vs α , $180 \leq \phi \leq 315$.

Figure 12. Continued.

DATA SET SYMBOL CONFIGURATION
 BU00N2 ○ F3.5 A7
 BU00N3 □ F3.5 A7
 BU00N4 ◇ F3.5 A7
 BU00N5 △ F3.5 A7

PHI-F PHI-A MACH
 180.000 .000 .250
 225.000 .000 .250
 270.000 .000 .250
 315.000 .000 .250

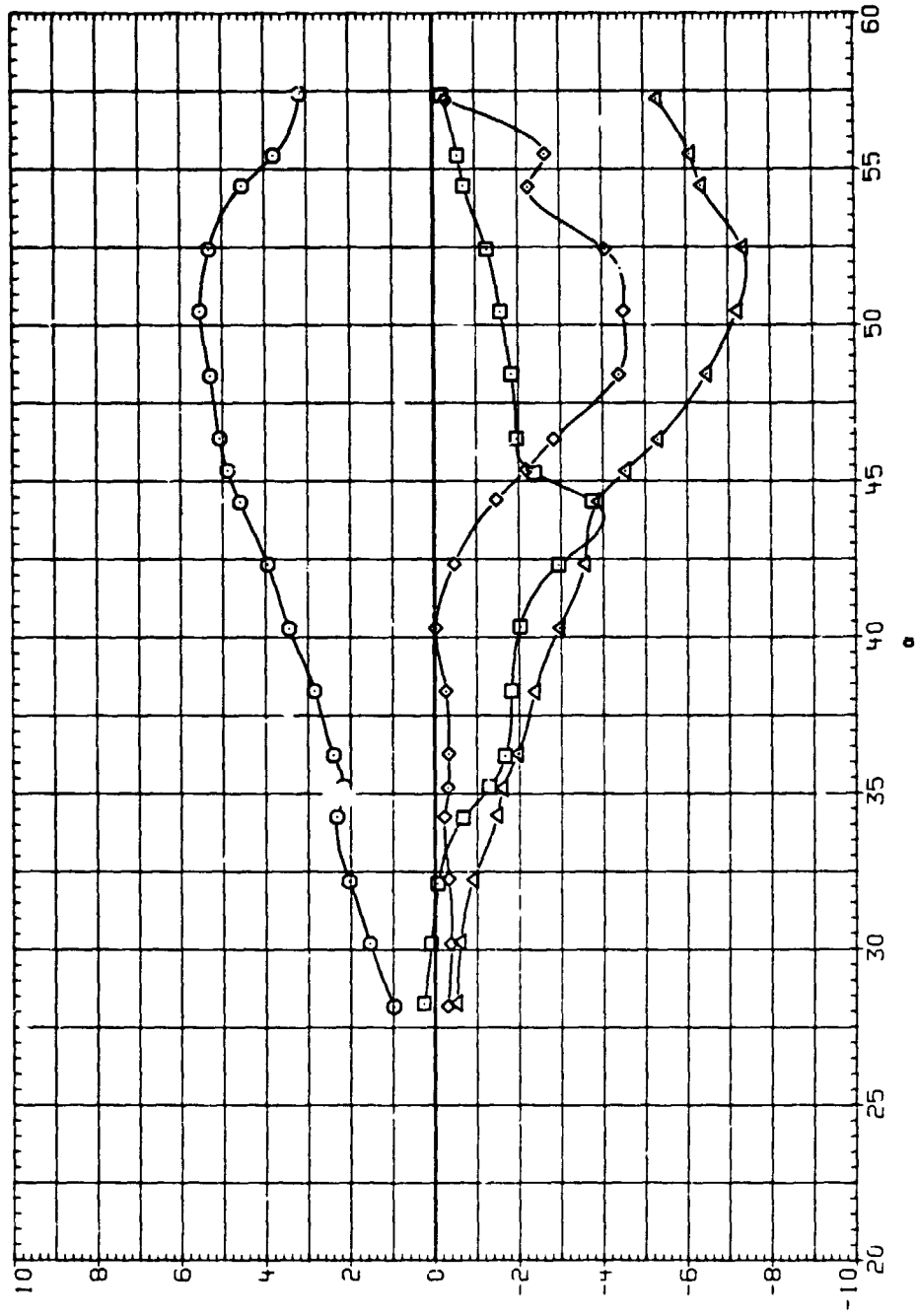


(d) C_l vs α , $180 \leq \phi F \leq 315$.

Figure 12.- Concluded.

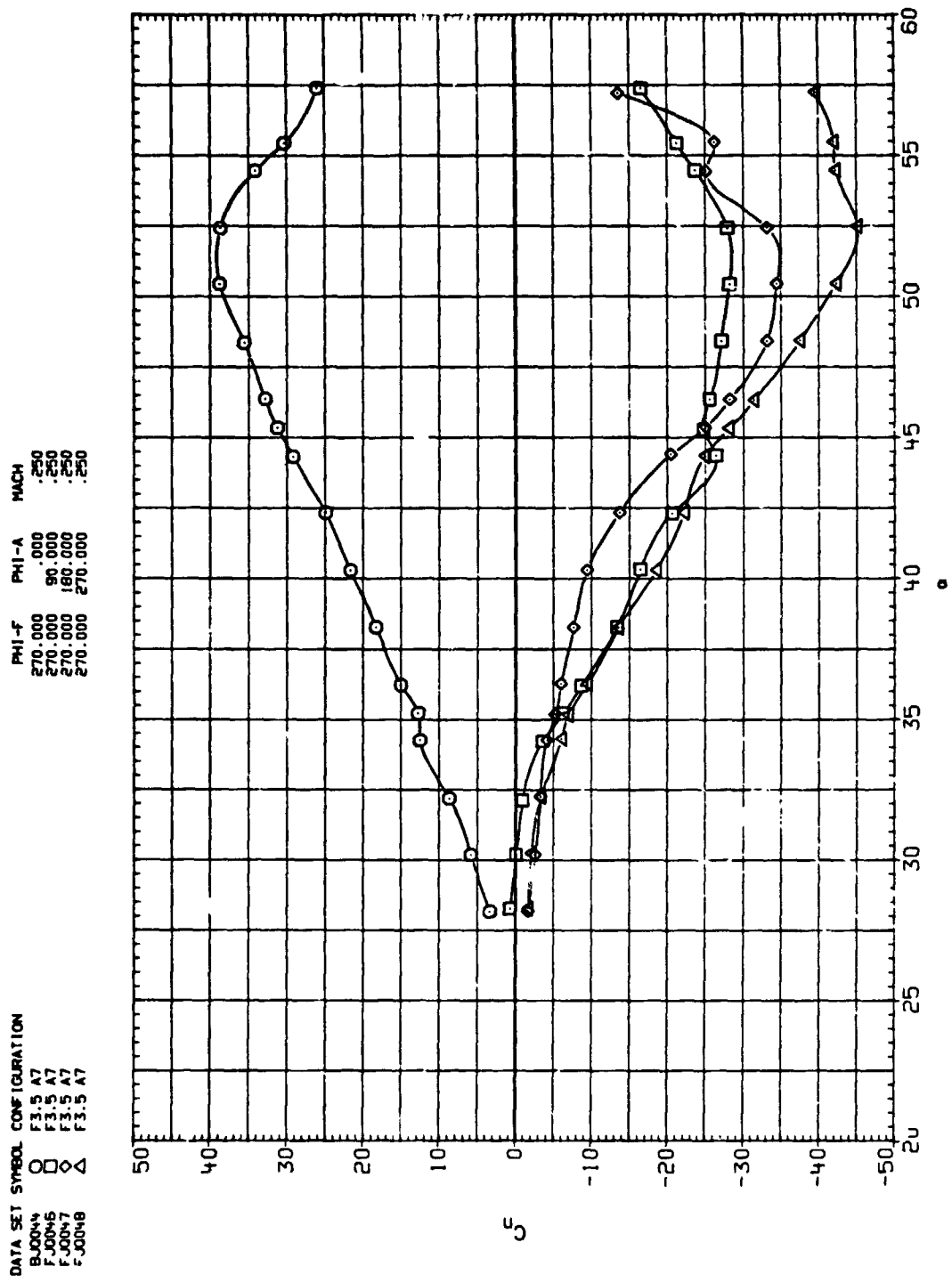
DATA SET SYMBOL CONFIGURATION
 B100N4 ○ F3.5 A7
 F100N6 □ F3.5 A7
 F100N7 ◇ F3.5 A7
 F100N8 △ F3.5 A7

PHI-F PHI-A MACH
 270.000 .000 .250
 270.000 90.000 .250
 270.000 180.000 .250
 270.000 270.000 .250



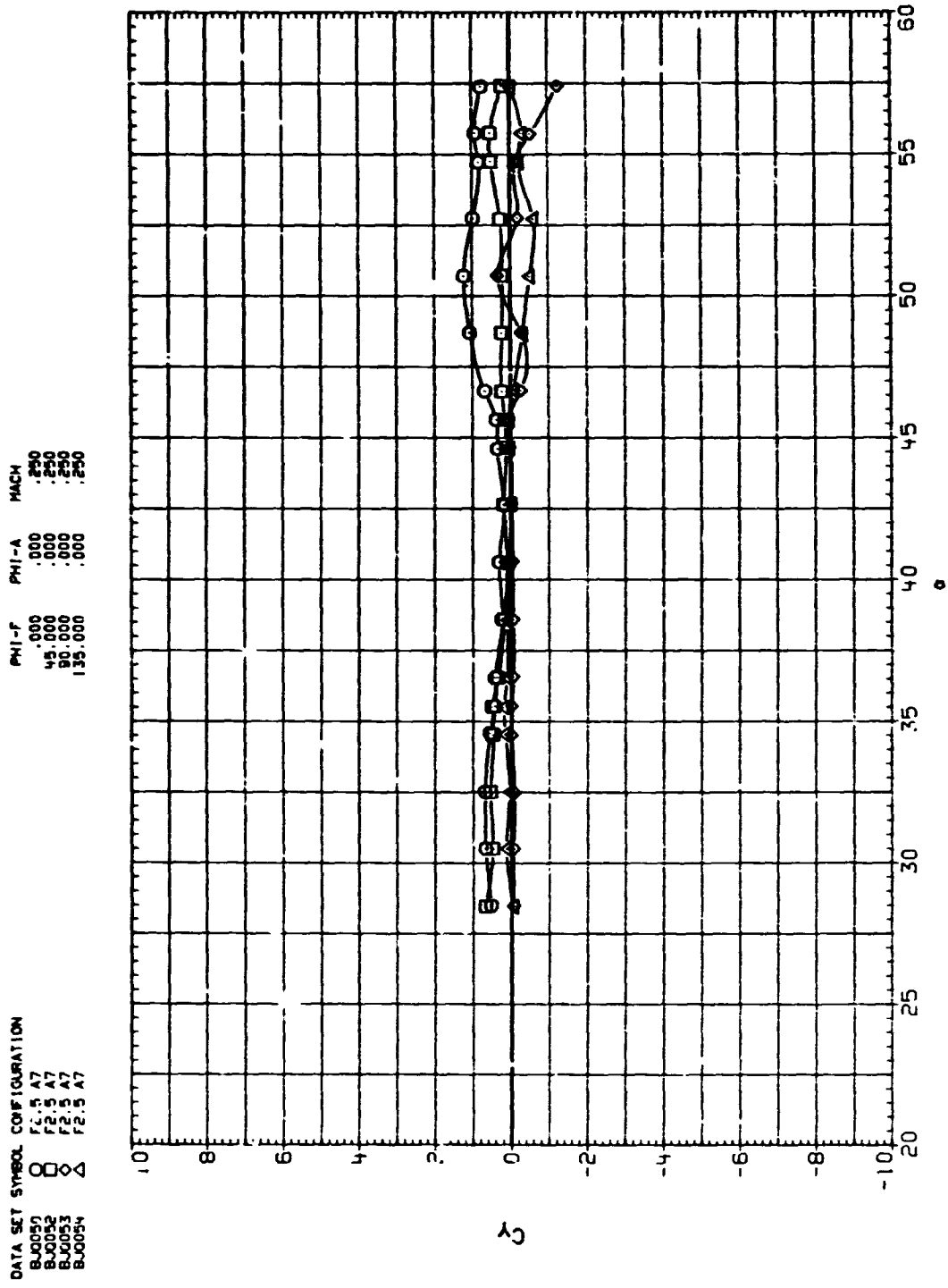
(a) C_y vs α .

Figure 13. - Effect of afterbody rotation, F3.5A7, forebody fixed. $Re = 0.32 \times 10^6$.



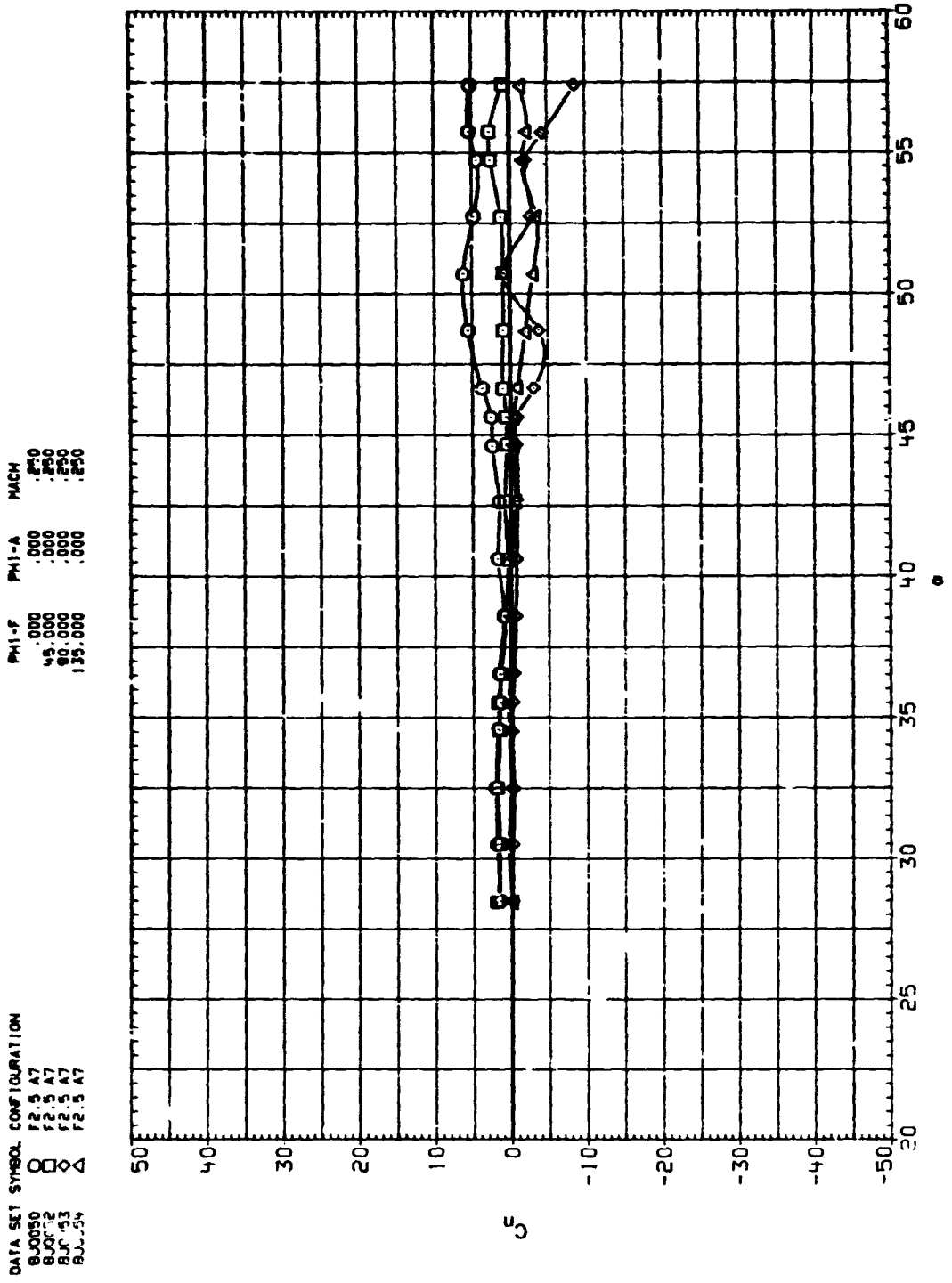
(b) C_D vs α .

Figure 13. Concluded.



(a) C_y vs α , $0 \leq \phi \leq 135$.

Figure 14. Effect of forebody rotation, F2.5A7, afterbody fixed, $R_e = 0.32 \times 10^6$.

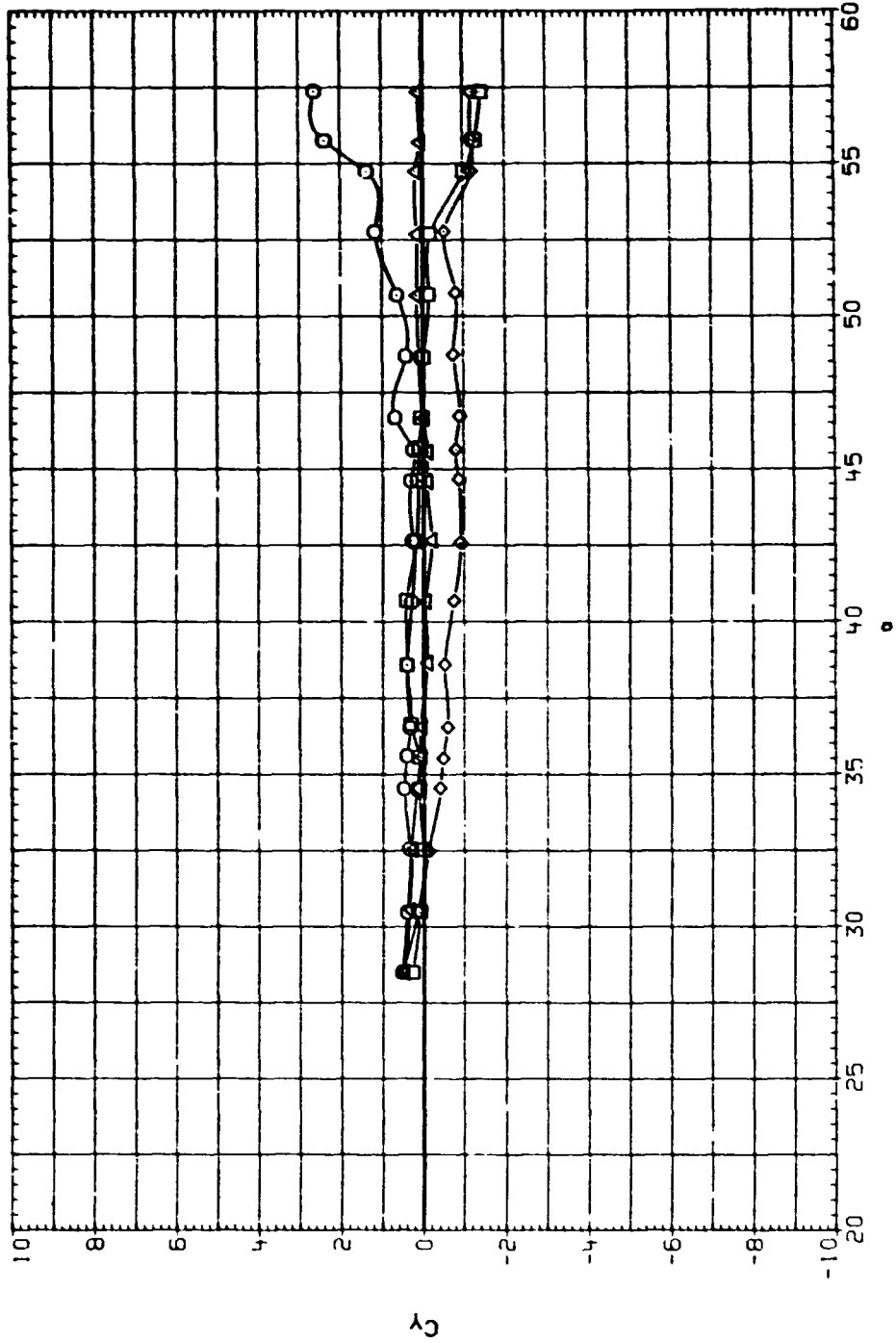


(b) C_{li} vs α , $0 \leq \phi_i \leq 135$.

Figure 14. Continued.

DATA SET SYMBOL CONFIGURATION
 B-J0055 F2.5 A7
 B-J0056 F2.5 A7
 B-J0057 F2.5 A7
 B-J0058 F2.5 A7

PHI-F PHI-A MACH
 180.000 .000 .250
 225.000 .000 .250
 270.000 .000 .250
 315.000 .000 .250



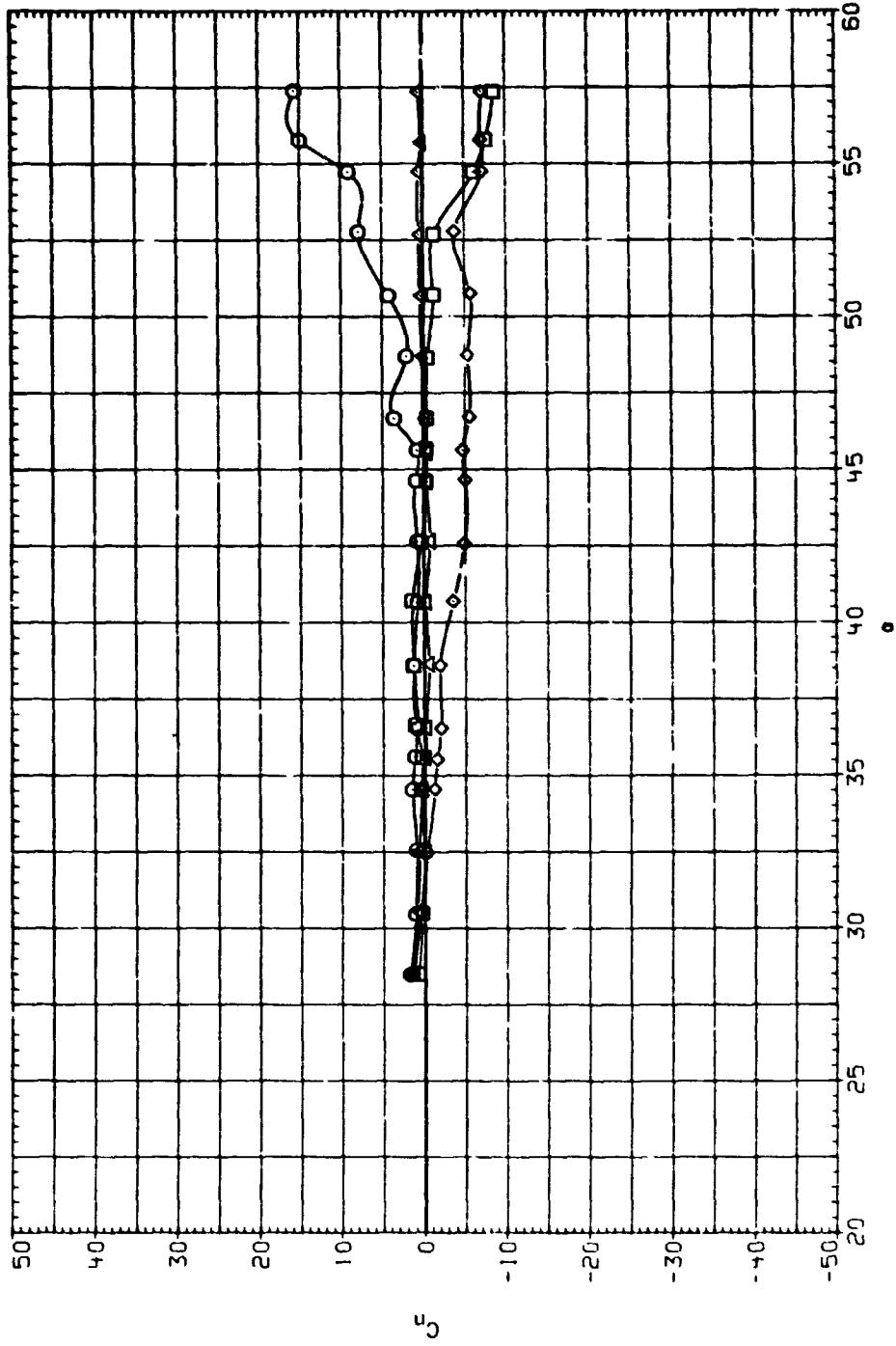
(c) C_y vs α , $180^\circ < \phi < 315^\circ$.

Figure 14. Continued.

DATA SET SYMBOL CONFIGURATION

BJ0055	○	F2.5 A7
BJ0056	□	F2.5 A7
BJ0057	◇	F2.5 A7
BJA1058	△	F2.5 A7

PHI-F	PHI-A	MACH
180.000	.000	.250
225.000	.000	.250
270.000	.000	.250
315.000	.000	.250

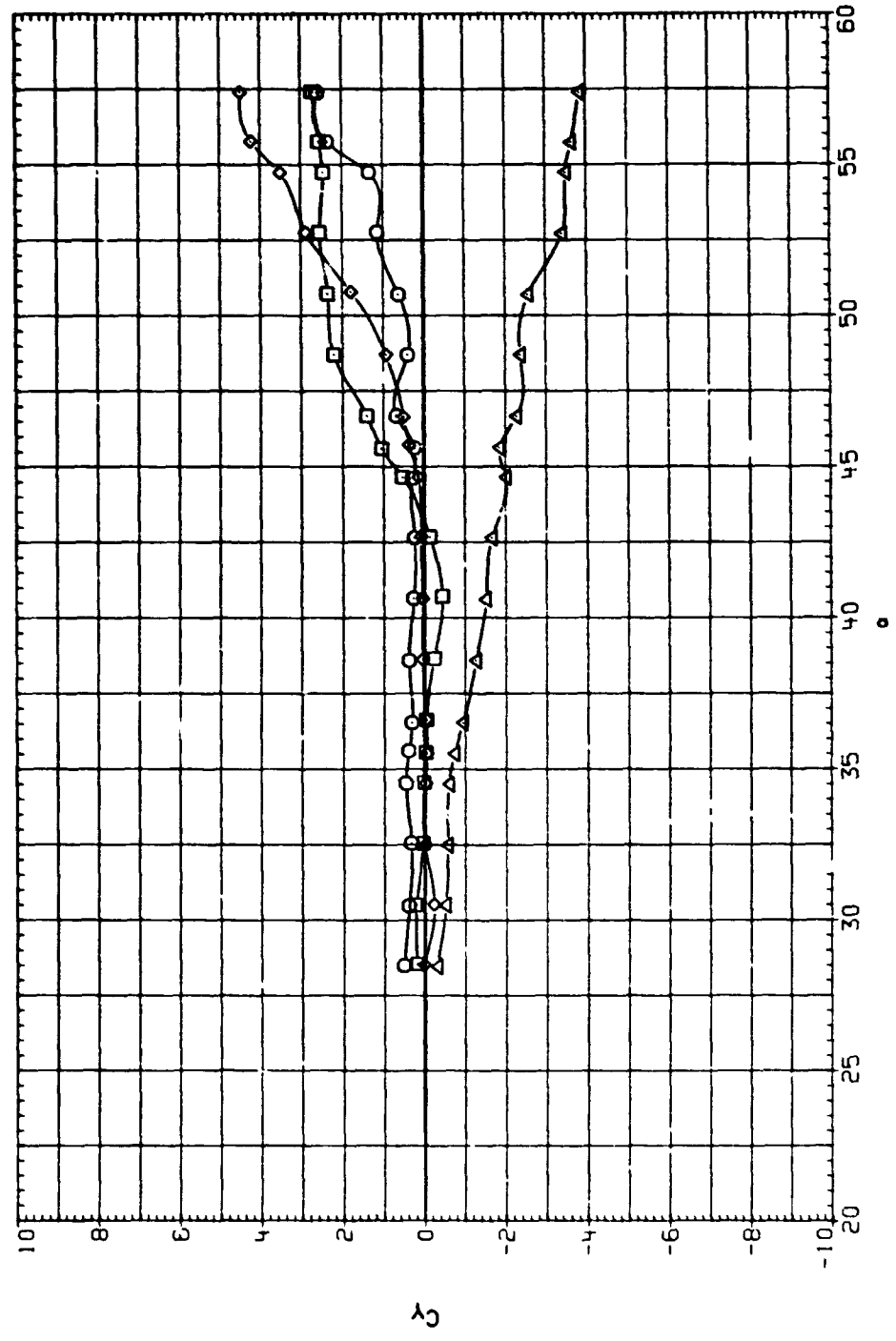


(d) $C_{l\alpha}$ vs α , $180 \leq \phi \leq 315$.

Figure 14. Concluded.

DATA SET SYMBOL CONFIGURATION
 B J0055 F2.5 A7
 F J0059 F2.5 A7
 F J0060 F2.5 A7
 F J0061 F2.5 A7

PHI-F PHI-A MACH
 180.000 .000 .250
 180.000 90.000 .250
 180.000 180.000 .250
 180.000 270.000 .250

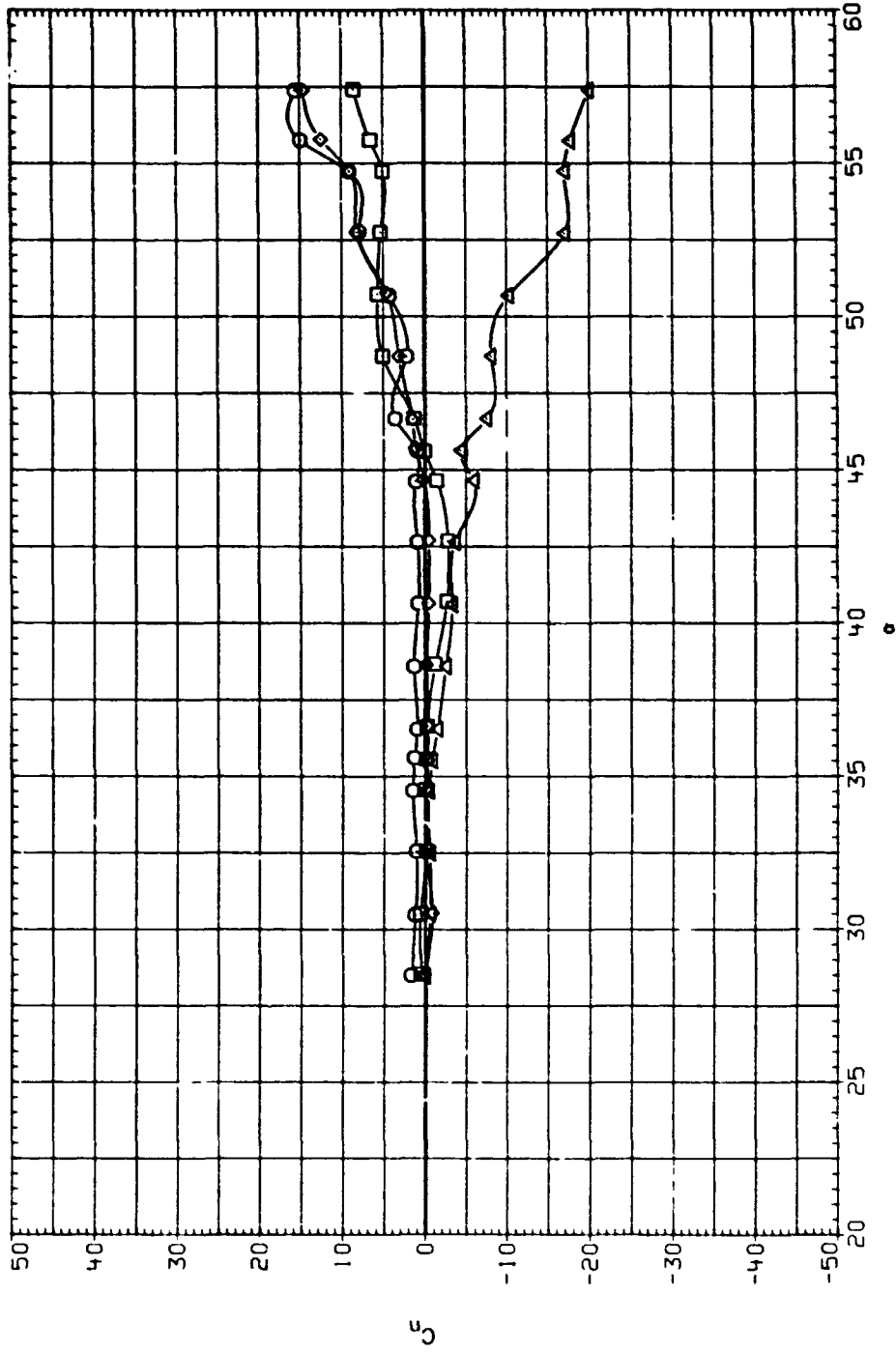


(a) C_y vs α .

Figure 15. Effect of afterbody rotation, F2.5.A7, forebody fixed, $Re = 0.32 \times 10^6$.

DATA SET SYMBOL CONFIGURATION
 B-J0055 F2.5 A7
 F-J0059 F2.5 A7
 F-J0060 F2.5 A7
 F-J0061 F2.5 A7

PHI-F PHI-A MACH
 180.000 .000 .250
 180.000 90.000 .250
 180.000 180.000 .250
 180.000 270.000 .250

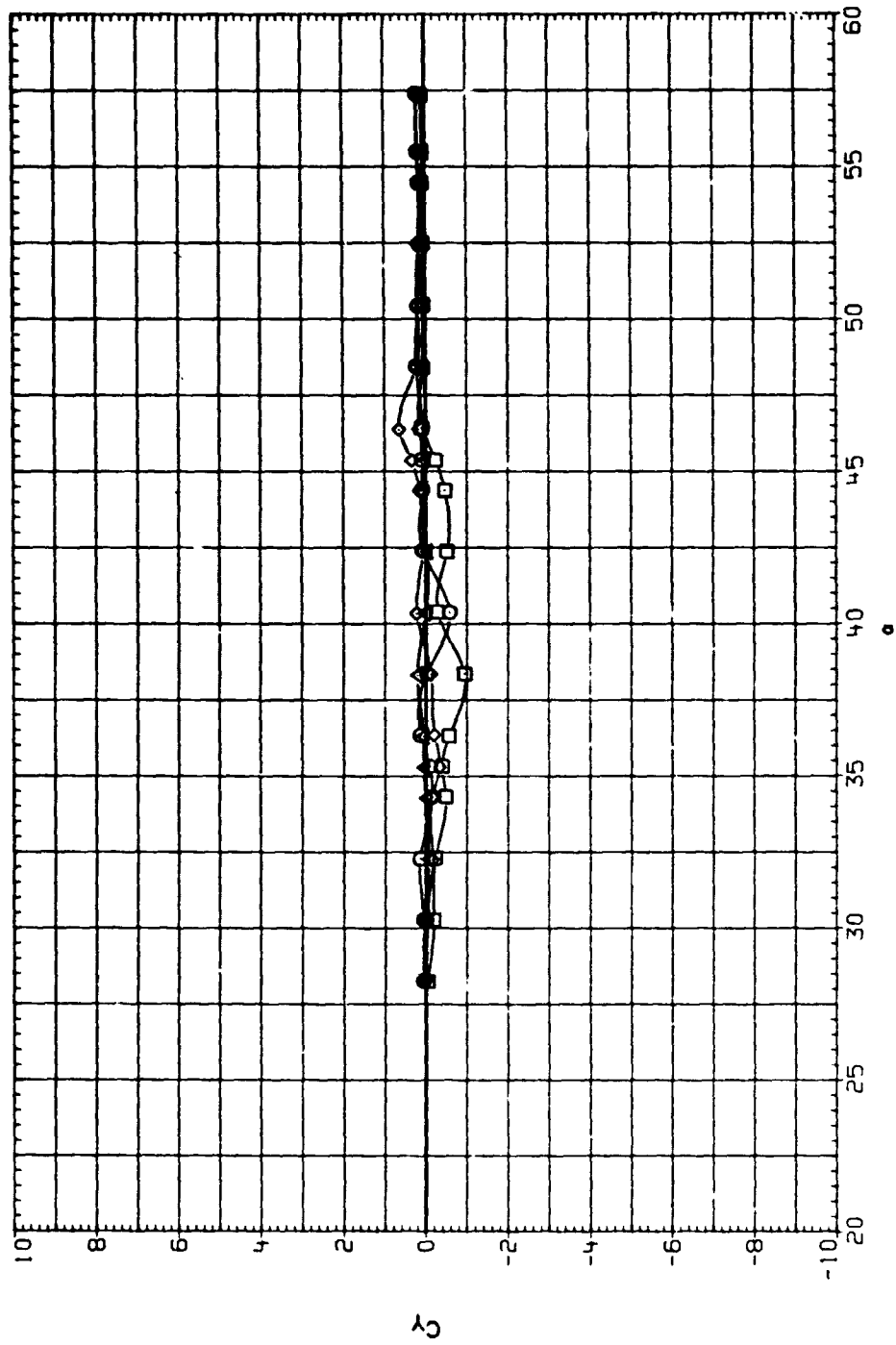


(h) C_L vs α .

Figure 15. - Concluded.

DATA SET SYMBOL CONFIGURATION
 B.J0029 F1.5 A7
 B.J0030 F1.5 A7
 B.J0031 F1.5 A7
 B.J0032 F1.5 A7

PHI-F PHI-A MACH
 .000 .000 .250
 90.000 .000 .250
 180.000 .000 .250
 270.000 .000 .250



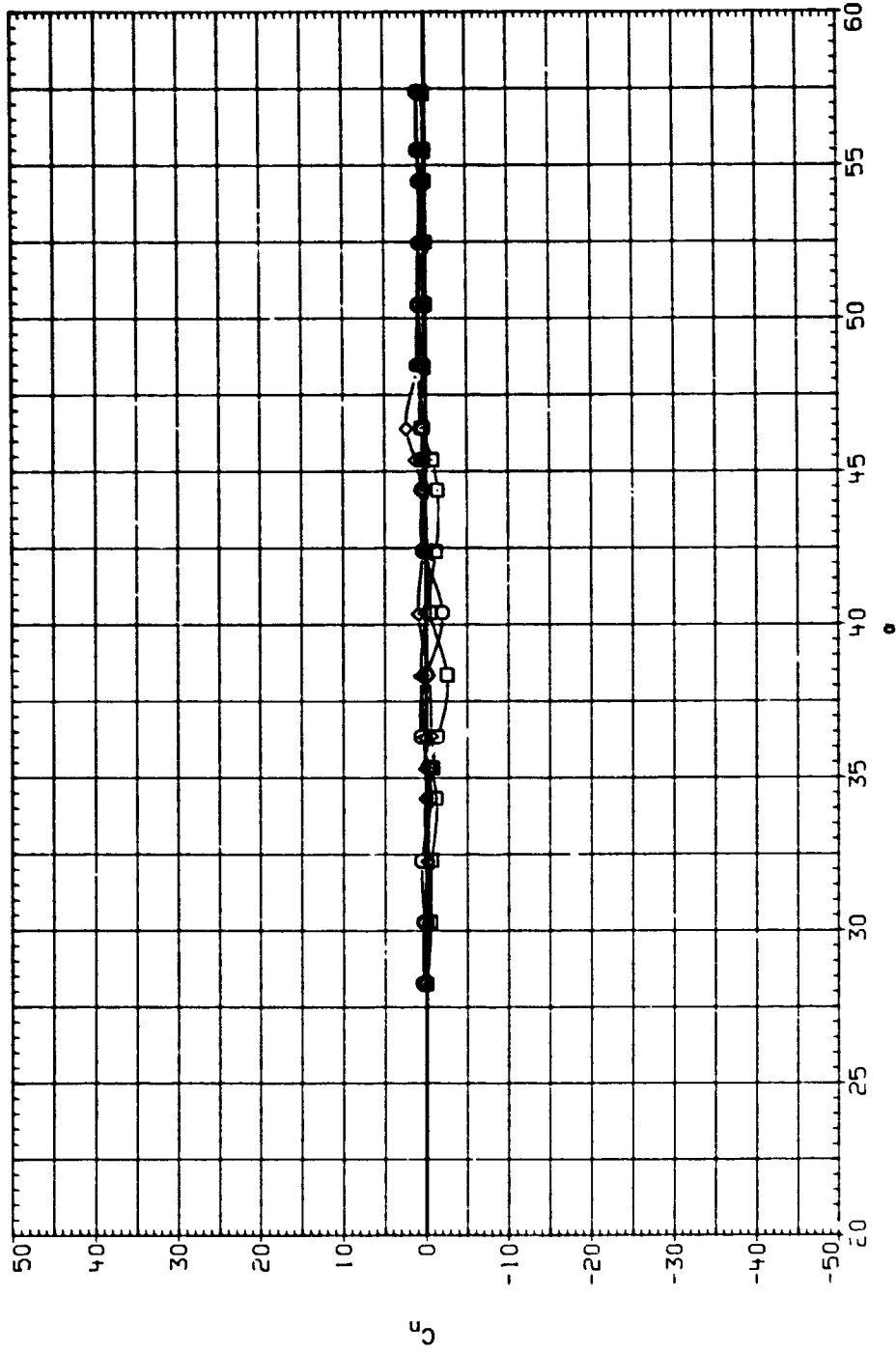
(a) C_L vs α .

Figure 16. Effect of forebody rotation, F1.5A7, afterbody fixed, $Re = 0.32 \times 10^6$.

DATA SET SYMBOL CONFIGURATION

BJ0029	□	F1.5 A7
BJ0030	◇	F1.5 A7
BJ0031	◇	F1.5 A7
BJ0032	△	F1.5 A7

PHI-F	PHI-A	MACH
.000	.000	.250
90.000	.000	.250
180.000	.000	.250
270.000	.000	.250

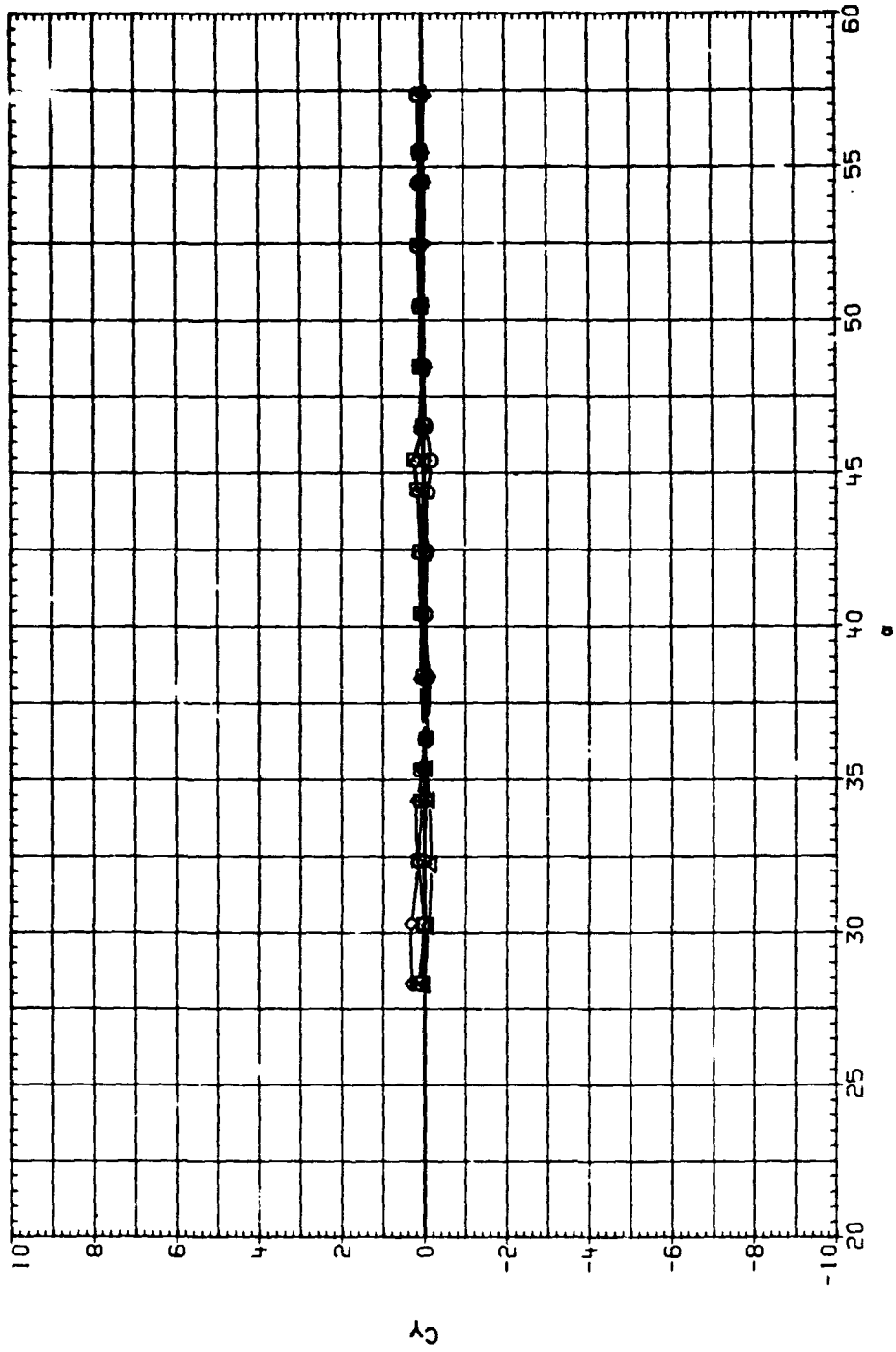


(b) C_H vs α .

Figure 16.--- Concluded.

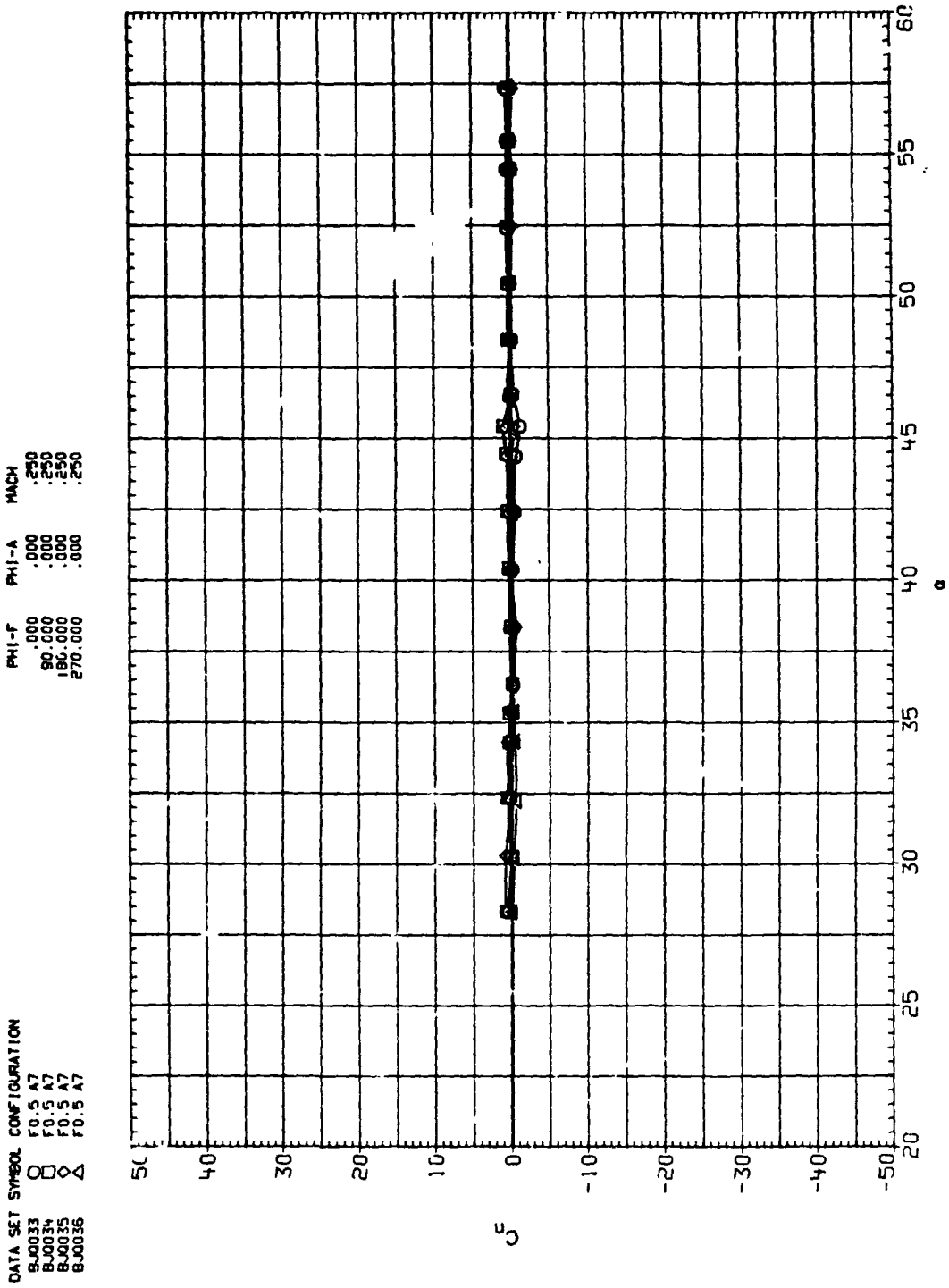
DATA SET SYMBOL CONFIGURATION
 B.0033 F0.5 A7
 B.0034 F0.5 A7
 B.0035 F0.5 A7
 B.0036 F0.5 A7

PHI-F PHI-A MACH
 .000 .000 .250
 90.000 .000 .250
 180.000 .000 .250
 270.000 .000 .250



(a) C_Y vs α .

Figure 17. Effect of forebody rotation, F0.5A7, afterbody fixed, $Re = 0.32 \times 10^6$.

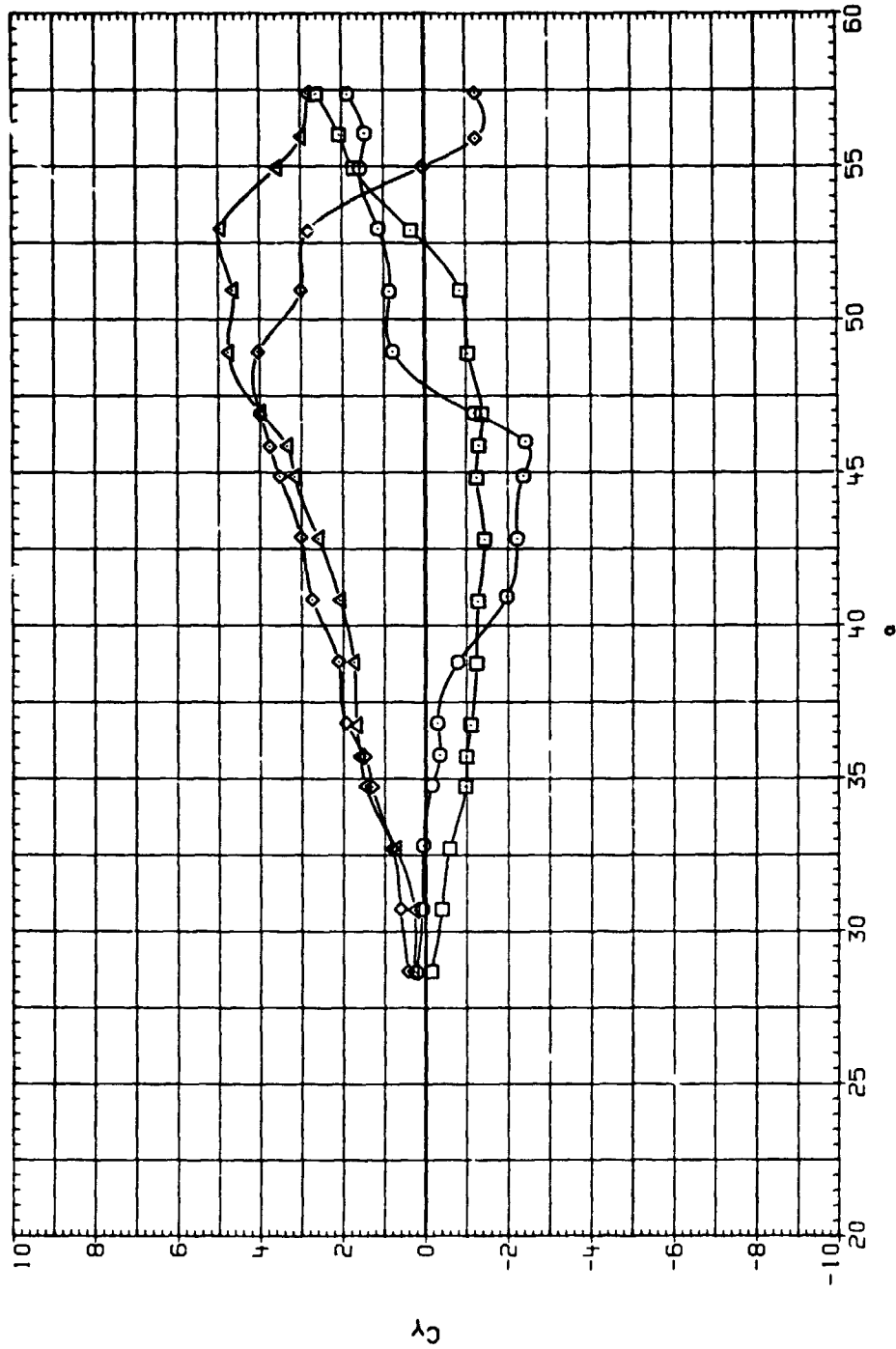


(b) C_L vs α .

Figure 17.— Concluded.

DATA SET SYMBOL CONFIGURATION
 BU0077 O F2.5 A13
 BU0078 □ F2.5 A13
 BU0079 ◇ F3.5 A13
 BU0080 △ F3.5 A13

PHI-F PHI-A MACH
 .000 .000 .250
 180.000 .000 .250
 .000 .000 .250
 180.000 .000 .250

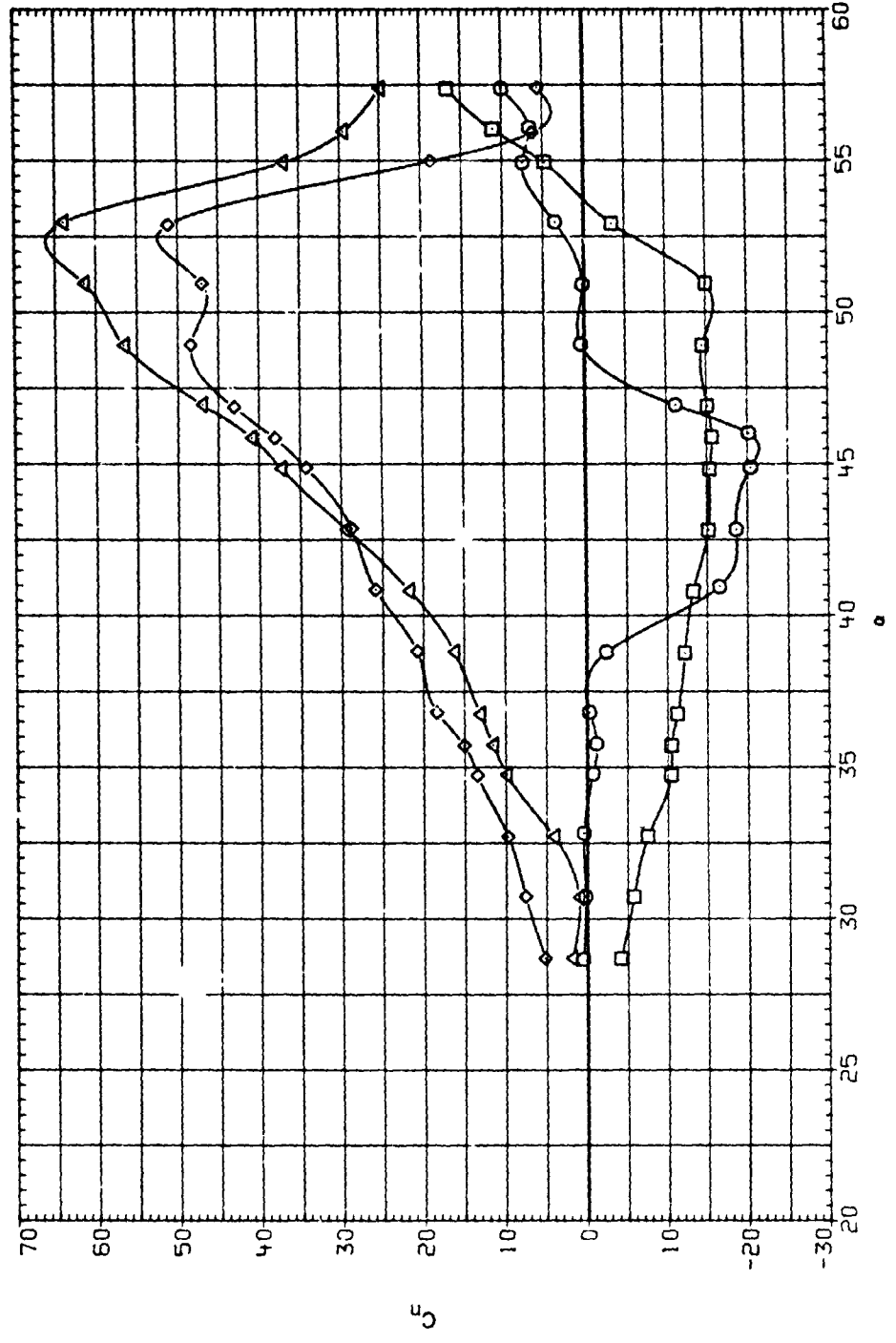


(a) C_y vs α .

Figure 18. - Effect of forebody rotation, F2.5A13 and F3.5A13, $Re = 0.32 \times 10^6$.

DATA SET SYMBOL CONFIGURATION
 B.J0077 □ F2.5 A13
 B.J0078 ○ F2.5 A13
 B.J0079 ◇ F3.5 A13
 B.J0080 △ F3.5 A13

PHI-F PHI-A MACH
 .000 .000 .250
 180.000 .000 .250
 .000 .000 .250
 180.000 .000 .250

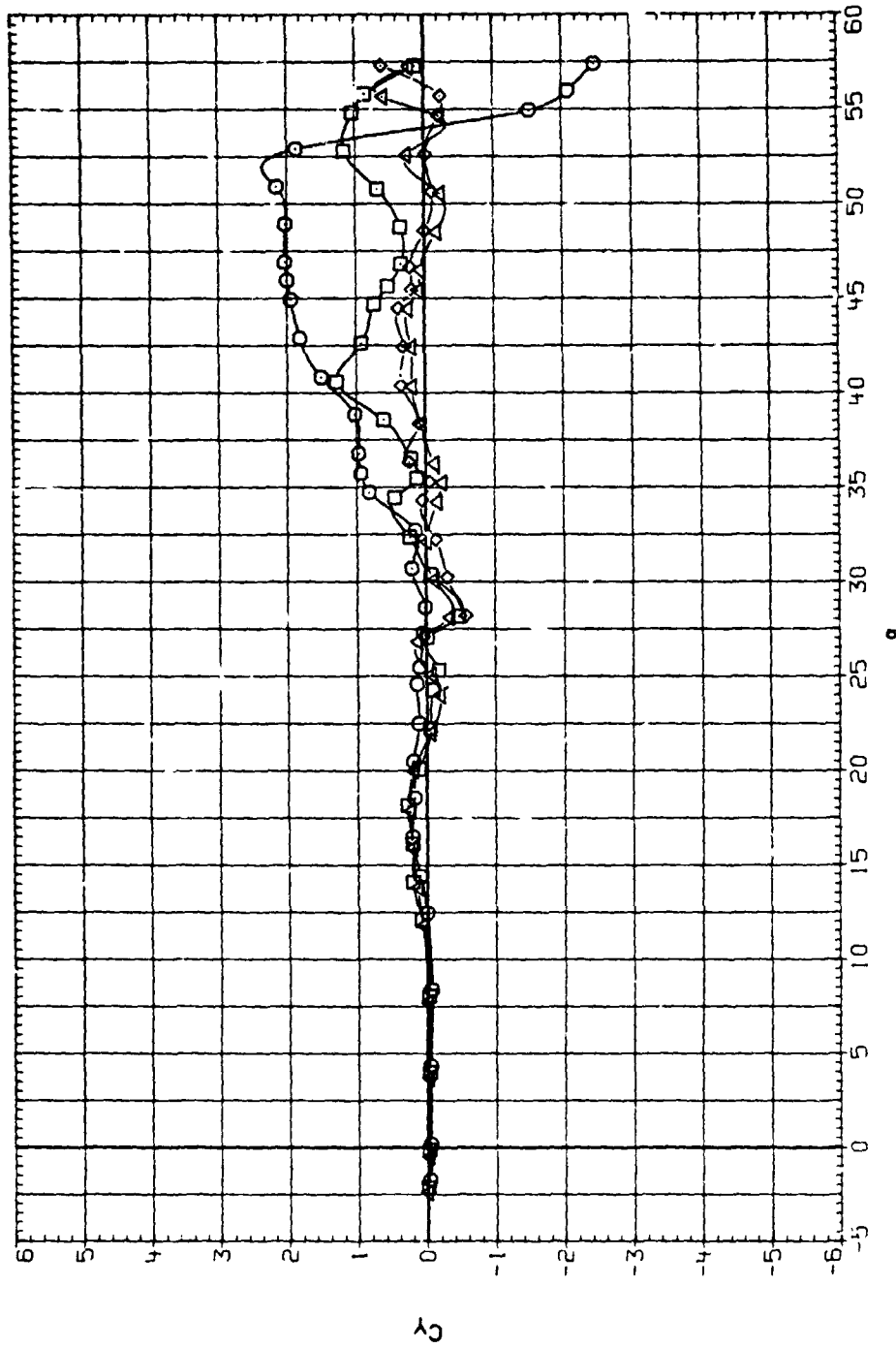


(b) C_L vs α .

Figure 18.- Concluded.

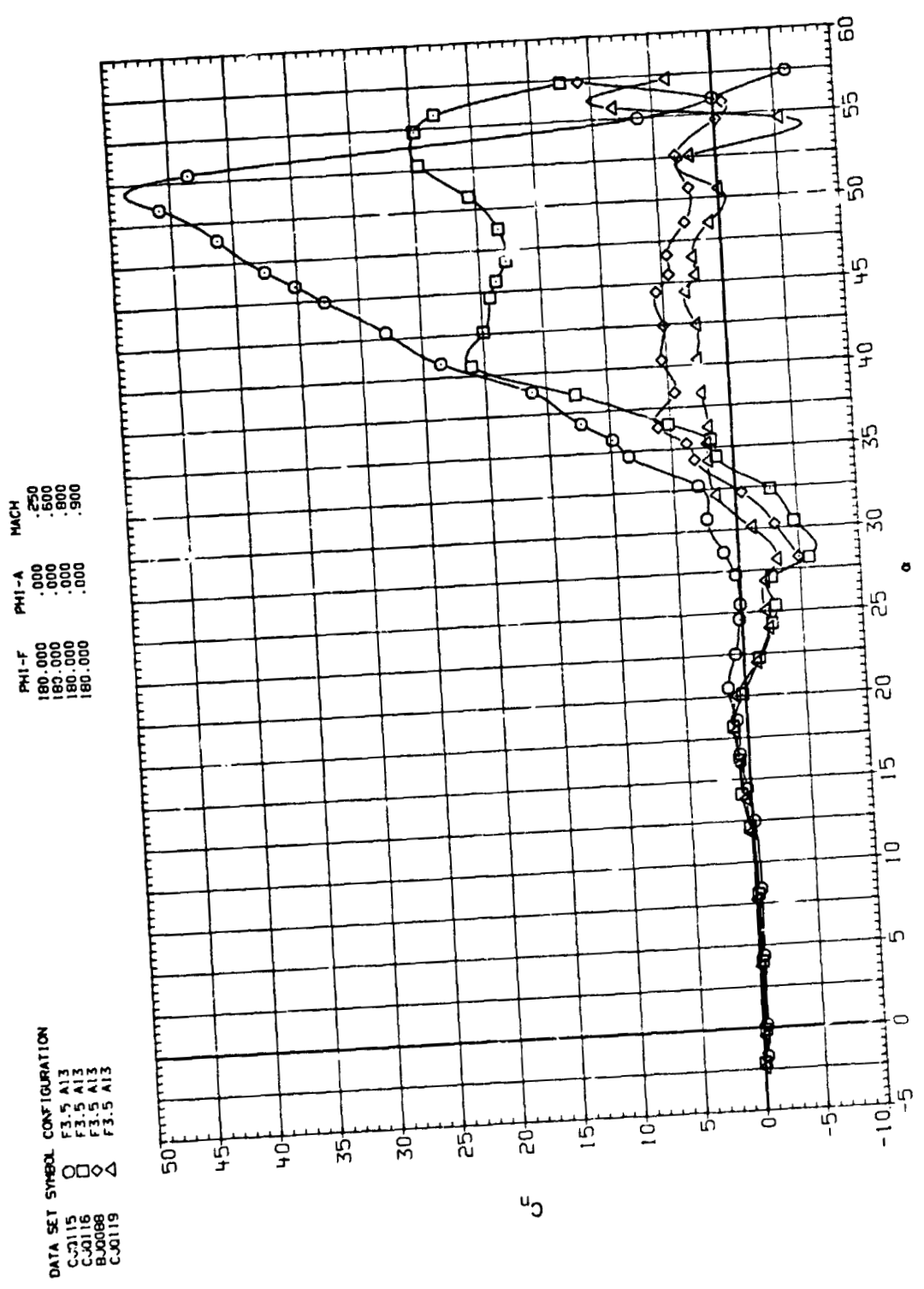
DATA SET SYMBOL CONFIGURATION
 CJO115 ○ F3.5 A13
 CJO116 □ F7.5 A13
 BJO088 ◇ F3.5 A13
 CJO119 △ F3.5 A13

PHI-F PHI-B MACH
 180.000 .000 .250
 180.000 .000 .500
 180.000 .000 .800
 180.000 .000 .900



(a) C_y vs α .

Figure 19. Effect of Mach number, F3.5A13, subsonic, $Re = 0.32 \times 10^6$.

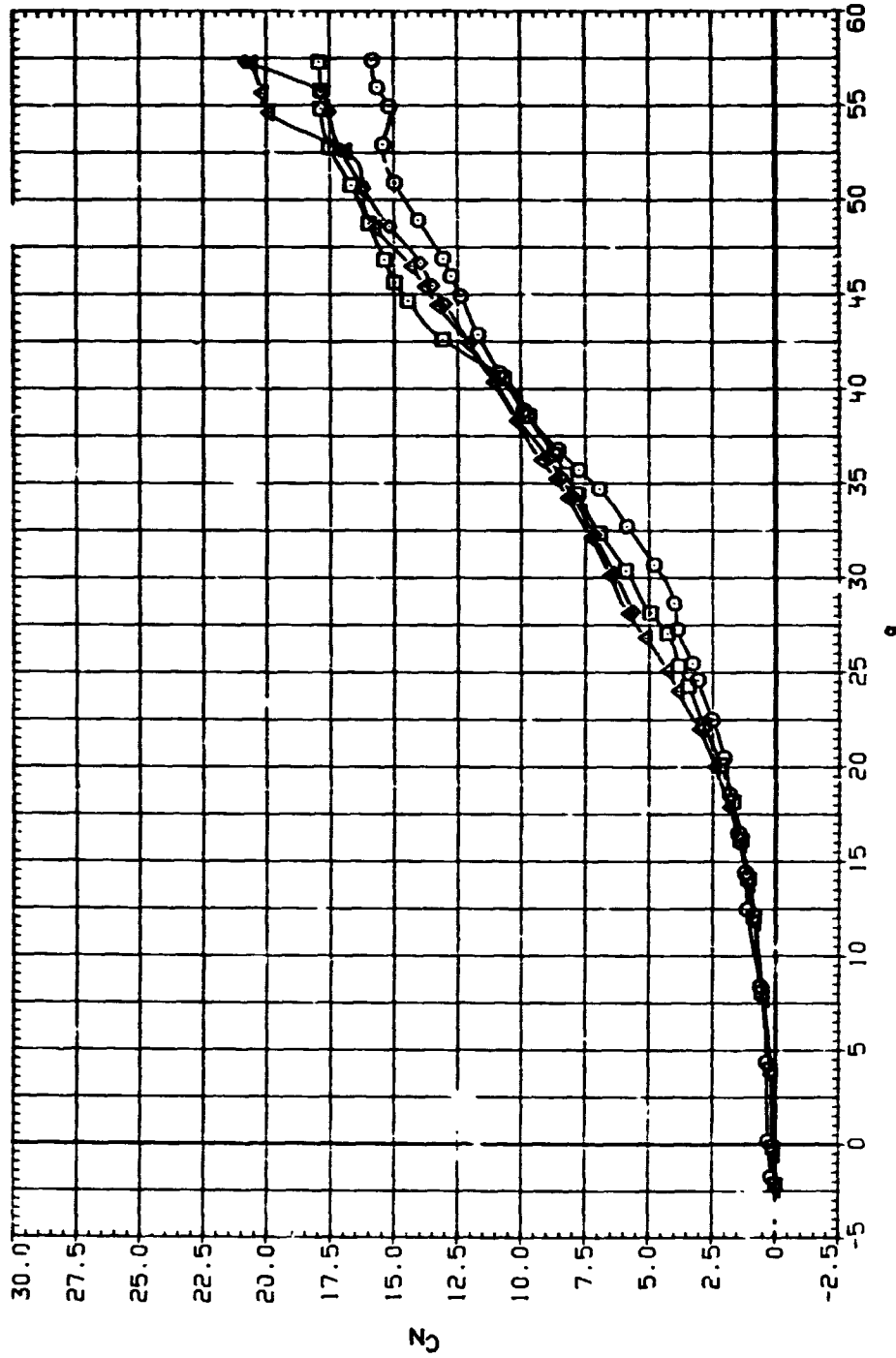


(b) C_H vs α .

Figure 19. Continued.

DATA SET SYMBOL CONFIGURATION
 C-J0115 F3.5 A13
 C-J0116 F3.5 A13
 B-J0088 F3.5 A13
 C-J0119 F3.5 A13

PHI-F PHI-A MACH
 180.000 .000 .250
 180.000 .000 .500
 180.000 .000 .800
 180.000 .000 .900

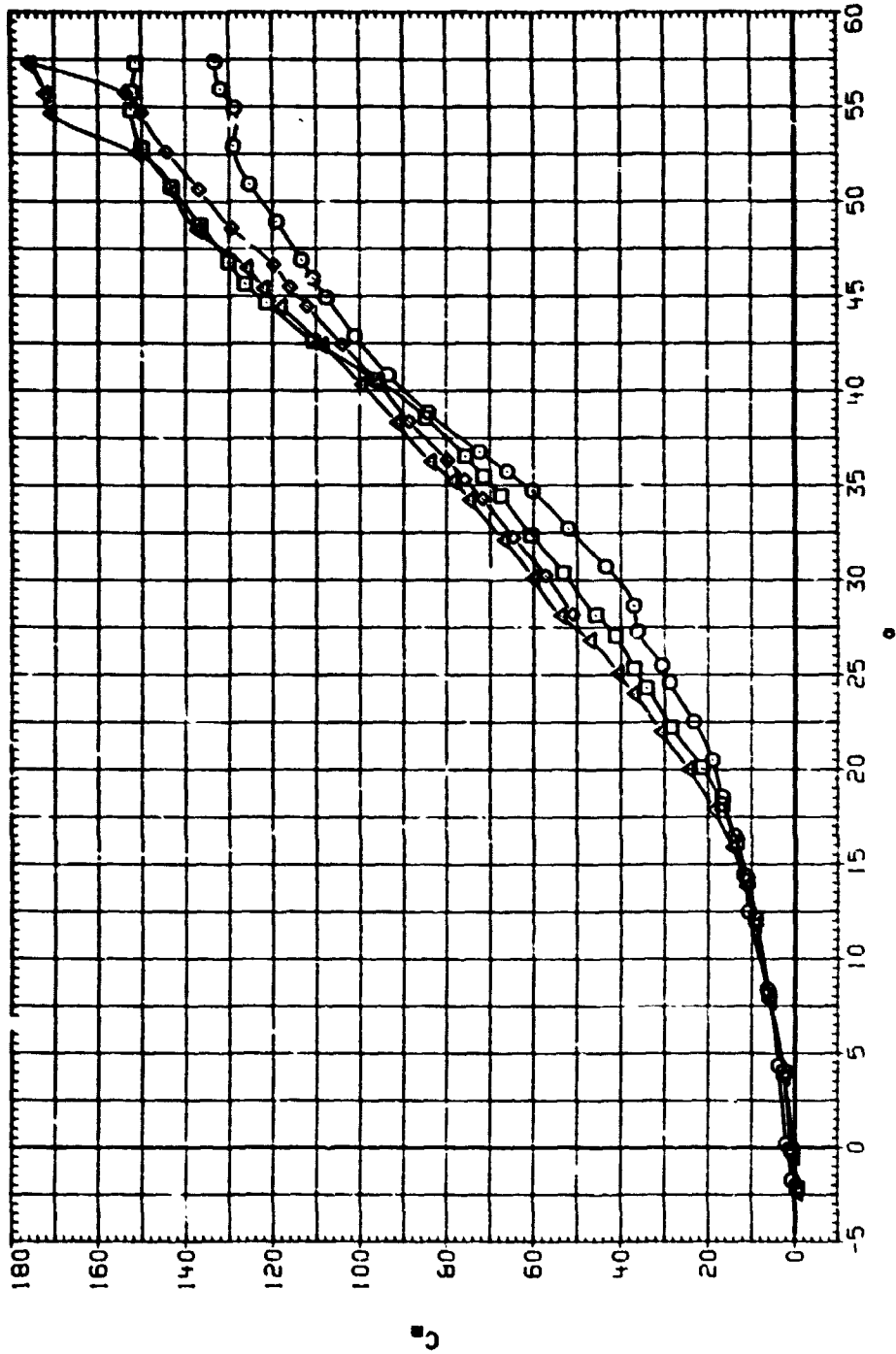


(c) C_N vs α .

Figure 19. Continued.

DATA SET SYMBOL CONFIGURATION
 C-0115 ○ F3.5 A13
 C-0116 □ F3.5 A13
 B-0008 ◇ F3.5 A13
 C-0119 △ F3.5 A13

PHI-7 PHI-A MACH
 180.000 .000 .250
 180.000 .000 .500
 180.000 .000 .800
 180.000 .000 .900

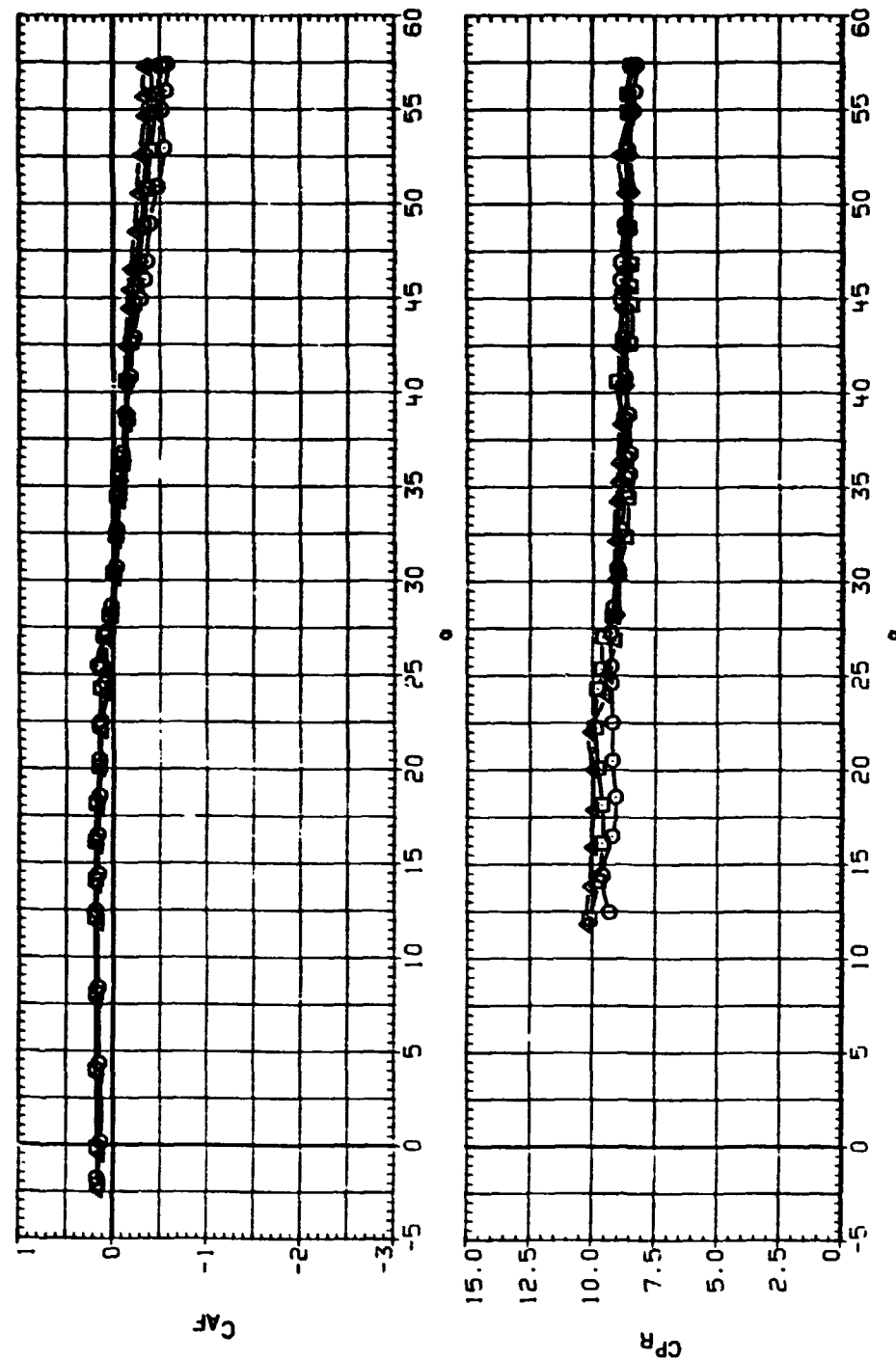


(d) C_m vs α .

Figure 19. Continued.

DATA SET SYMBOL CONFIGURATION
 C-0115 □ 3.5 A13
 C-0116 □ 3.5 A13
 B-0098 □ 3.5 A13
 C-0119 □ 3.5 A13

PHI-T PHI-A MACH
 180.000 .000 .850
 180.000 .000 .600
 180.000 .000 .800
 180.000 .000 .900

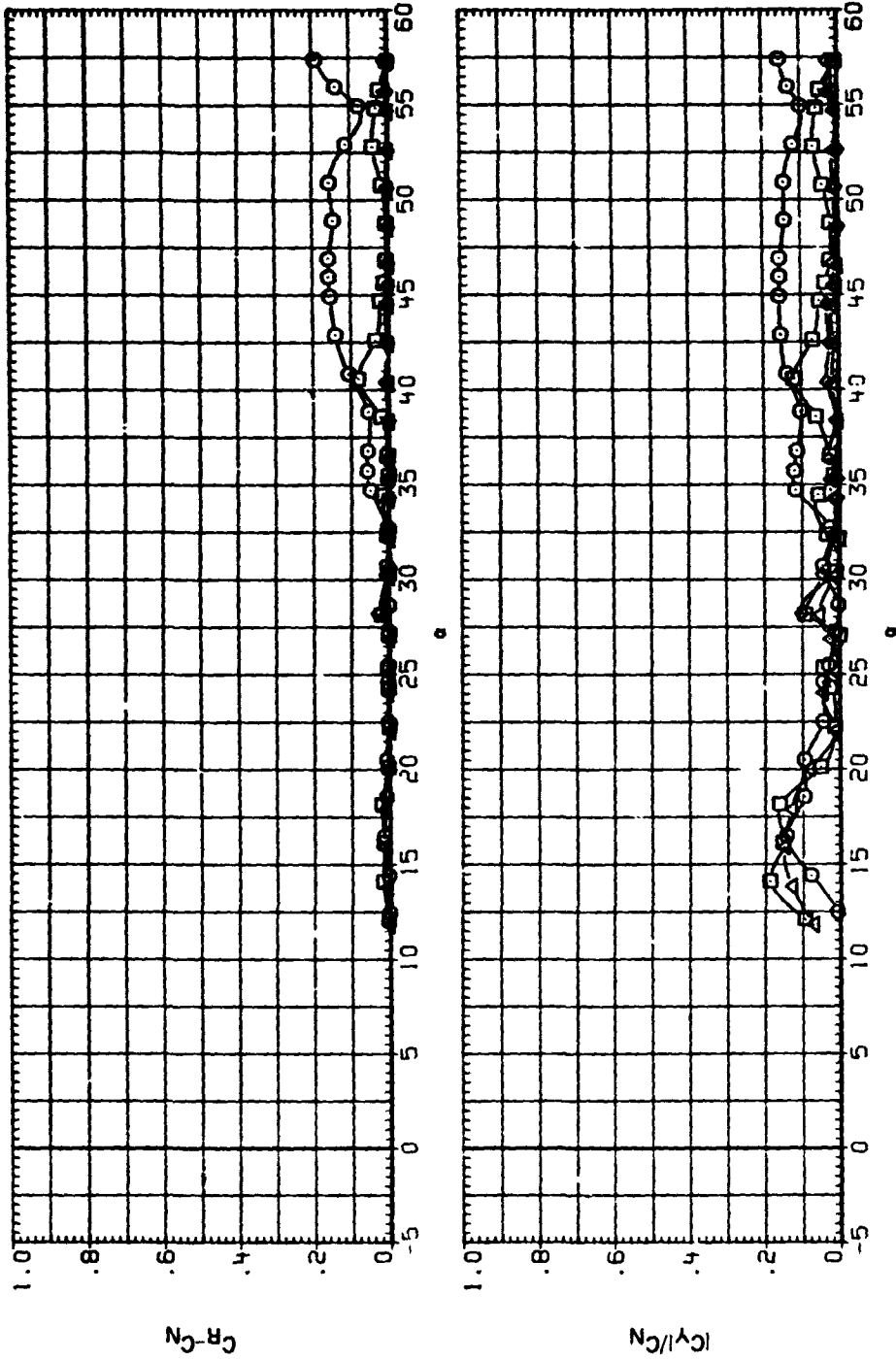


(c) C_{AF} and C_{PR} vs α .

Figure 19.- Continued.

DATA SET SYMBOL CONFIGURATION
 C.0115 ○ F4.5 A13
 C.0116 □ F3.5 A13
 S.0068 △ F3.5 A13
 C.0119 ○ F3.5 A13

PHI-F PHI-A MACH
 180.000 .000 .250
 180.000 .000 .500
 180.000 .000 .800
 180.000 .000 .900

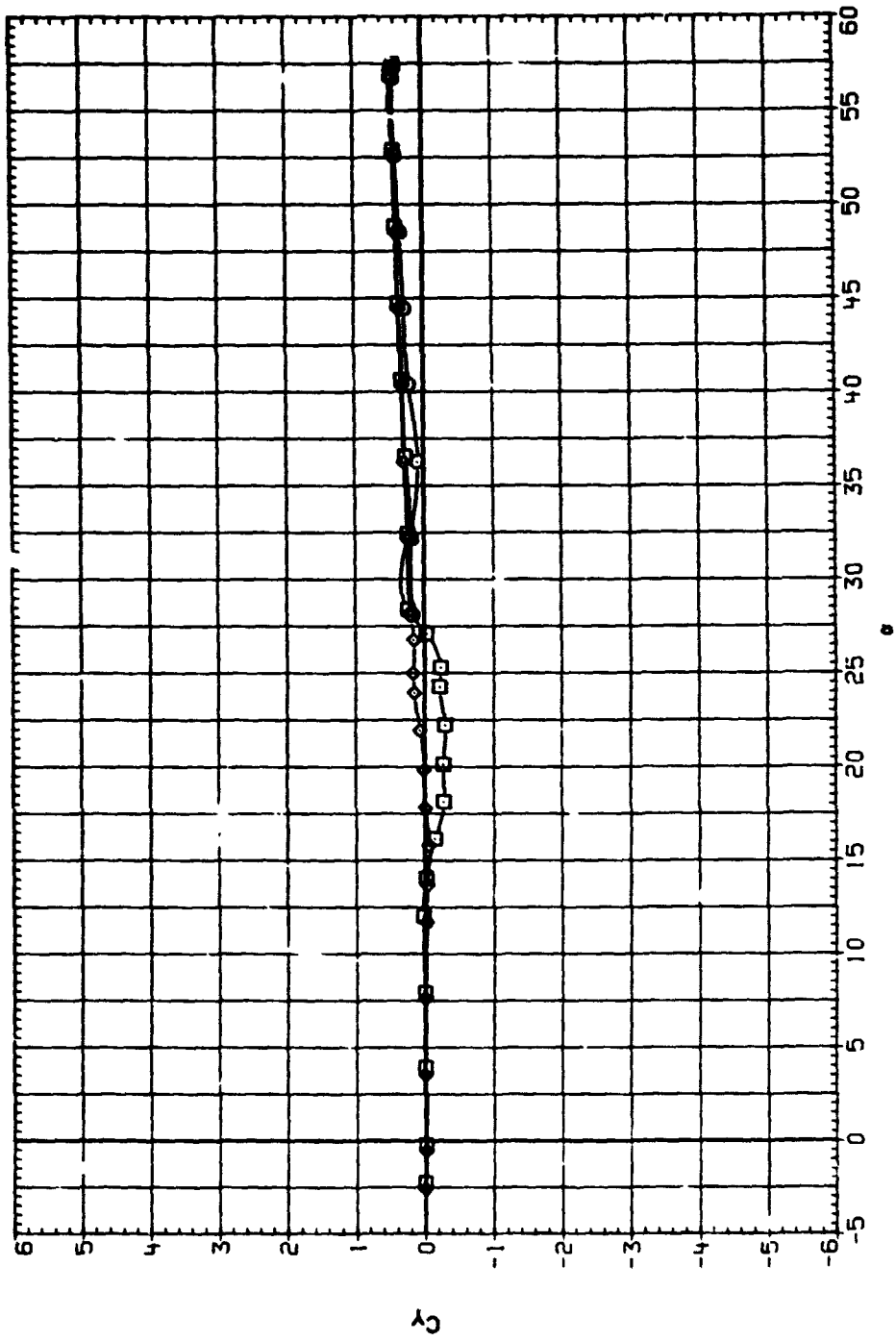


(f) $C_R - C_N$ and $|C_Y|/C_N$ vs α .

Figure 19. — Concluded.

DATA SET SYMBOL CONFIGURATION
 B-0081 F3.5 A13
 C-0120 F3.5 A13
 C-0121 F3.5 A13

PHI-F PHI-A MACH
 180.000 .000 1.200
 180.000 .000 1.500
 180.000 .000 2.000

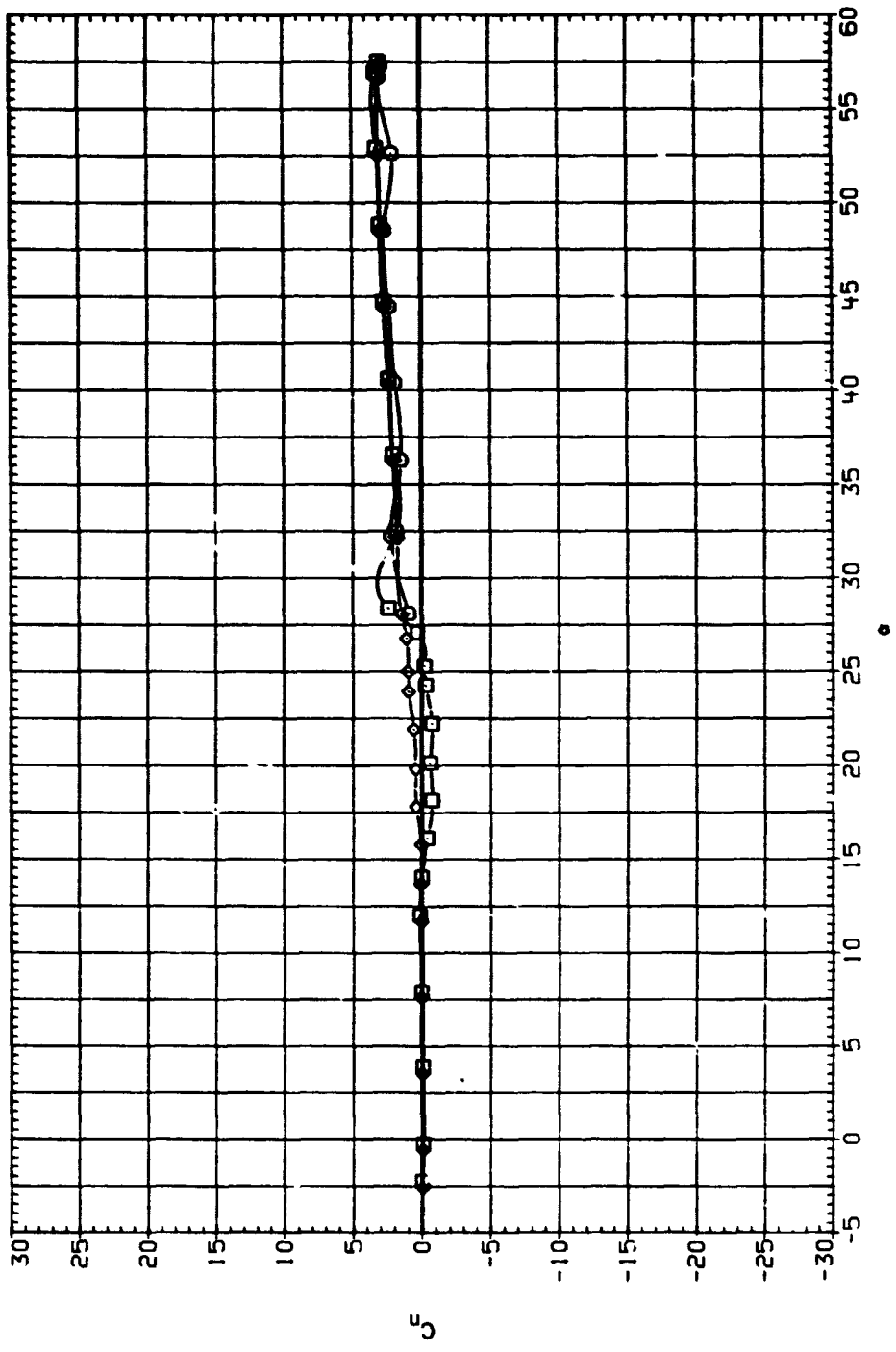


(a) C_y vs α .

Figure 20. — Effect of Mach number, F3.5A13, supersonic, $Re = 0.32 \times 10^6$.

DATA SET SYMBOL CONFIGURATION
 B-0081 F3.5 A13
 C-0120 F3.5 A13
 C-0121 F3.5 A13

PHI-F PHI-A MACH
 180.000 .000 1.200
 180.000 .000 1.500
 180.000 .000 2.000

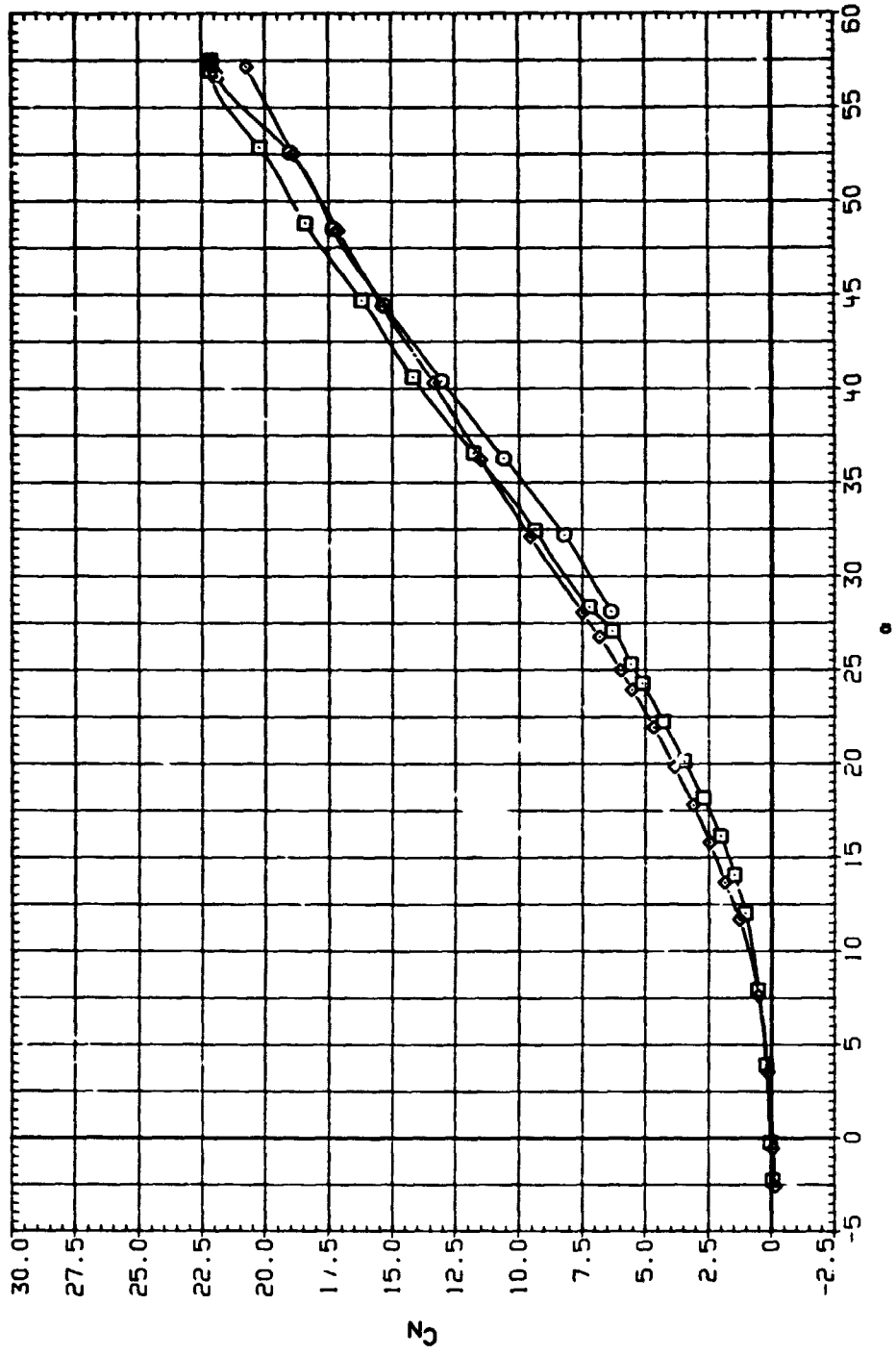


(b) C_N vs α .

Figure 20.— Continued.

DATA SET SYMBOL CONFIGURATION
 BU0081 F3.5 A13
 CU0120 F3.5 A13
 CU0121 F3.5 A13

PHI-F PHI-A MACH
 180.000 .000 1.200
 180.000 .000 1.500
 180.000 .000 2.000

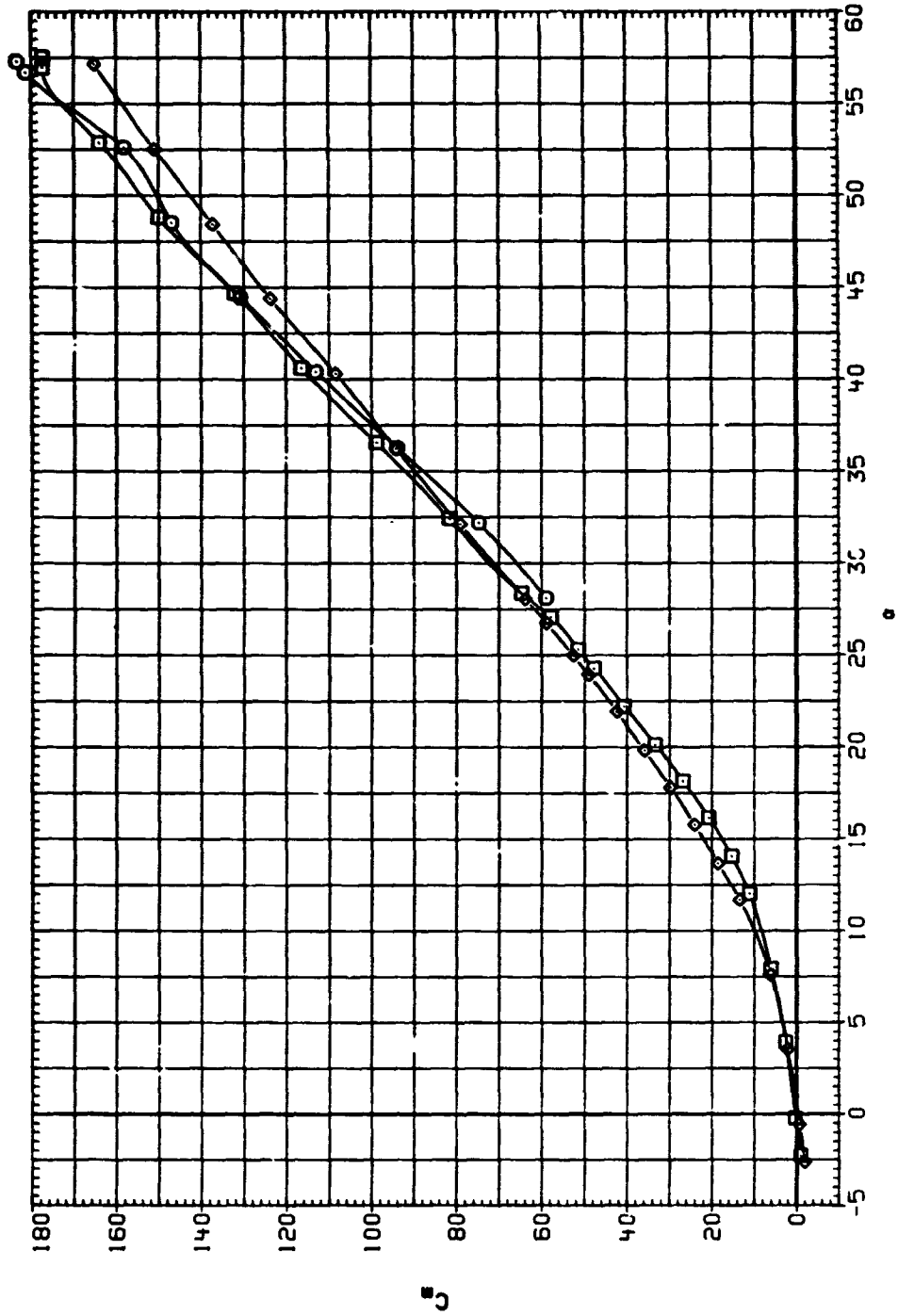


(c) C_N vs α .

Figure 20. - Continued.

DATA SET SYMBOL CONFIGURATION
 B:0081 F3.5 A13
 C:0120 □ F3.5 A13
 C:0121 ◇ F3.5 A13

PHI-F PHI-A MACH
 180.000 .000 1.200
 180.000 .000 1.500
 180.000 .000 2.000

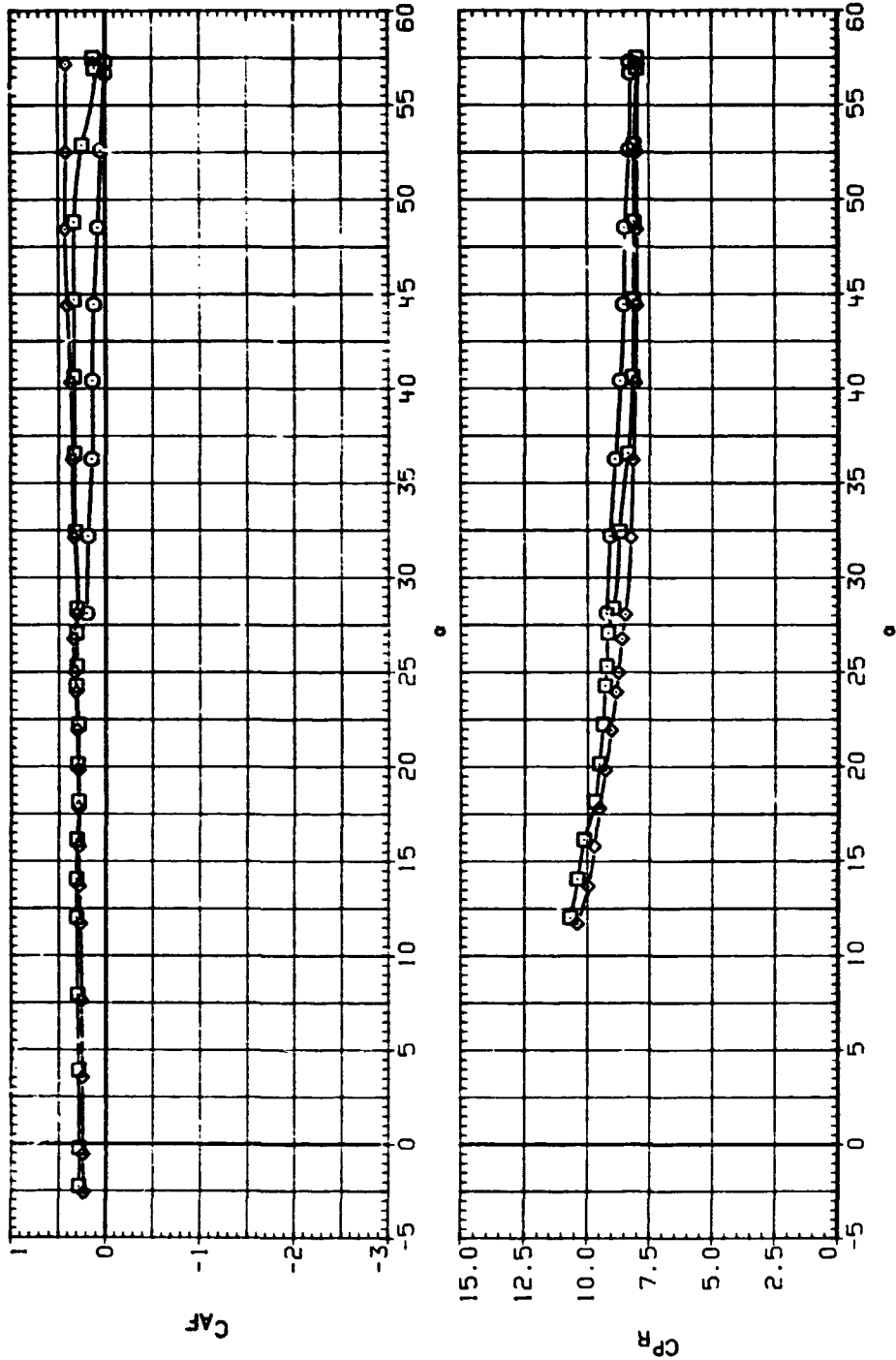


(d) C_m vs α .

Figure 20. - Continued.

DATA SET SYMBOL CONFIGURATION
 B-00081 F3.5 A13
 C-00120 F3.5 A13
 C-00121 F3.5 A13

PHI-F PHI-A MACH
 180.000 .000 1.200
 180.000 .000 1.500
 180.000 .000 2.000

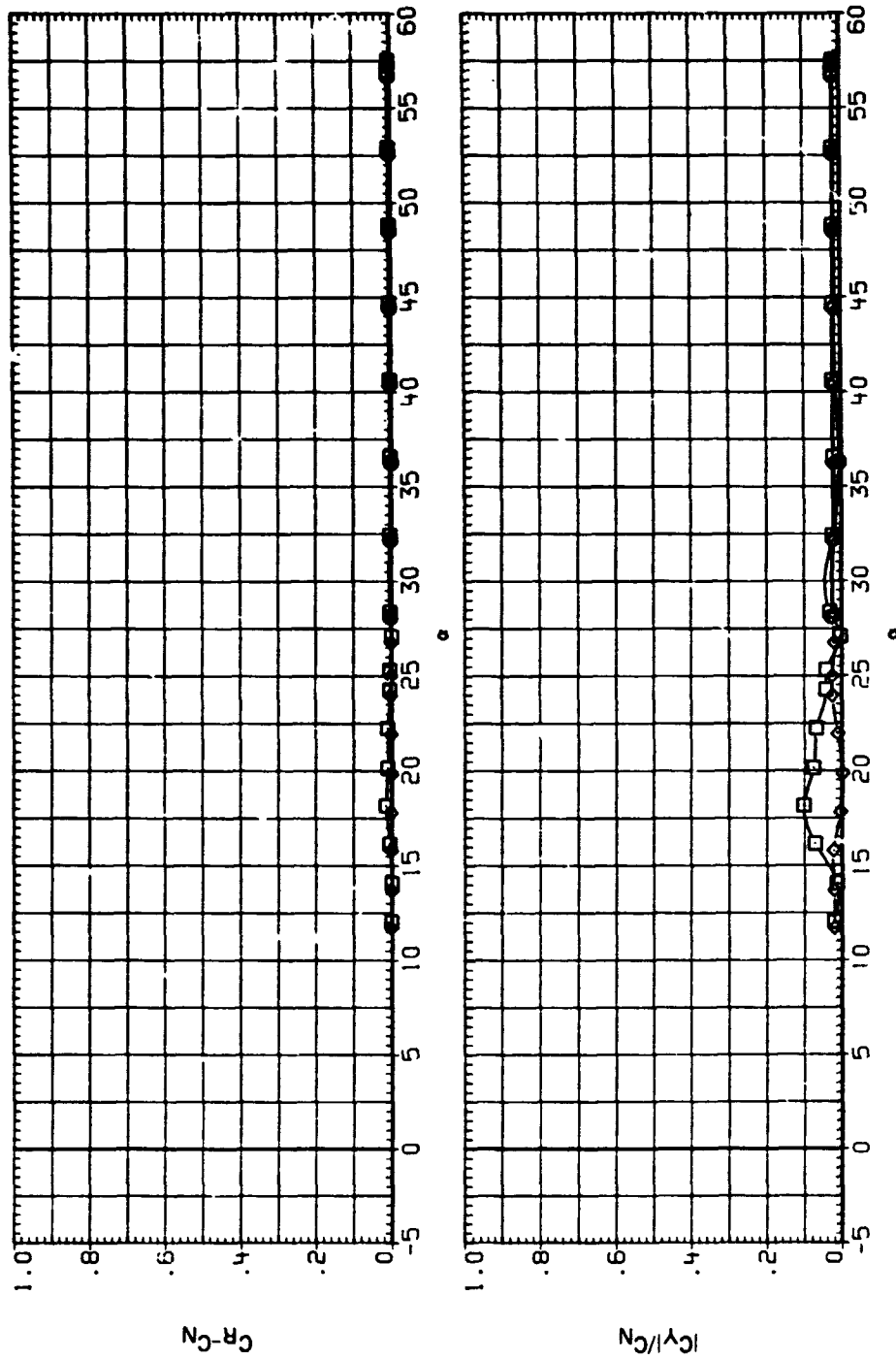


(c) C_{AF} and C_{PR} vs α .

Figure 20.-- Continued.

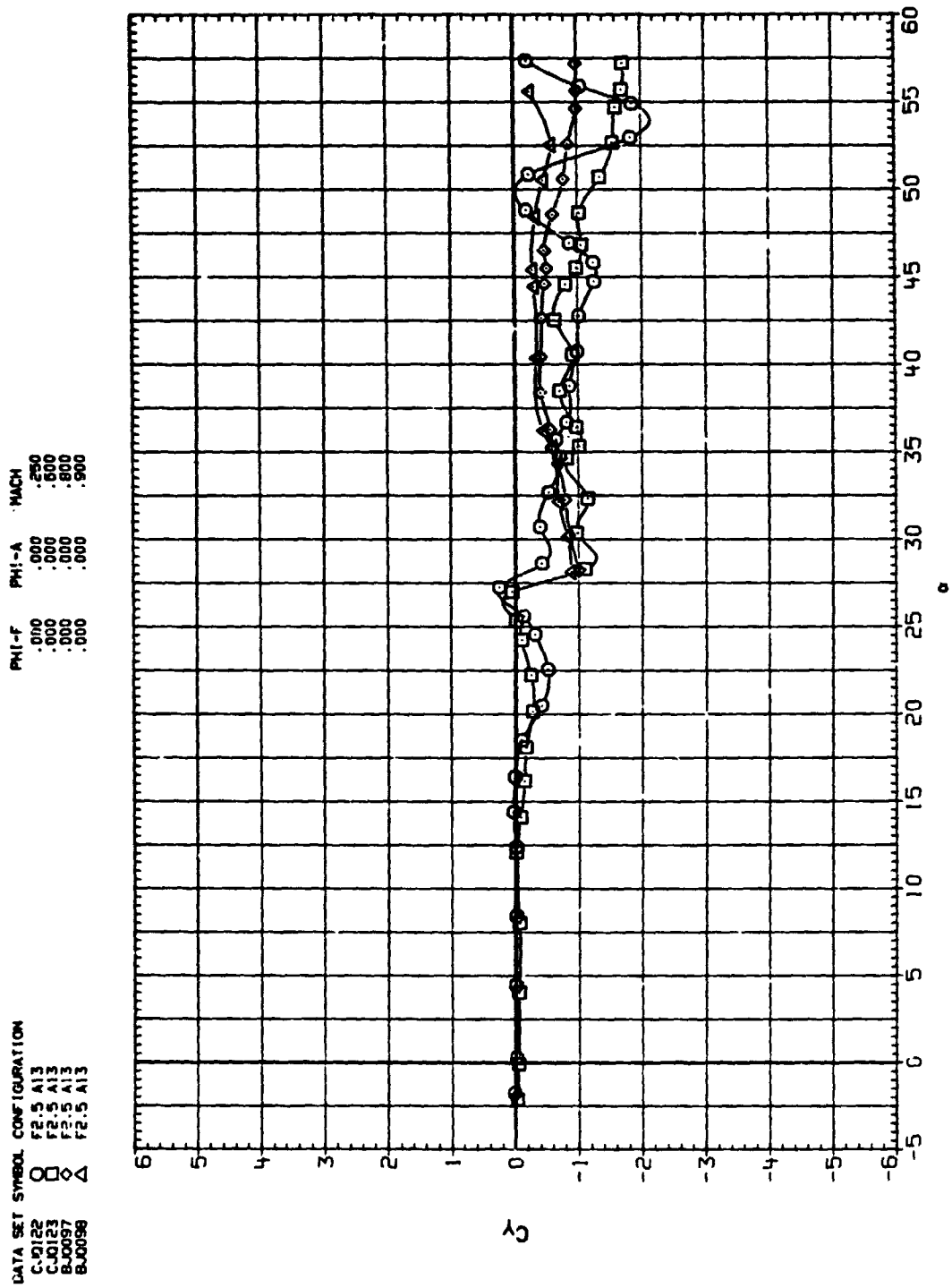
DATA SET SYMBOL CONFIGURATION
 8J0081 F3.5 A13
 C.J0120 F3.5 A13
 C.W121 F3.5 A13

PHI-F PHI-A MACH
 180.000 .000 1.200
 180.000 .000 1.500
 180.000 .000 2.000



(1) $C_R - C_N$ and $|C_Y|/C_N$ vs α .

Figure 20. - Concluded.

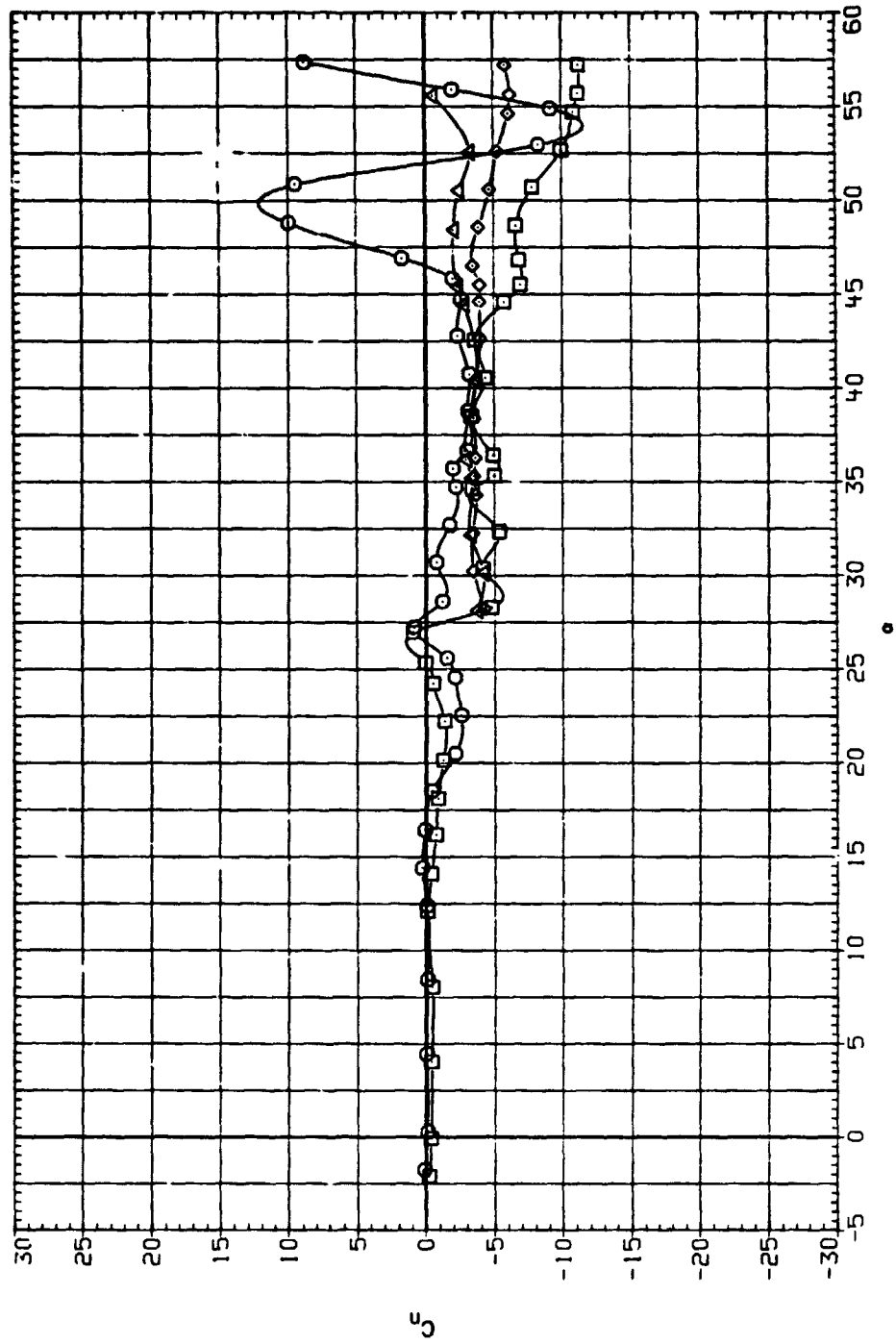


(a) C_y vs α .

Figure 21.— Effect of Mach number, F2.5A13, subsonic, $Re = 0.32 \times 10^6$.

DATA SET SYMBOL CONFIGURATION
 C-J0122 ○ F2.5 A13
 C-J0123 □ F2.5 A13
 B-J0097 ◇ F2.5 A13
 B-J0098 △ F2.5 A13

PHI-F PHI-A MACH
 .000 .000 .250
 .000 .000 .600
 .000 .000 .800
 .000 .000 .900

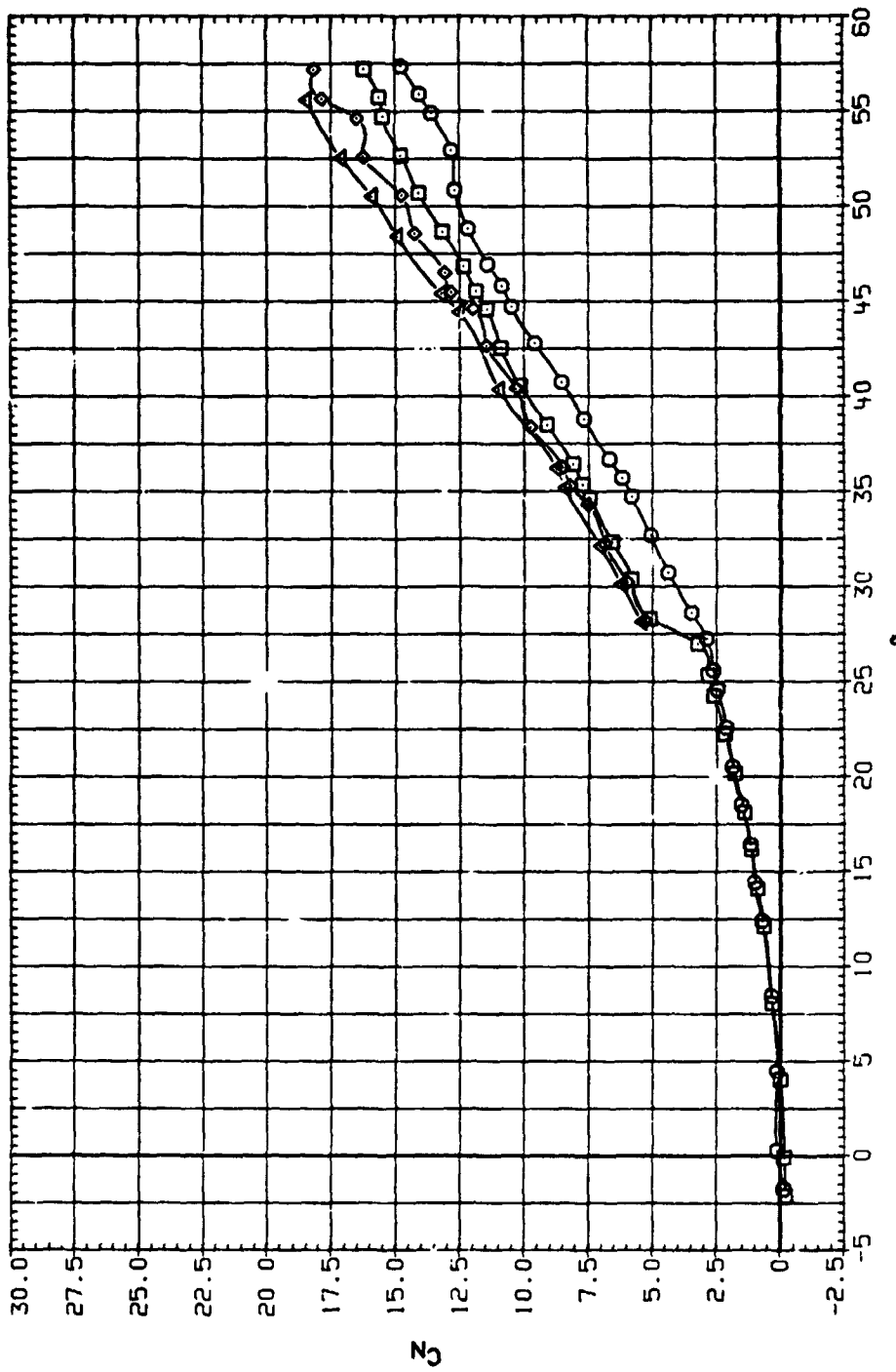


(b) C_n vs α .

Figure 21. — Continued.

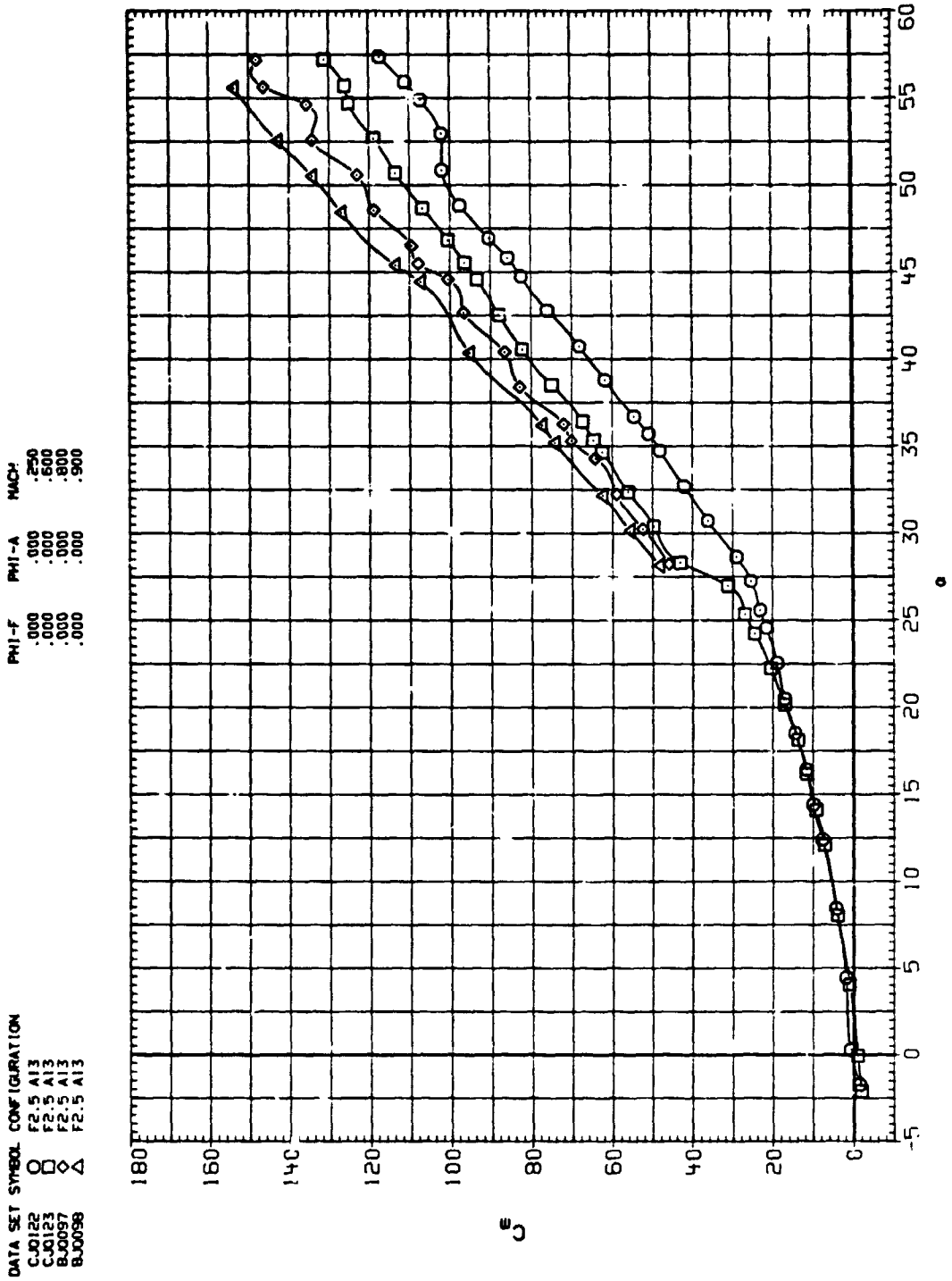
DATA SET SYMBOL CONFIGURATION
 C.00122 O F2.5 A13
 C.00123 O F2.5 A13
 B.00057 O F2.5 A13
 B.00098 O F2.5 A13

PHI-F PHI-A MACH
 .000 .000 .250
 .000 .000 .571
 .000 .000 .800
 .000 .000 .900



C_N vs α .

Figure 21.-- Continued.

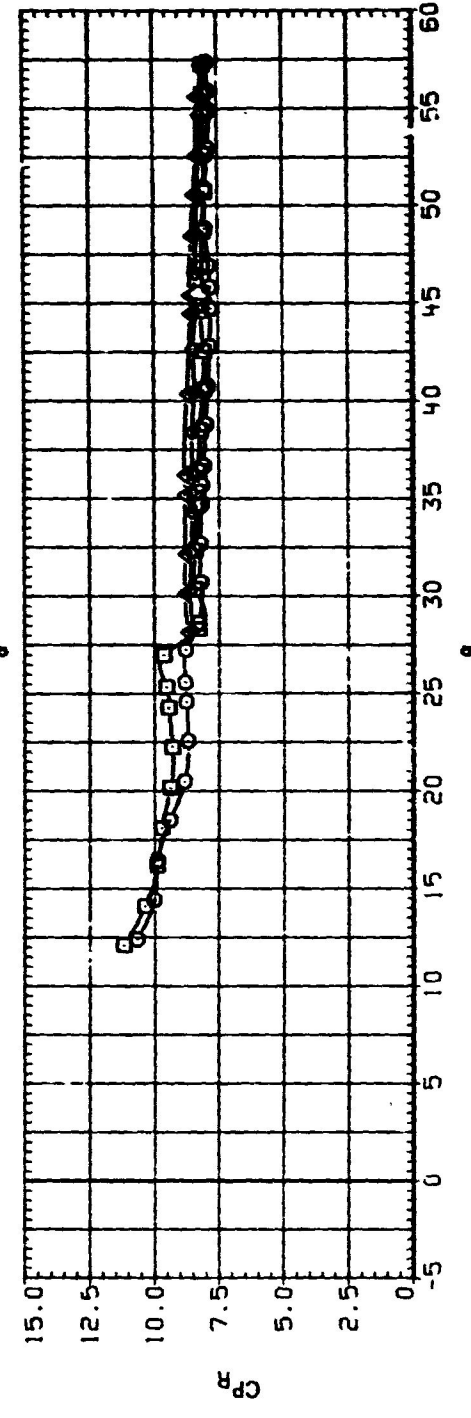
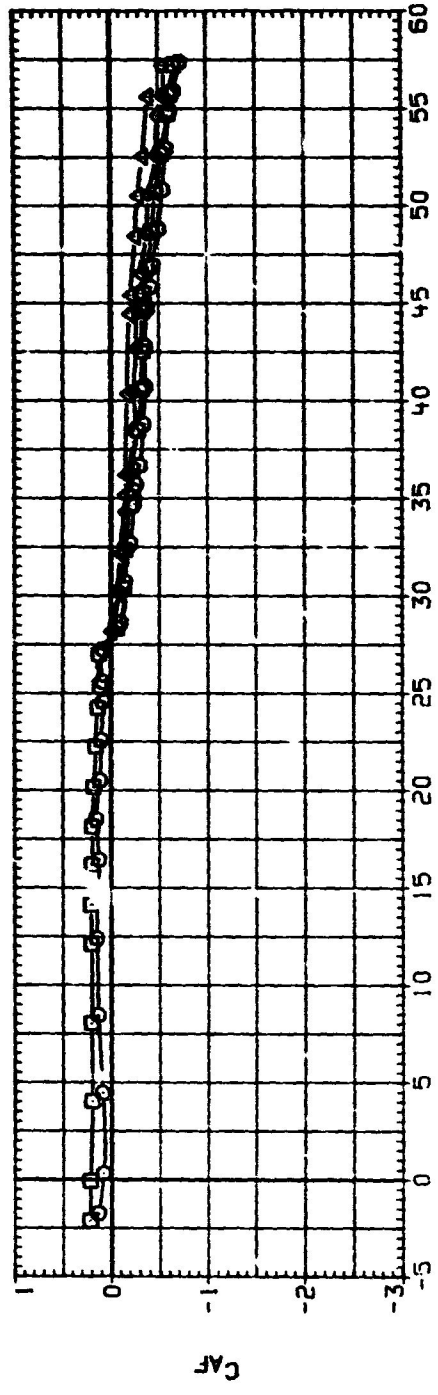


(d) C_m vs α .

Figure 21.-- Continued.

DATA SET SYMBOL CONFIGURATION
 C-0122 ○
 C-0123 □
 B-0053 △
 B-0057 ○
 B-0058 △

PHI-F PHI-A KACH
 .000 .000 .000
 .000 .000 .000
 .000 .000 .000
 .000 .000 .000

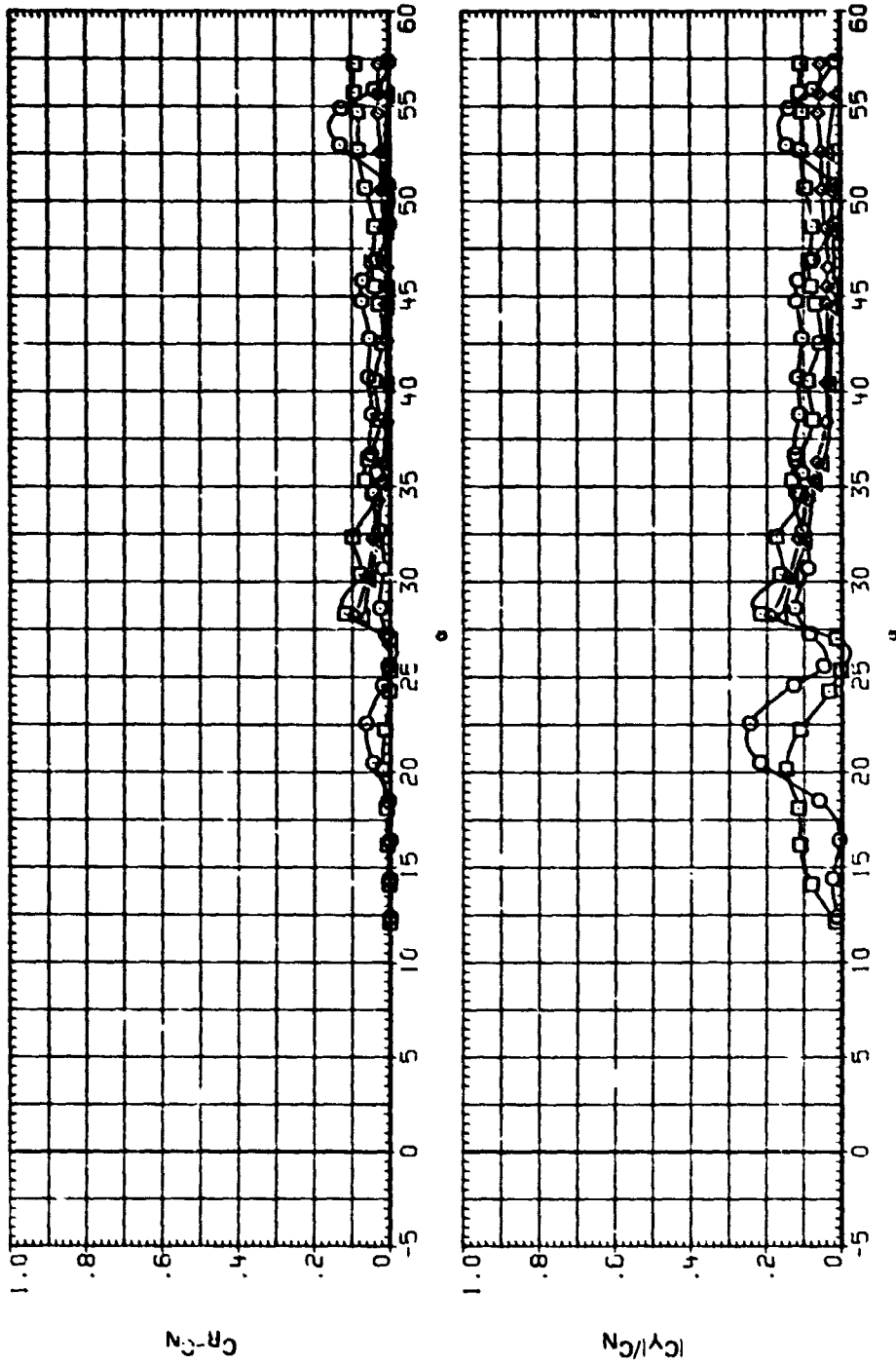


(c) C_{AF} and C_{PR} vs α .

Figure 21.- Continued.

DATA SET SYMBOL CONFIGURATION
 CJO122 F2.5 A13
 CJO123 F2.5 A13
 BJ0097 F2.5 A13
 BJ0098 F2.5 A13

PHI-F PHI-A MACH
 .000 .000 .750
 .000 .000 .800
 .000 .000 .850
 .000 .000 .900

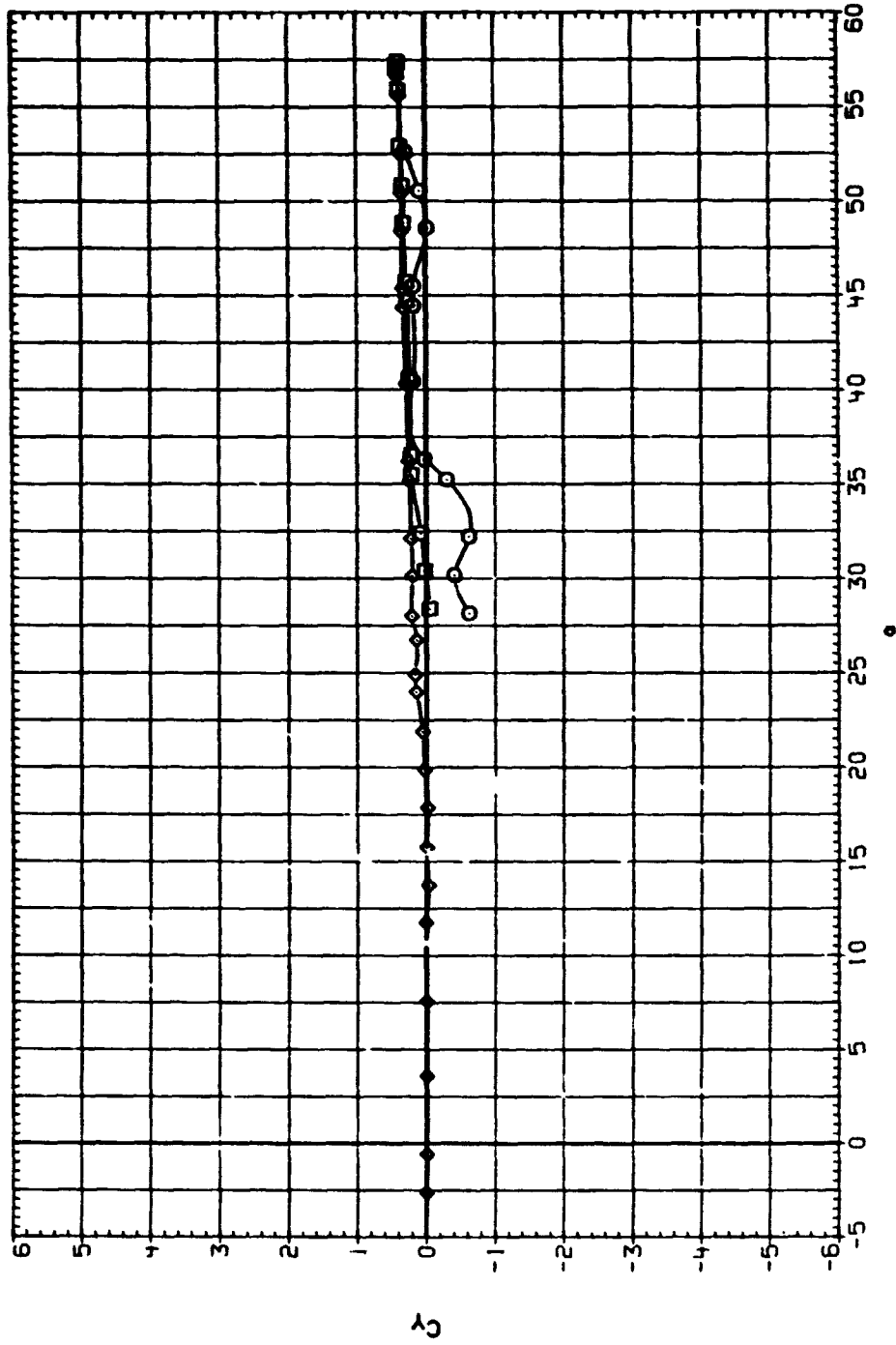


(f) $C_R - C_N$ and $|C_Y|/C_N$ vs α .

Figure 21. - Concluded.

DATA SET SYMBOL CONFIGURATION
 B.0090 F2.5 A13
 B.0091 F2.5 A13
 C.0126 F2.5 A13

PHI-F PHI-A MACH
 .000 .000 1.200
 .000 .000 1.500
 .000 .000 2.000

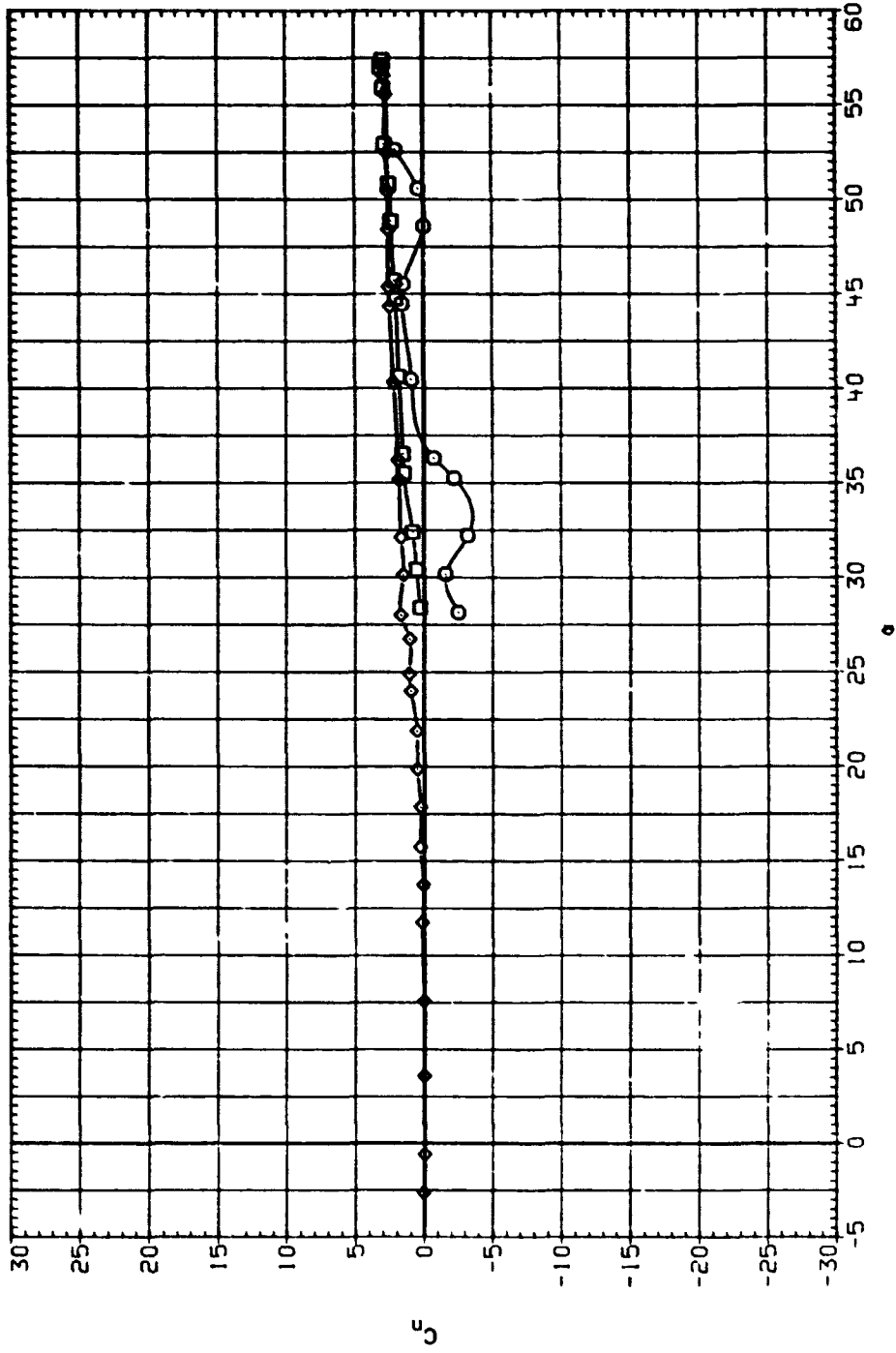


(a) C_L vs α .

Figure 22. - Effect of Mach number, F2.5A13, supersonic, $K_c = 0.32 \times 10^6$.

DATA SET SYMBOL CONFIGURATION
 B-0090 F2.5 A13
 B-0091 F2.5 A13
 C-0026 F2.5 A13

PHI-F PHI-A MACH
 .000 .000 1.200
 .000 .000 1.500
 .000 .000 2.000

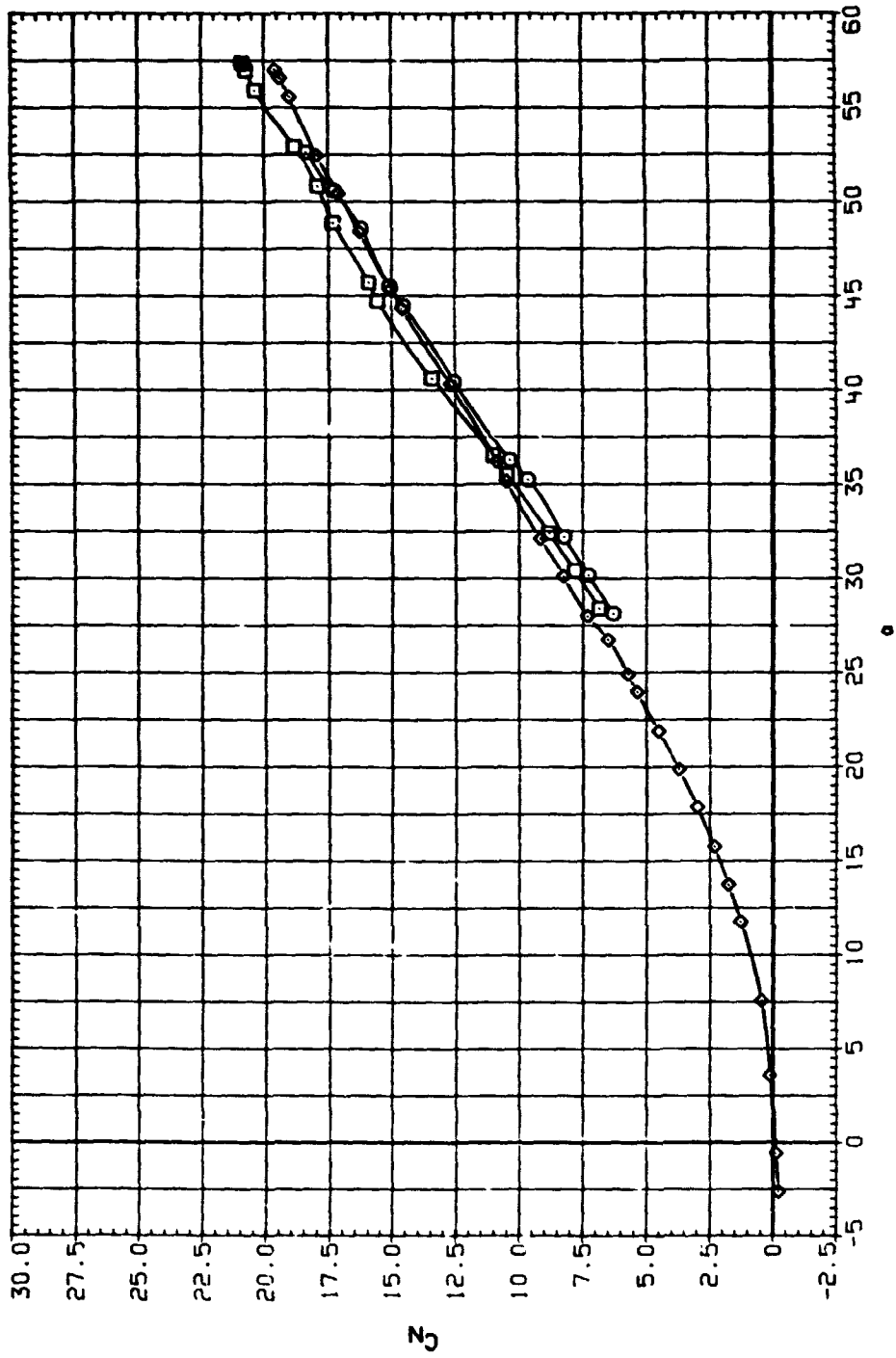


(b) C_l vs α .

Figure 22. -- Continued.

DATA SET SYMBOL CONFIGURATION
 B.J0090 F2.5 A13
 D.J0091 F2.5 A13
 C.J0126 F2.5 A13

PHI-F PHI-A MACH
 .000 .000 1.200
 .000 .000 1.500
 .000 .000 2.000

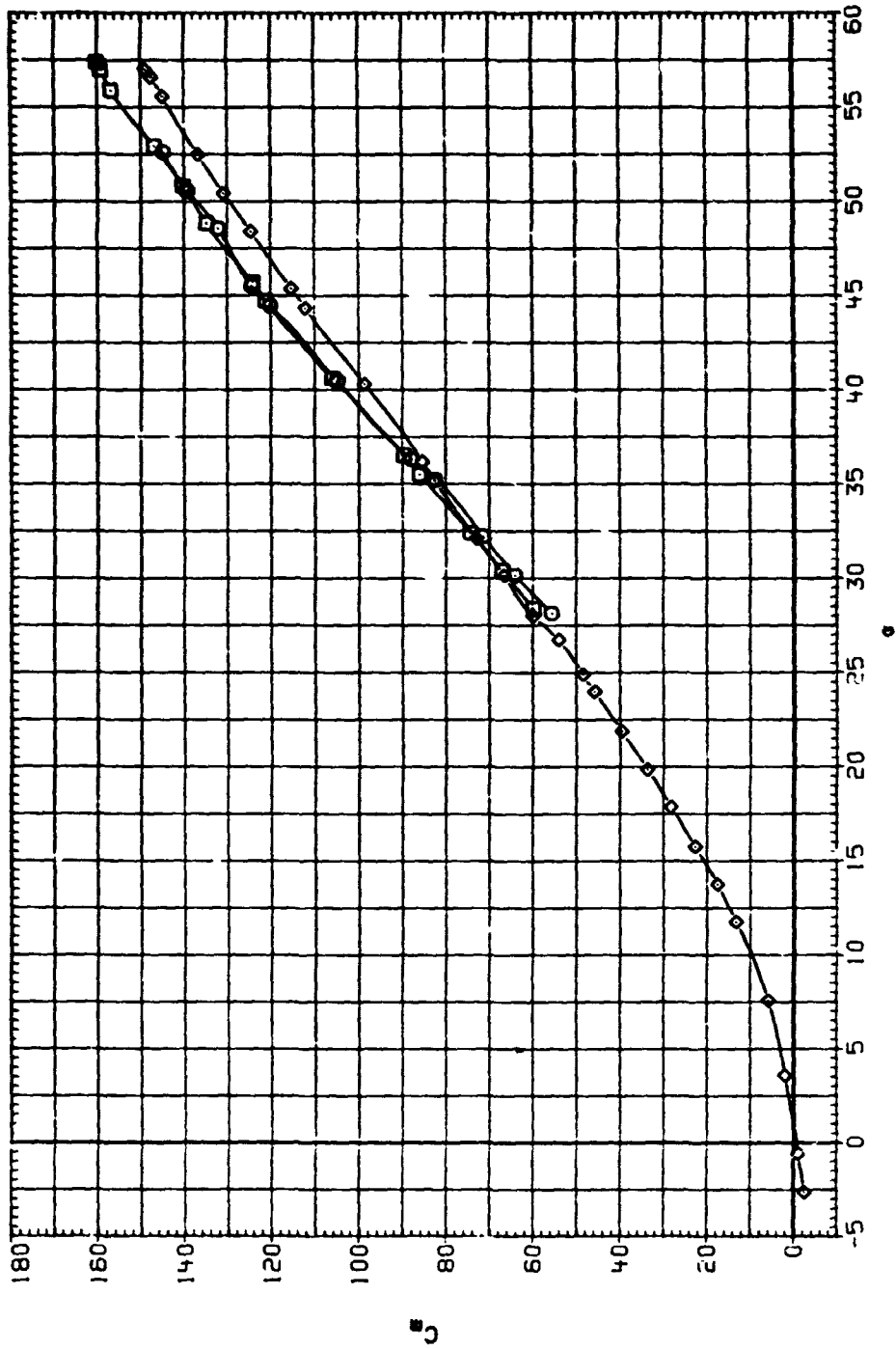


(c) C_N vs α .

Figure 22. Continued.

DATA SET SYMBOL CONFIGURATION
 B-0080 □ F2.5 A13
 B-0081 □ F2.5 A13
 C-00126 ◇ F2.5 A13

PHI-F PHI-A MACH
 .000 .000 1.200
 .000 .000 1.500
 .000 .000 2.000

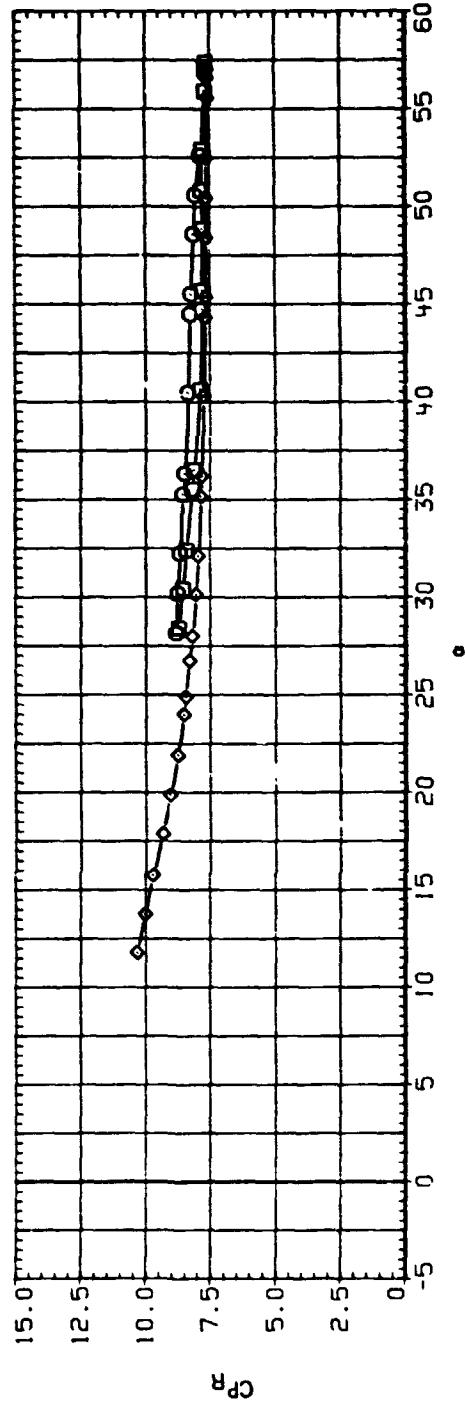
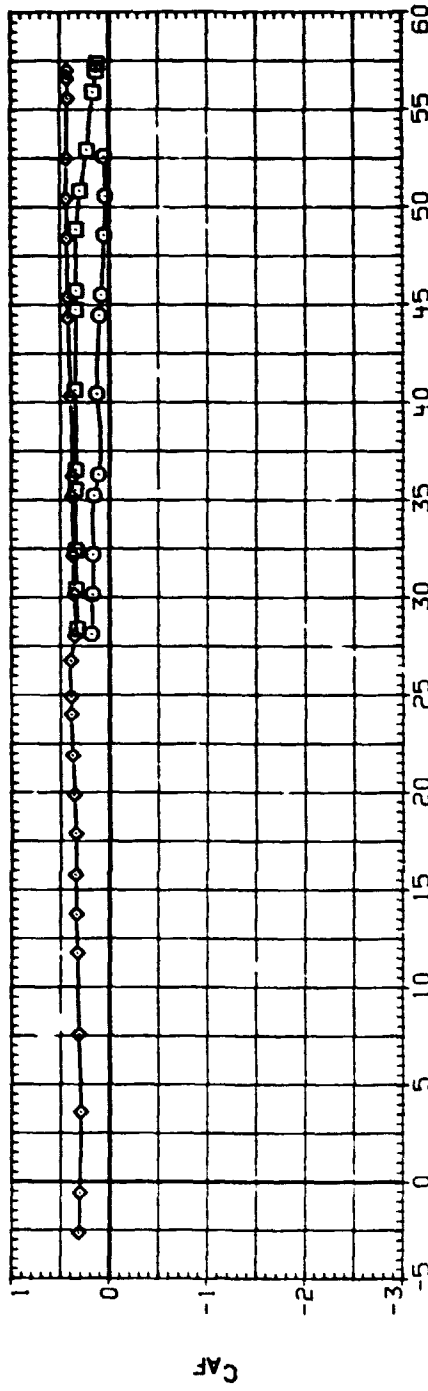


(d) C_m vs α .

Figure 22. Continued.

DATA SET SYMBOL CONFIGURATION
 B-0090 □ F2.5 A13
 B-0091 □ F2.5 A13
 C-0126 ◇ F2.5 A13

PHI-F PHI-A MACH
 .000 .000 1.200
 .000 .000 1.500
 .000 .000 2.000

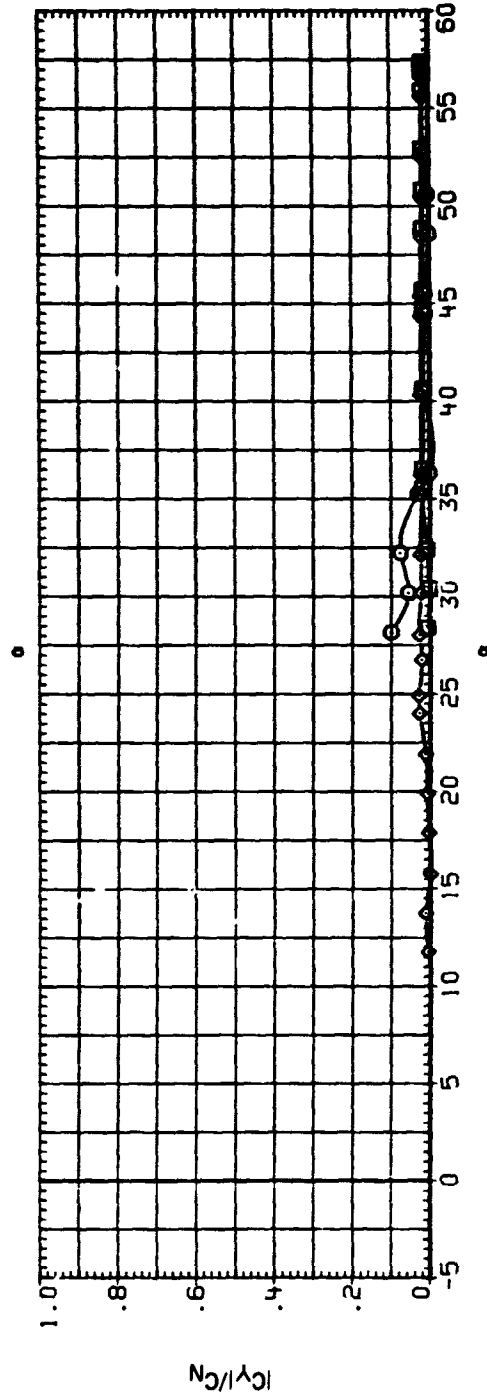
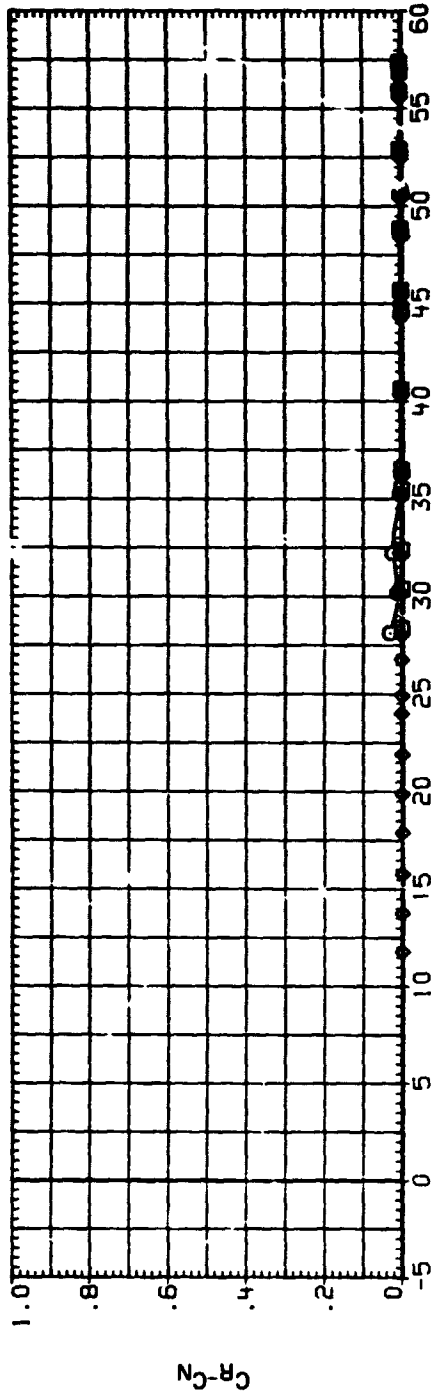


(c) C_{AF} and C_{PR} vs α .

Figure 22. Continued.

DATA SET SYMBOL CONFIGURATION
 8J0090 O F2.5 A13
 8J0091 □ F2.5 A13
 C.0126 ◇ F2.5 A13

PHI-F PHI-A MACH
 .000 .000 1.200
 .000 .000 1.500
 .000 .000 2.000

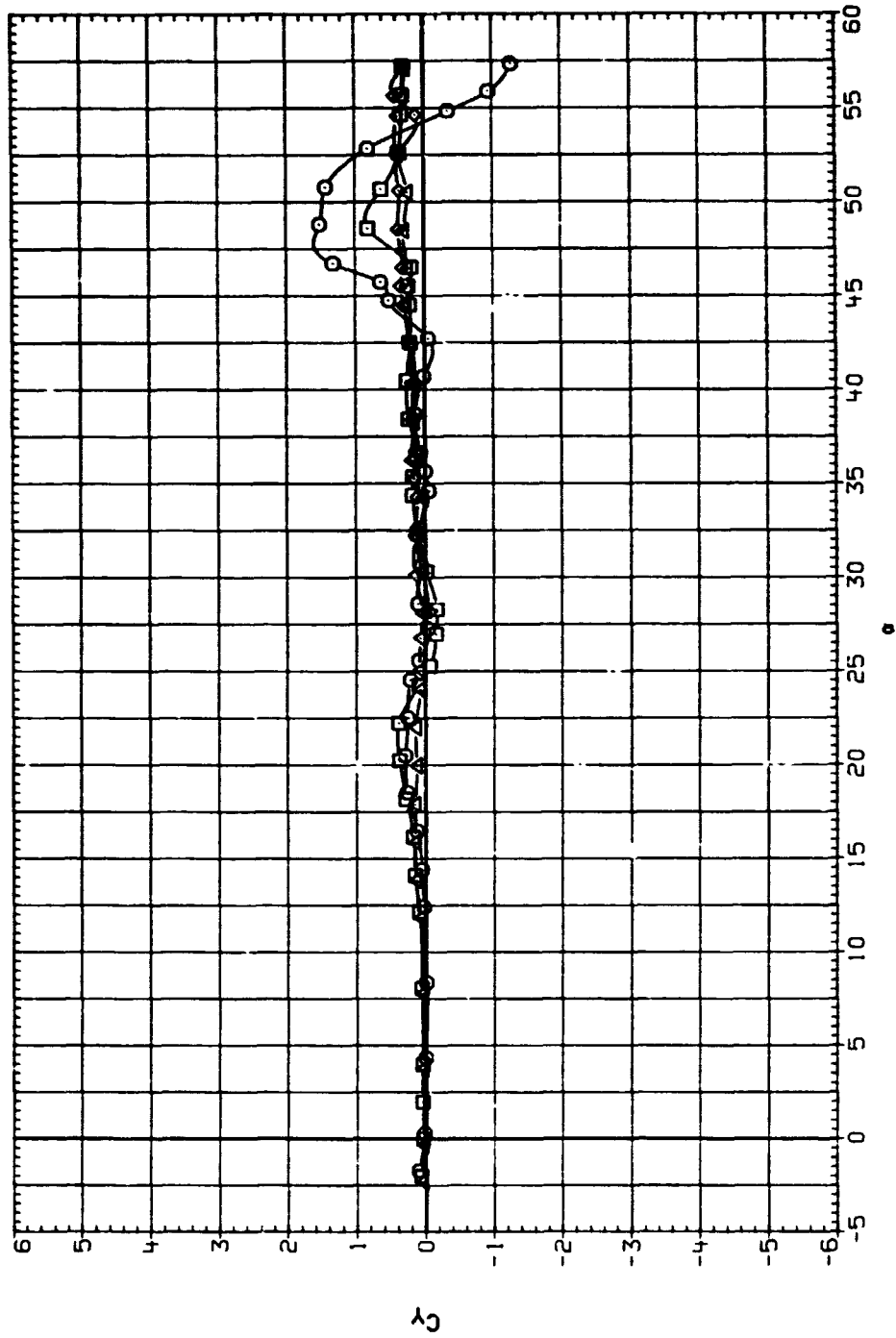


(D) $C_R - C_N$ and $|C_Y|/C_N$ vs α .

Figure 22.— Concluded.

DATA SET SYMBOL CONFIGURATION
 C-J0108 F1.5 A13
 C-J0109 F1.5 A13
 B-J0106 F1.5 A13
 C-J0112 F1.5 A13

PHI-F PHI-A MACH
 .000 .000 .250
 .000 .000 .400
 .000 .000 .600
 .000 .000 .900

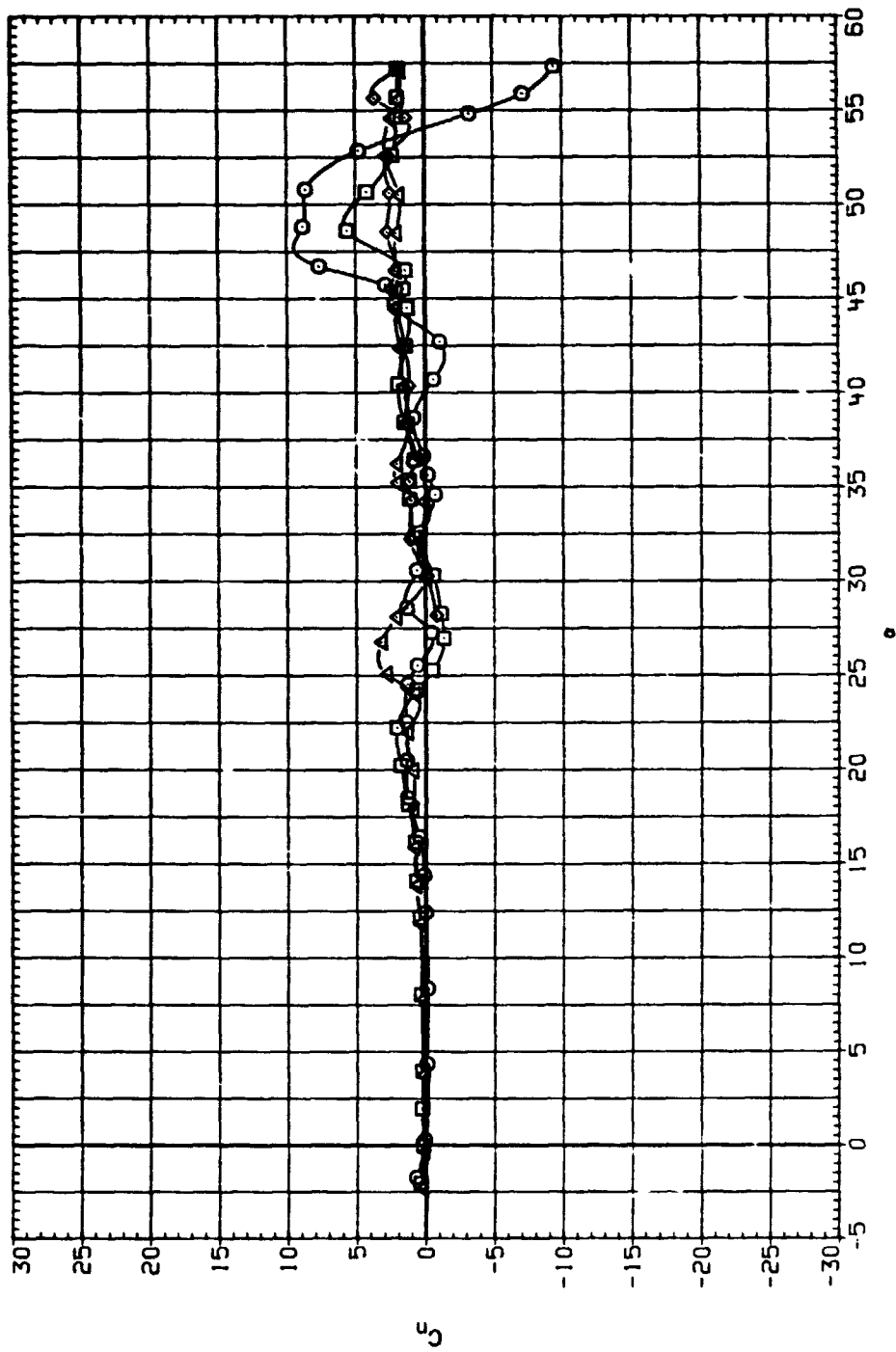


(a) C_L vs α .

Figure 23.-- Effect of Mach number, F1.5A13, subsonic, $Re = 0.32 \times 10^6$.

DATA SET SYMBOL CONFIGURATION
 C-0108 ○ F1.5 A13
 B-0108 □ F1.5 A13
 C-0112 △ F1.5 A13

PHI-F PHI-A MACH
 .000 .000 .750
 .000 .000 .800
 .000 .000 .800
 .000 .000 .900

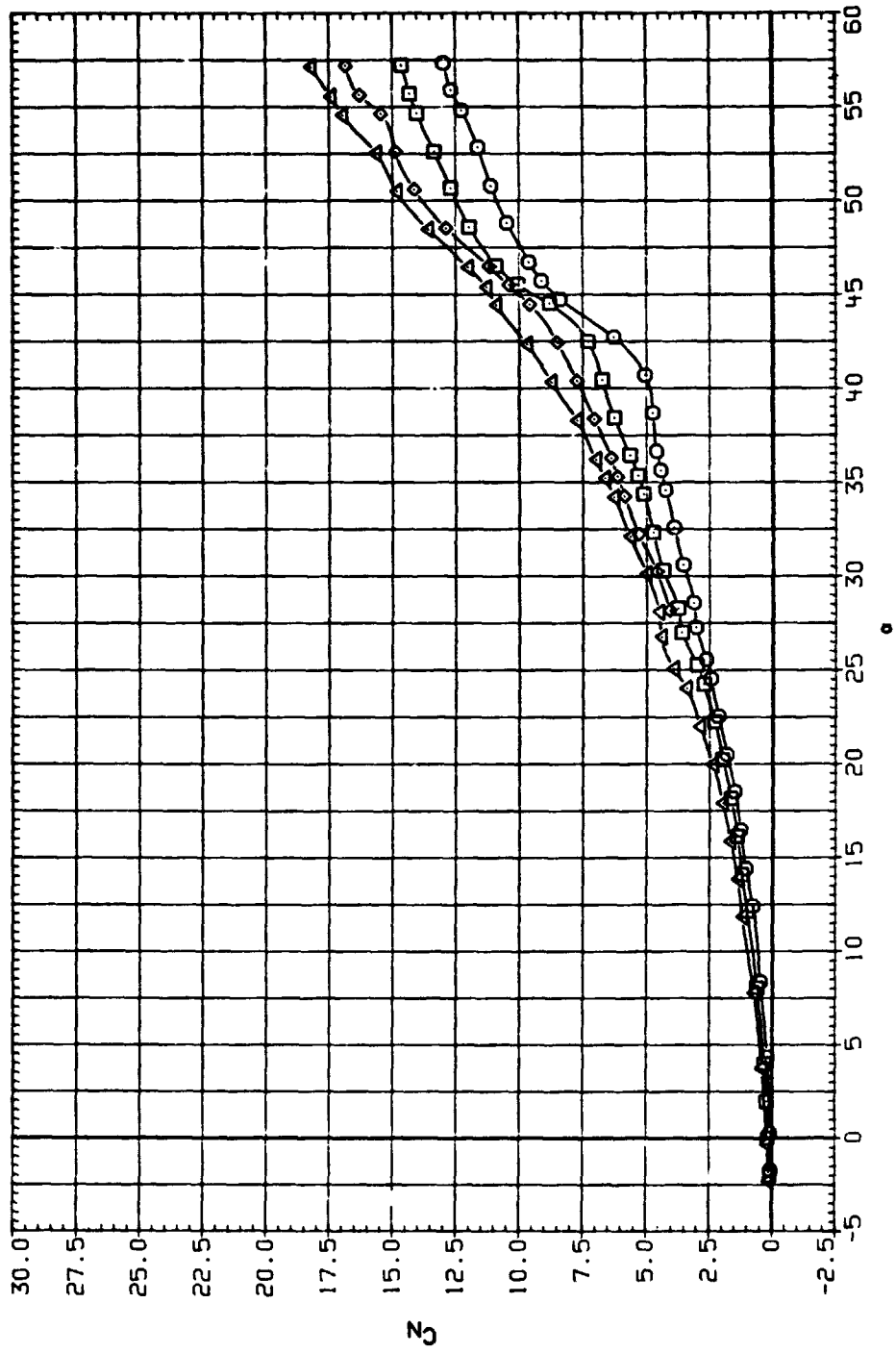


(b) C_m vs α .

Figure 23. - Continued.

DATA SET SYMBOL CONFIGURATION
 C.J0108 O F1.5 A13
 C.J0109 □ F1.5 A13
 B.J0106 △ F1.5 A13
 C.J0112 ○ F1.5 A13

PHI-F PHI-A MACH
 .000 .000 .250
 .000 .000 .500
 .000 .000 .800
 .000 .000 .900

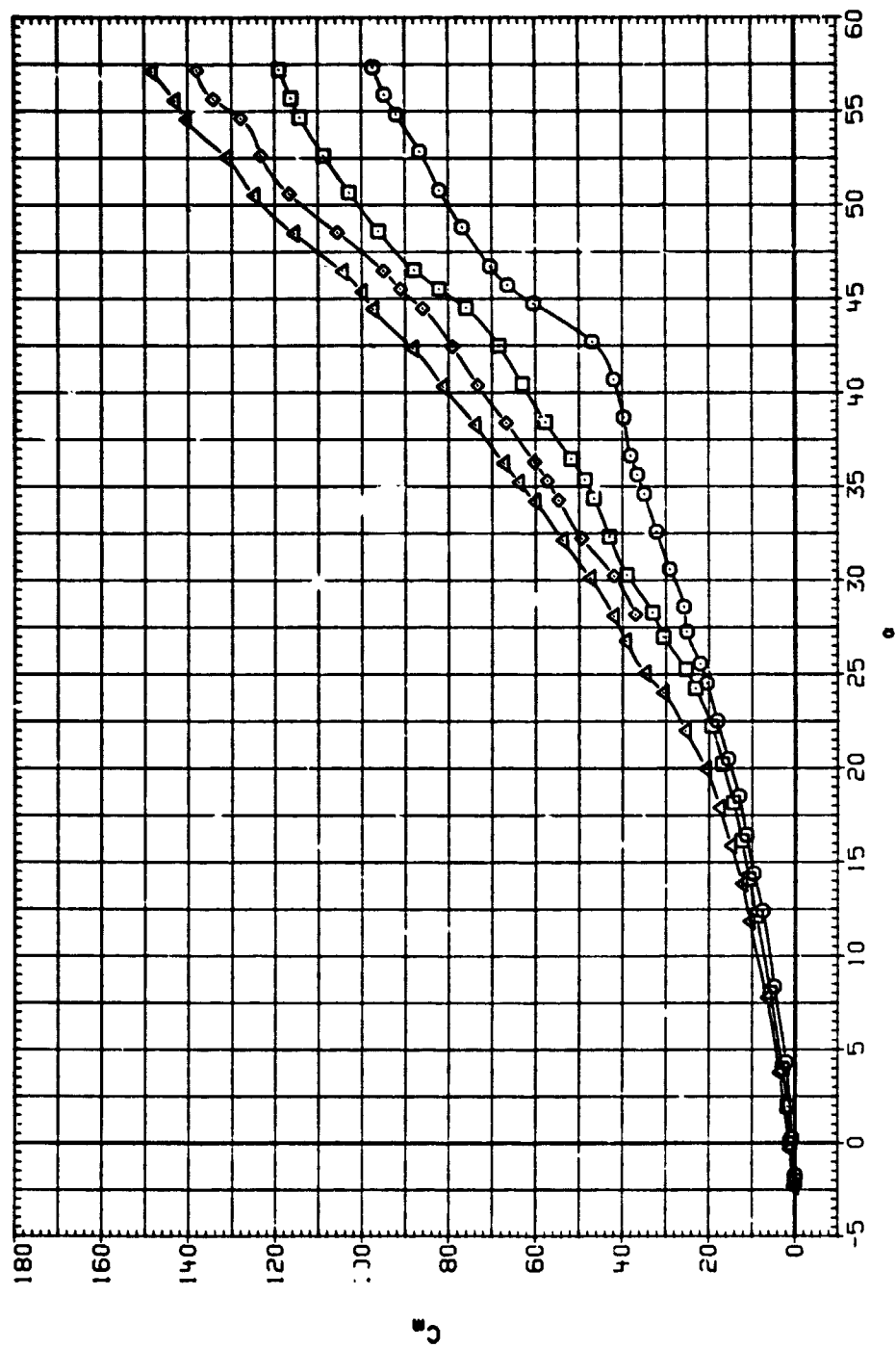


(c) C_N vs α .

Figure 23.— Continued.

DATA SET SYMBOL CONFIGURATION
 C-J0108 O F1.5 A13
 C-J0109 □ F1.5 A13
 B-J0106 ◇ F1.5 A13
 C-J0112 △ F1.5 A13

PHI-F PHI-A MACH
 .000 .000 .250
 .000 .000 .600
 .000 .000 .800
 .000 .000 .900

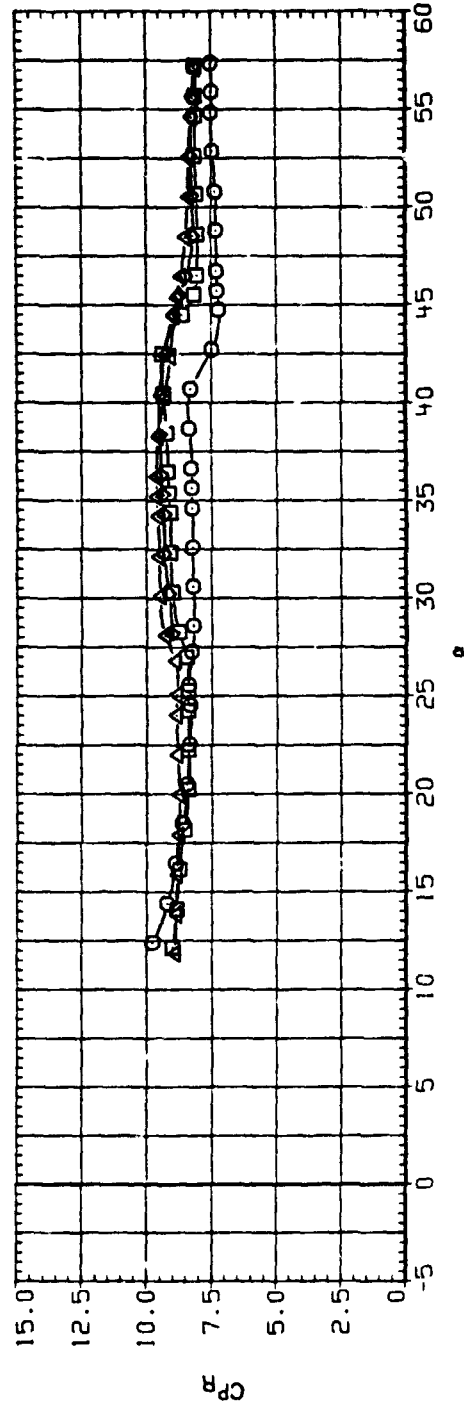
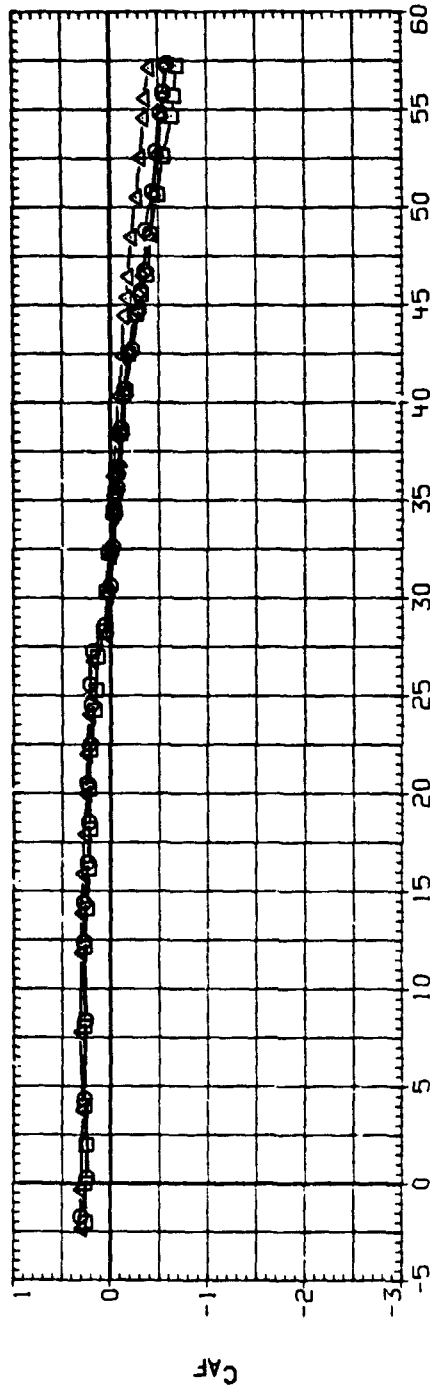


(d) C_m vs α .

Figure 23.— Continued.

DATA SET SYMBOL CONFIGURATION
 C.01.09 □ F1.5 A13
 C.01.09 □ F1.5 A13
 B.01.05 △ F1.5 A13
 C.01.12 △ F1.5 A13

PHI-F PHI-A I
 .000 .000 .250
 .000 .000 .500
 .000 .000 .800
 .000 .000 .900

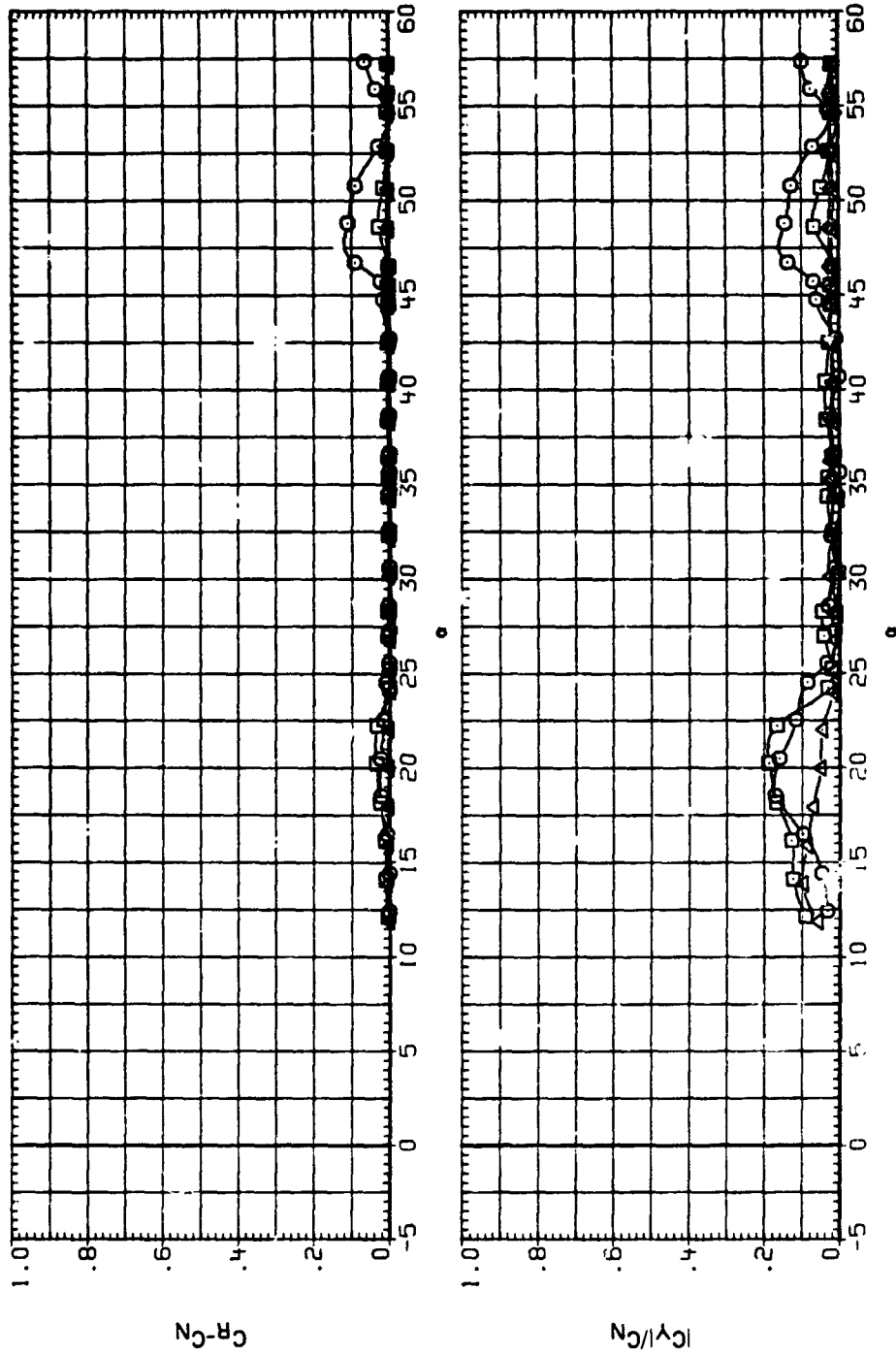


(c) C_{AF} and C_{PR} vs α .

Figure 23.- Continued.

DATA SYMBOL CONFIGURATION
 C-01109 \square F1.5 A13
 C-01109 \square F1.5 A13
 B-01106 \triangle F1.5 A13
 C-01112 \square F1.5 A13

PHI-F PHI-A MACH
 .000 .000 .250
 .000 .000 .500
 .000 .000 .800
 .000 .000 .900

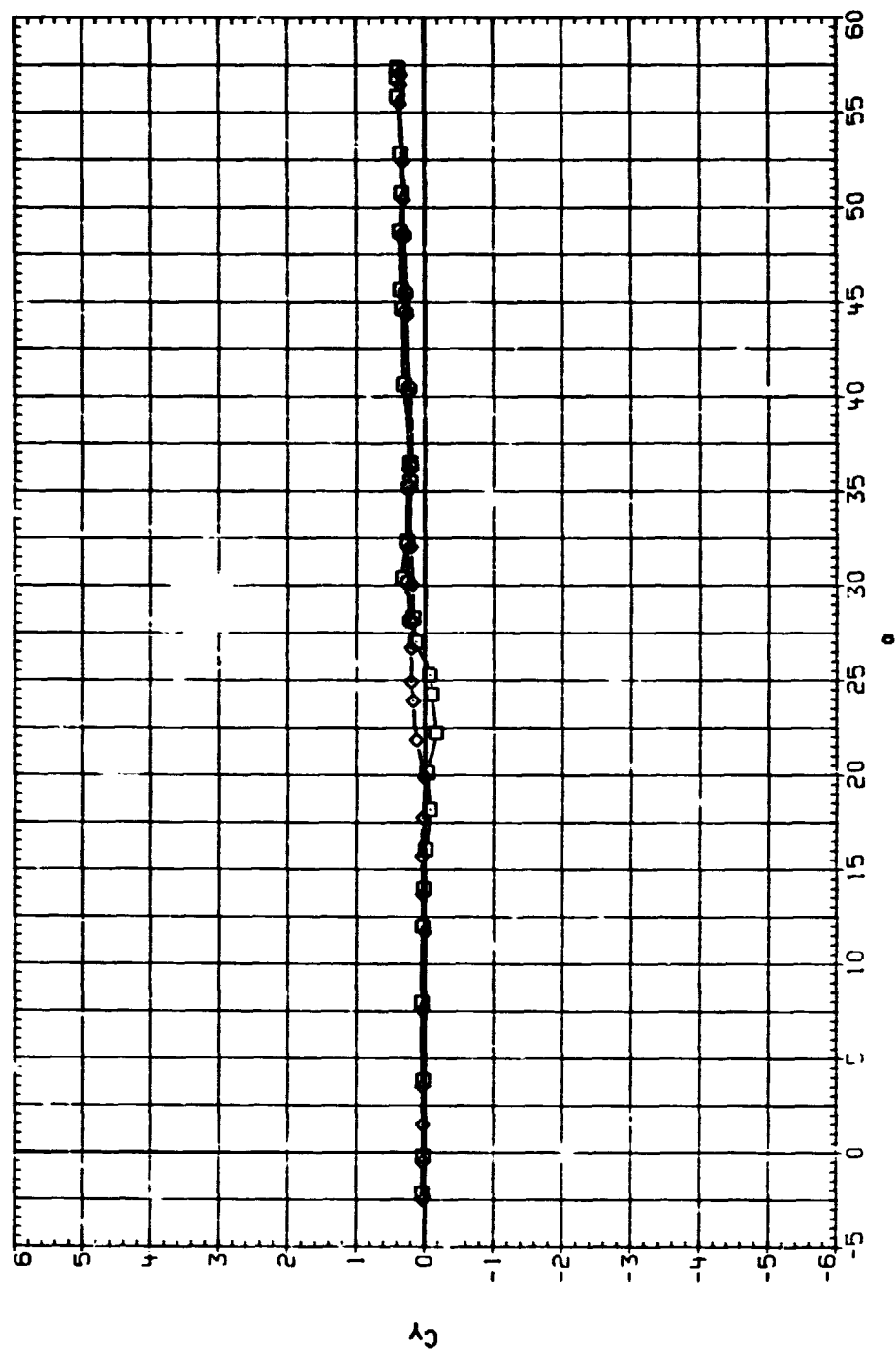


(f) C_R/C_N and $|C_Y/C_N|$ vs α .

Figure 2? Concluded.

DATA SET SYMBOL CONFIGURATION
 B.0099 F1.5 A13
 C.0113 F1.5 A13
 C.0114 F1.5 A13

PHI-F PHI-A MACH
 .000 .000 1.200
 .000 .000 1.500
 .000 .000 2.000

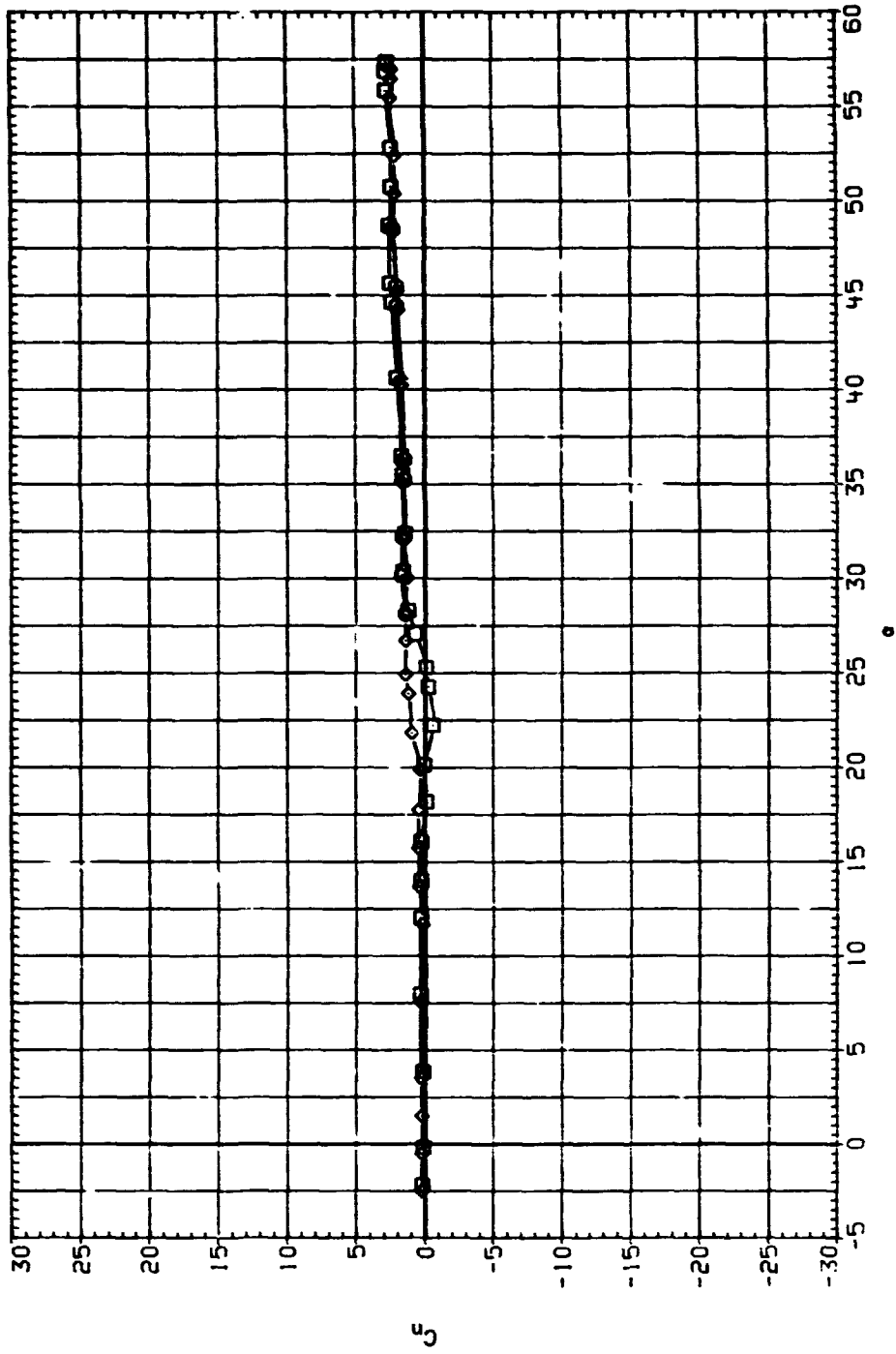


(a) C_y vs α .

Figure 24. - Effect of Mach number, F1.5A13, supersonic, $Re = 0.32 \times 10^6$.

DATA SET SYMBOL CONFIGURATION
 8J0099 F1.5 A13
 CJ0113 F1.5 A13
 CJ0114 F1.5 A13

PHI-F PHI-A MACH
 .000 .000 1.200
 .000 .000 1.500
 .000 .000 2.000

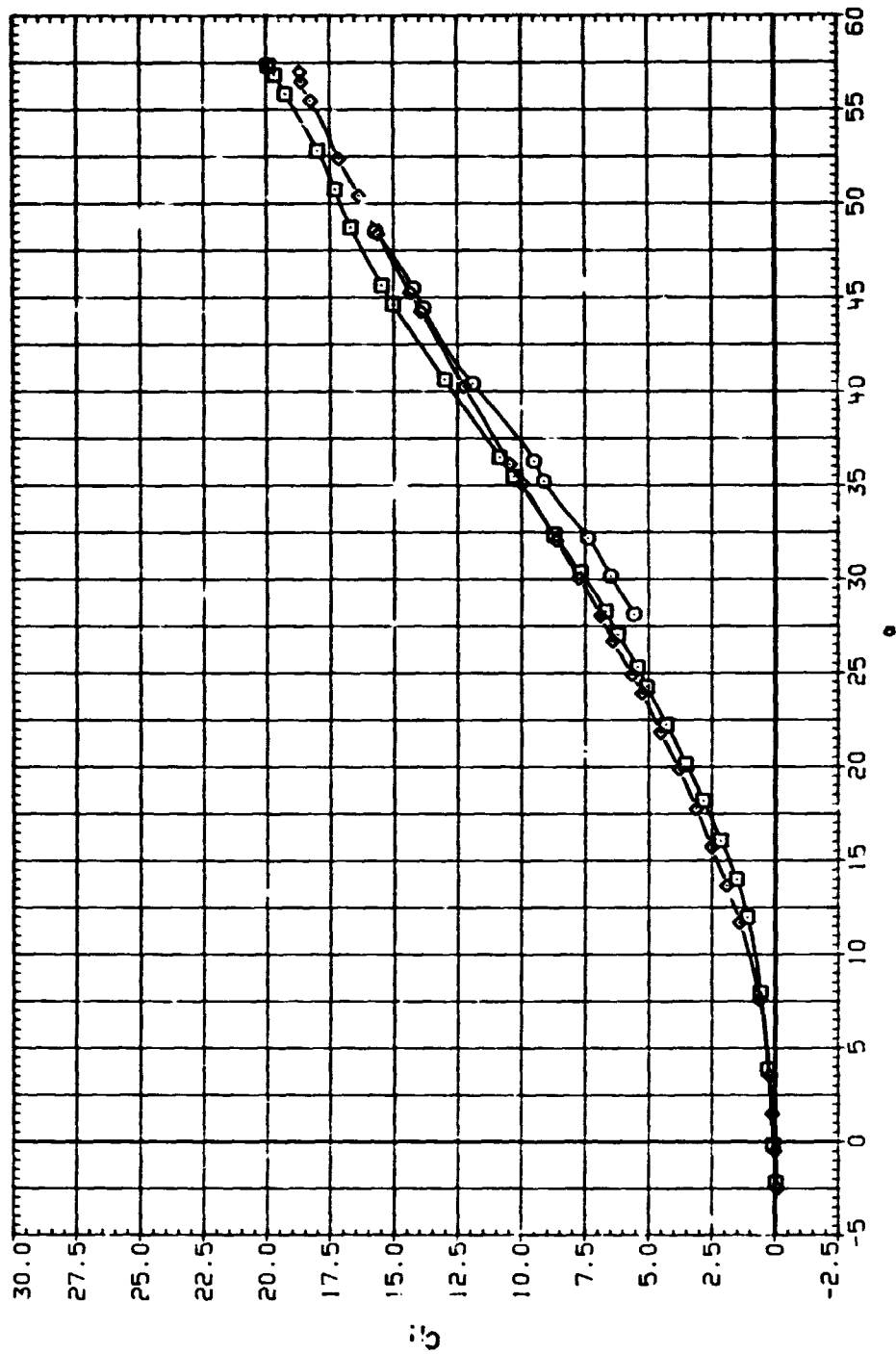


(b) C_l vs α .

Figure 24. Continued.

DATA SET SYMBOL CONFIGURATION
 B-0099 O F1.5 A13
 C-0113 □ F1.5 A13
 C-0114 ◇ F1.5 A13

PHI-F PHI-A MACH
 .000 .000 1.200
 .000 .000 1.500
 .000 .000 2.000

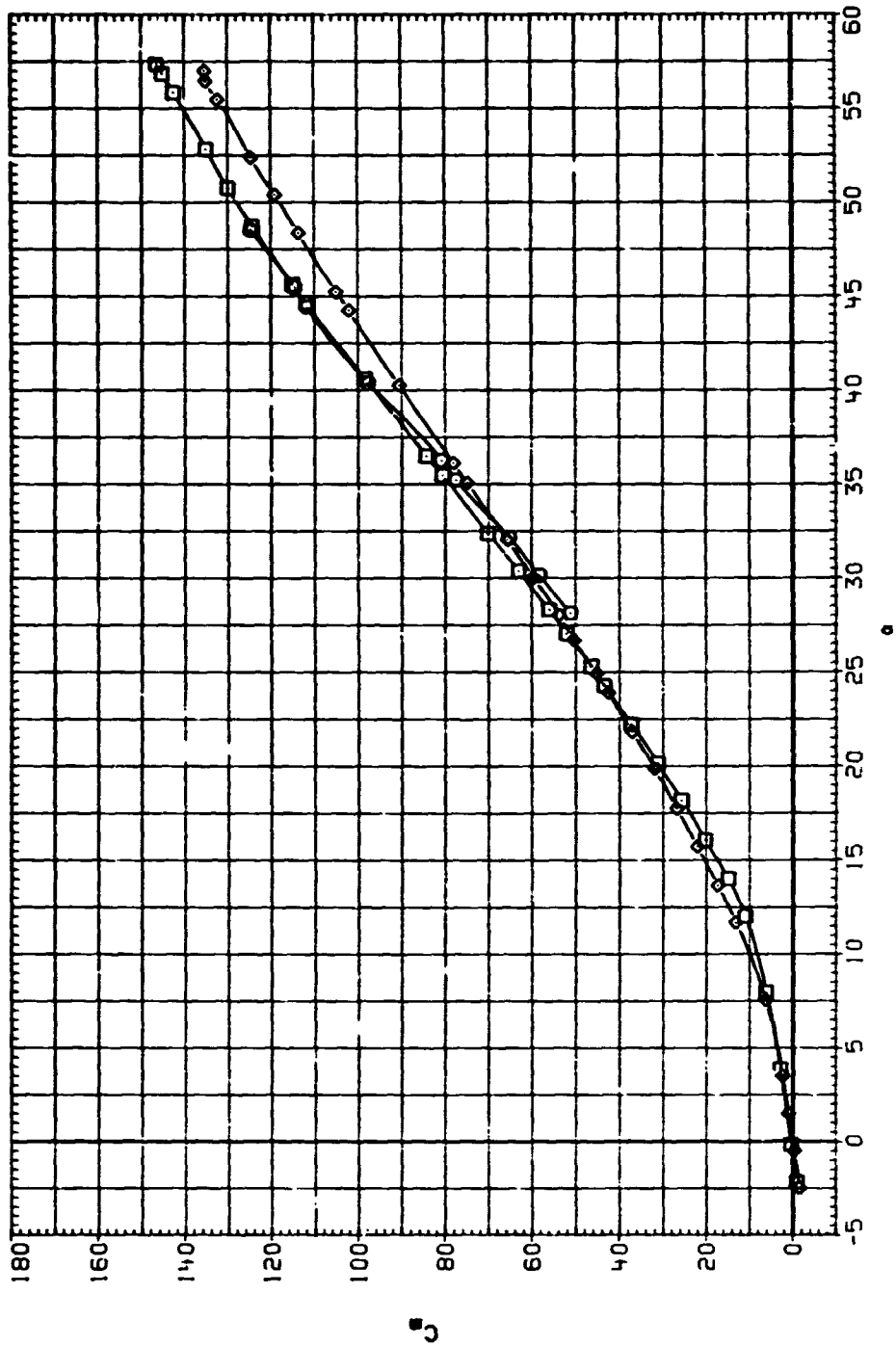


(c) C_N vs α .

Figure 24.--- Continued.

DATA SET SYMBOL CONFIGURATION
 B-0089 F1.5 A13
 C-0113 F1.5 A13
 C-0114 F1.5 A13

PHI-F PHI-A MACH
 .000 .000 1.200
 .000 .000 1.500
 .000 .000 2.000

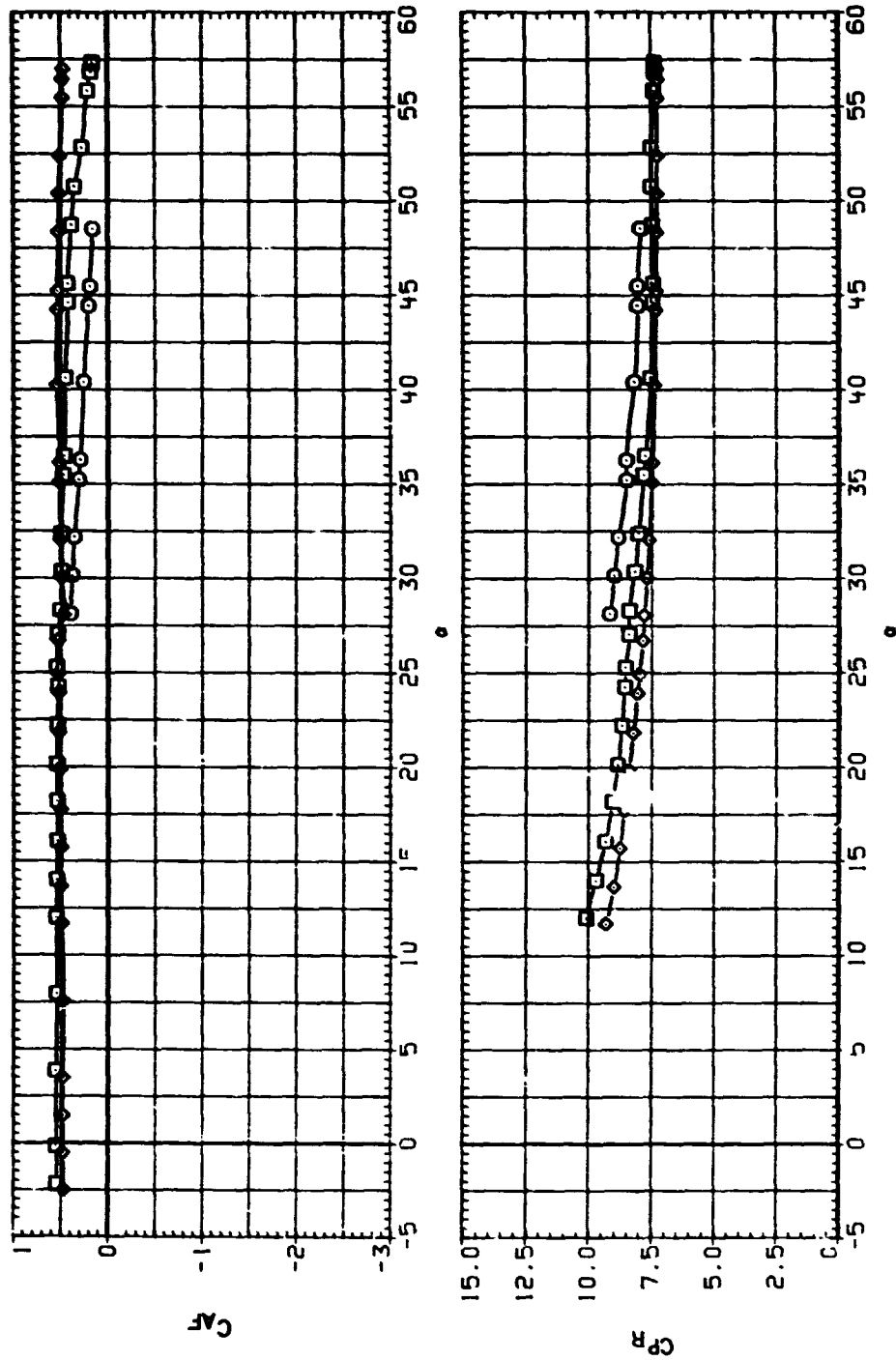


(d) C_m vs α .

Figure 24. Continued.

DATA SET SYMBOL CONFIGURATION
 B-0099 O F1.5 A13
 C-0113 O F1.5 A13
 C-0114 O F1.5 A13

PHI-F PHI-A MACH
 .000 .000 1.200
 .000 .000 1.500
 .000 .000 2.000

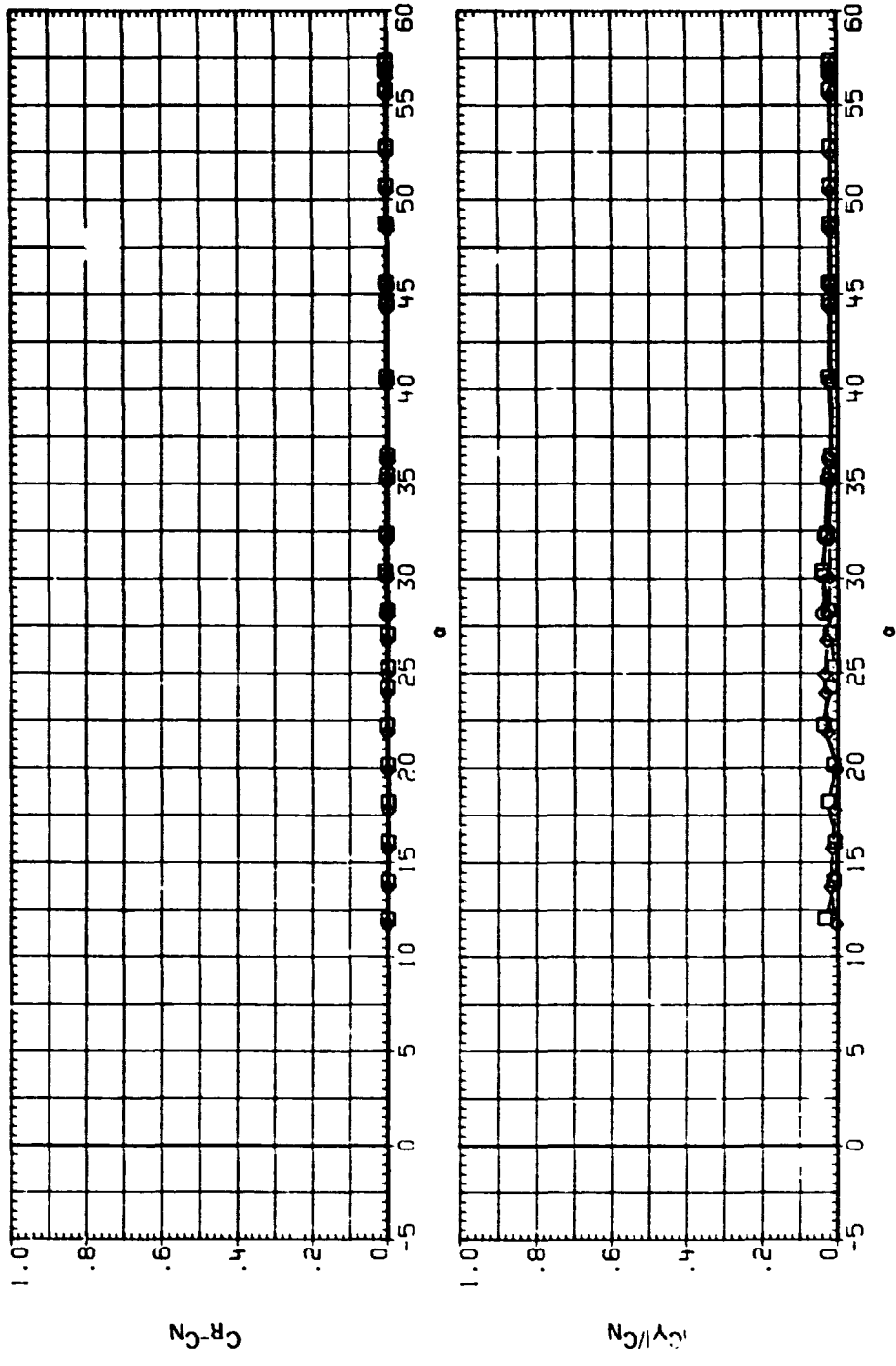


(c) C_{Af} and $C'P_R$ vs α .

Figure 24. - Continued.

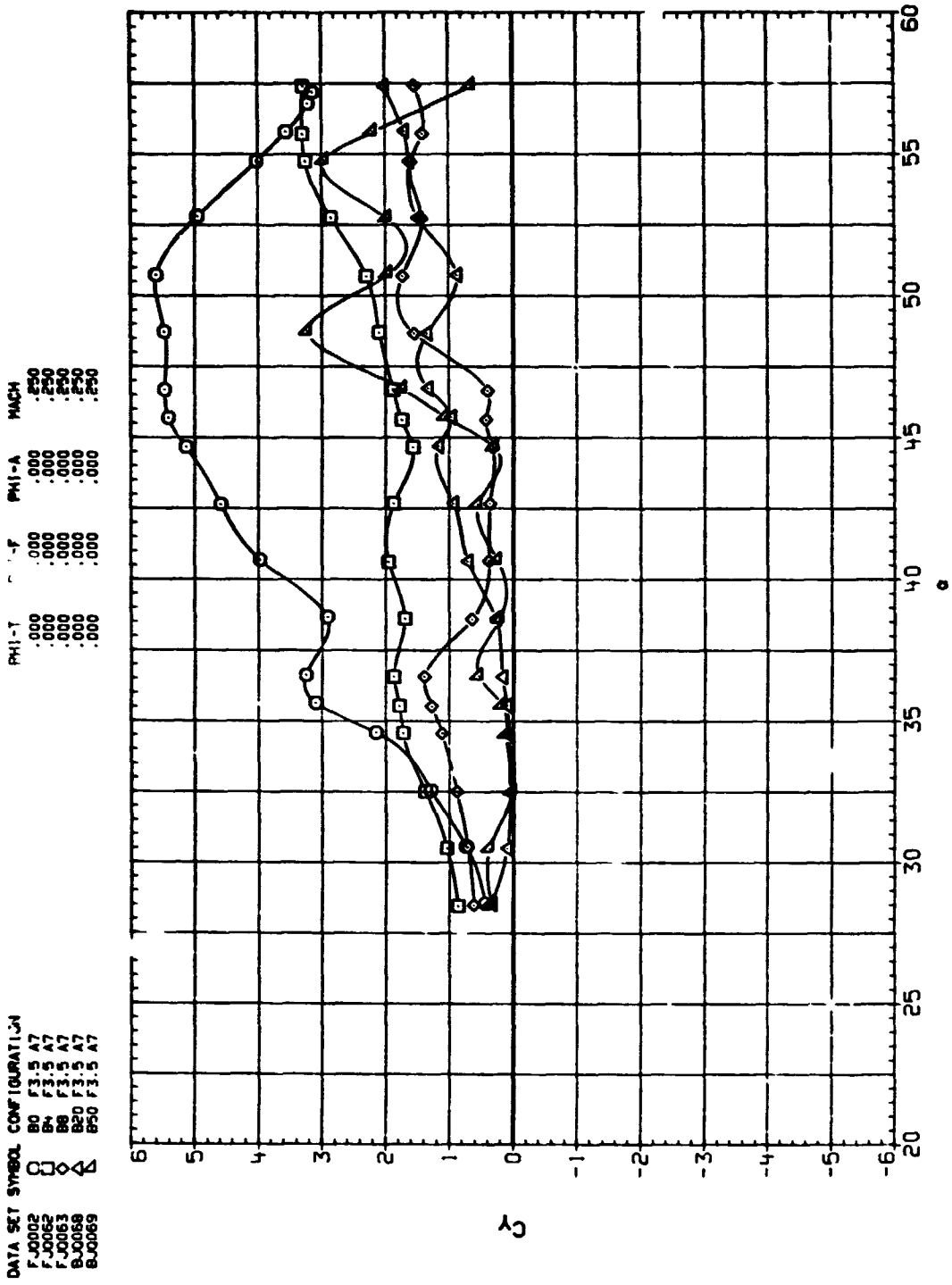
DATA SET SYMBOL CONFIGURATION
 BU099 \square F1.5 A13
 CU113 \square F1.5 A13
 CU114 \diamond F1.5 A13

PHI-F PHI-A MACH
 .000 .000 1.200
 .000 .000 1.500
 .000 .000 2.000



(f) $C_R - C_N$ and $|C_Y|/C_N$ vs α .

Figure 24. Conclude 1.

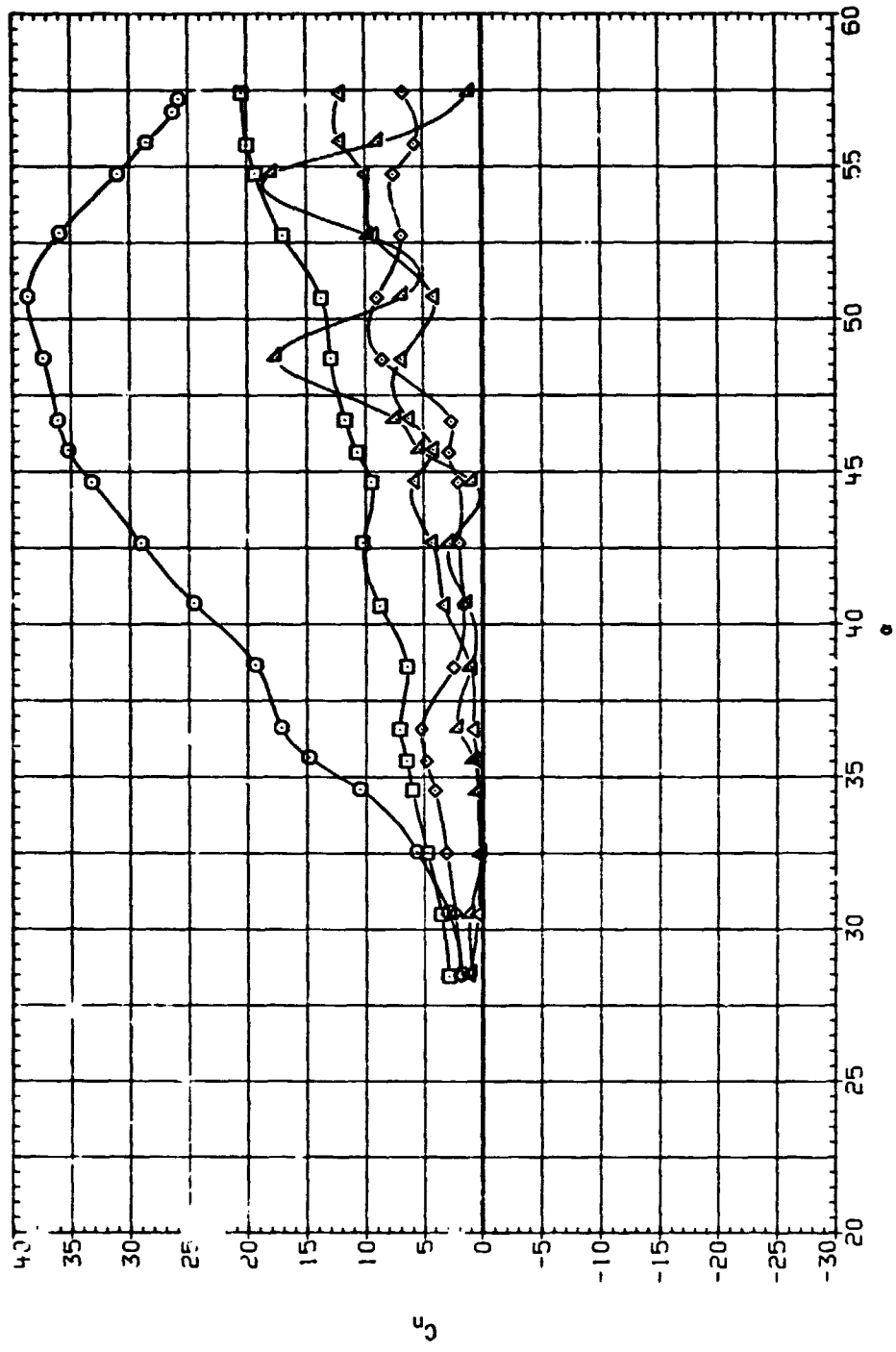


(a) C_y vs α .

Figure 25. Effect of bluntness, blunted F3.5A7, Mach number = 0.25, $Re = 0.32 \times 10^6$.

DATA SET SYMBOL CONFIGURATION
 F-00002 R0 F3.5 A7
 F-00062 B4 F3.5 A7
 F-00063 B8 F3.5 A7
 B-00068 B20 F3.5 A7
 B-00069 B50 F3.5 A7

PHI-T PHI-F PHI-A MACH
 .000 .000 .000 .250
 .000 .000 .000 .250
 .000 .000 .000 .250
 .000 .000 .000 .250

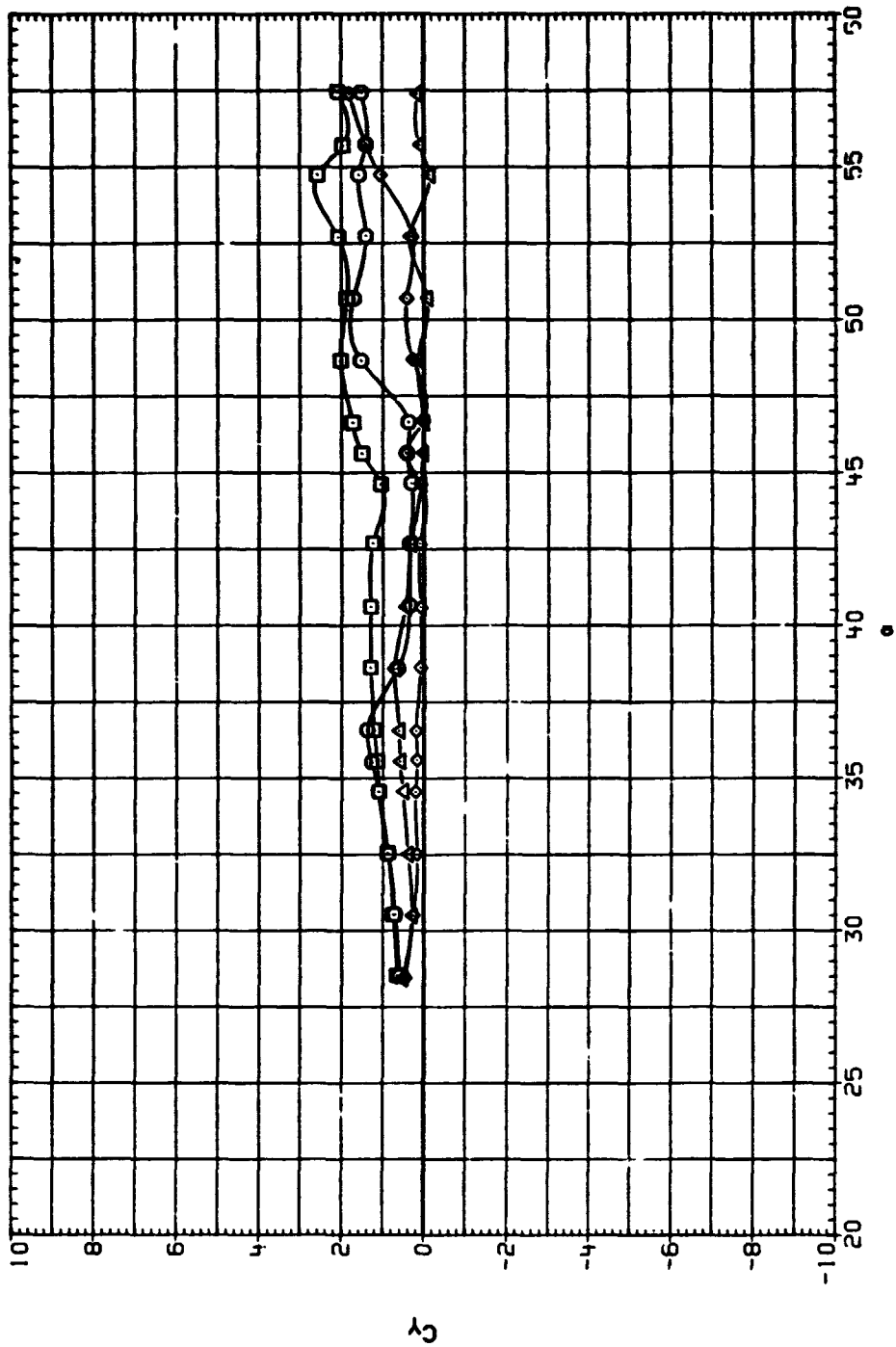


(b) C_{l} vs α .

Figure 25. Concluded.

DATA SET SYMBOL CONFIGURATION
 F-J0063 88 F3.5 A7
 F-J0064 88 F3.5 A7
 F-J0463 88 F3.5 A7
 F-J0066 88 F3.5 A7

PHI-T PHI-F PHI-A MACH
 .000 .000 .000 .250
 90.000 .000 .000 .250
 180.000 .000 .000 .250
 270.000 .000 .000 .250

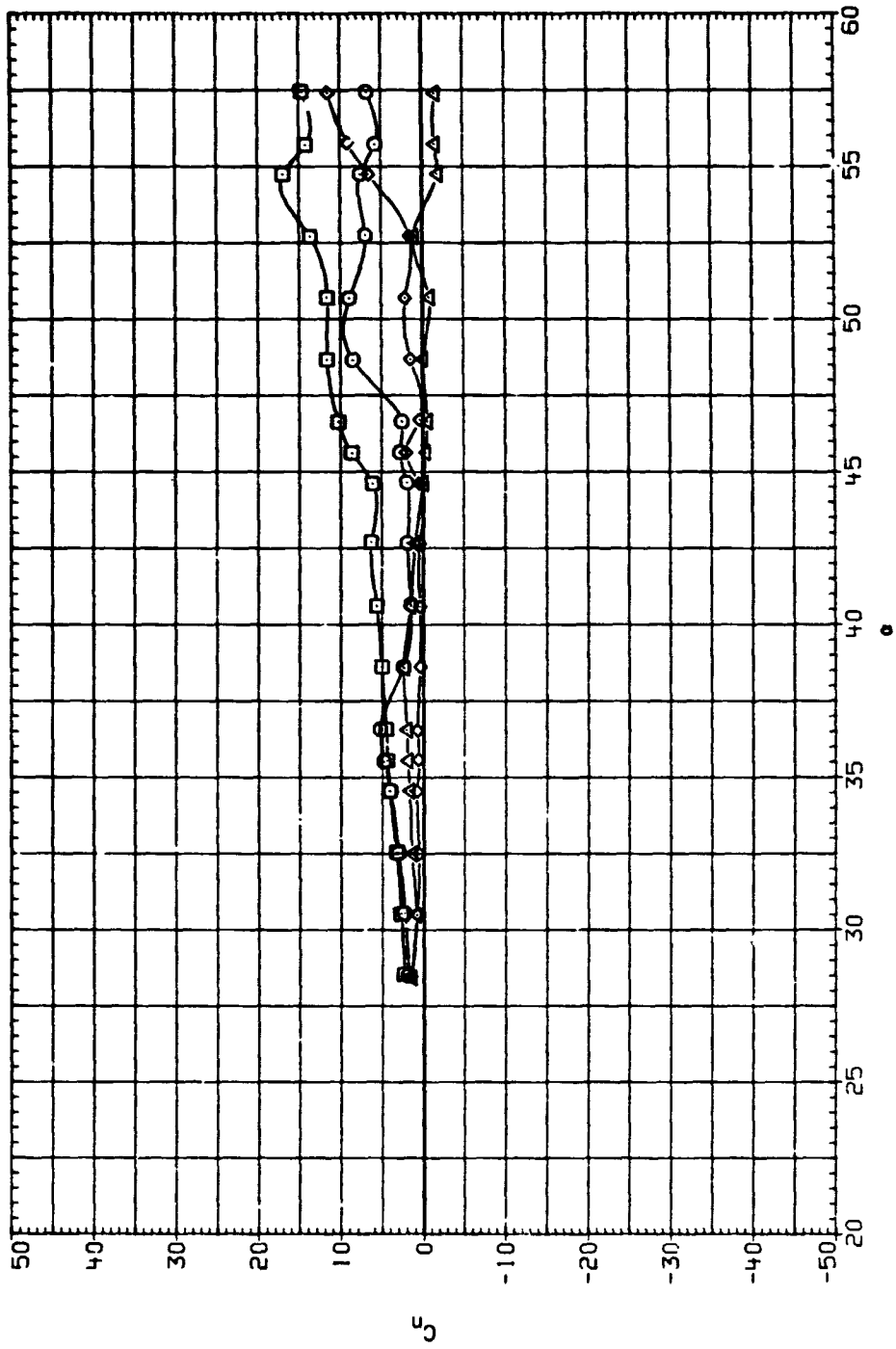


(a) C_l vs α .

Figure 26.— Effect of rotation of blunted tip, B8F3.5A7, forebody and afterbody fixed, Mach number = 0.25, $Re = 0.32 \times 10^6$.

DATA SET SYMBOL CONFIGURATION
 FJ0063 ○ 88 F3.5 A7
 FJ0064 □ 88 F3.5 A7
 FJ0065 ◇ 88 F3.5 A7
 FJ0066 △ 88 F3.5 A7

PHI-T PHI-F PHI-A MACH
 .000 .000 .000 .250
 90.000 .000 .000 .250
 180.000 .000 .000 .250
 270.000 .000 .000 .250

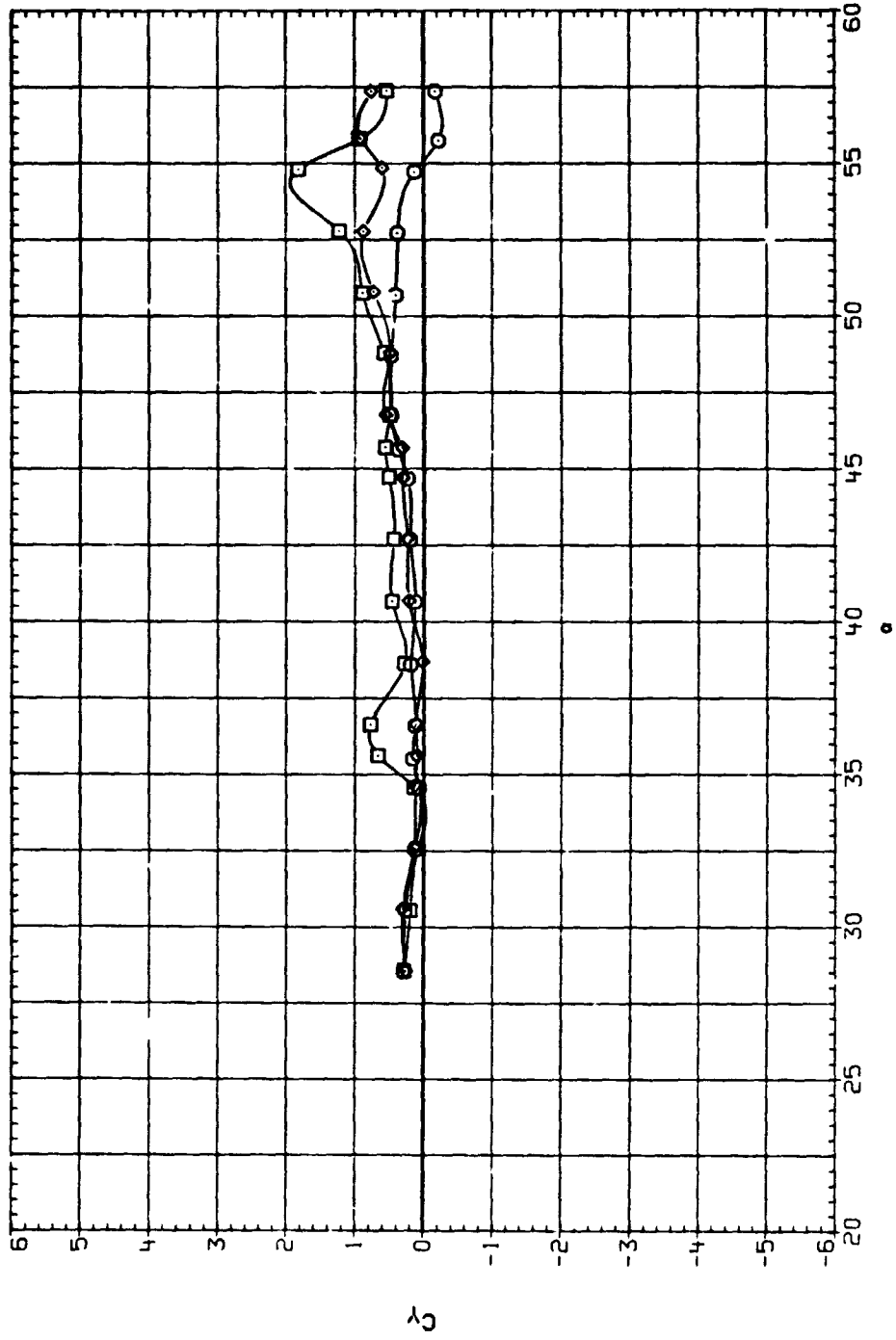


(b) C_L vs α .

Figure 26. Concluded.

DATA SET SYMBOL CONFIGURATION
 FJ0070 ○ 88 F2.5 A7
 BJ0075 □ 820 F2.5 A7
 BJ0076 ◇ 850 F2.5 A7

PHI-T PHI-F PHI-A MACH
 .000 .000 .000 .250
 .000 .000 .000 .250
 .000 .000 .000 .250

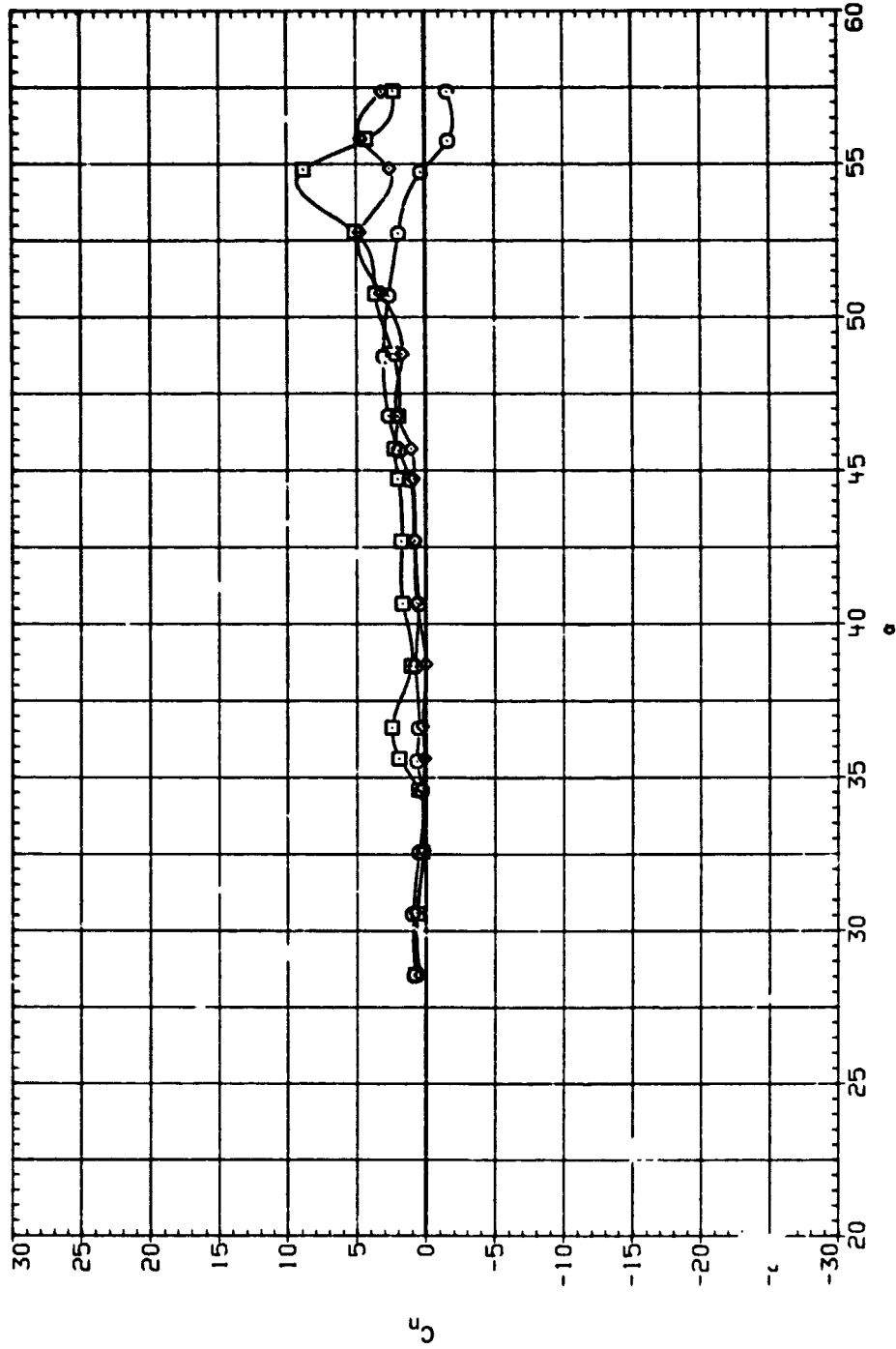


(a) C_y vs α .

Figure 27. Effect of bluntness, blunted F2.5A7, Mach number = 0.25, $Re = 0.32 \times 10^6$.

DATA SET SYMBOL CONFIGURATION
 F.00070 ○ B8 F2.5 A7
 B.00075 □ B20 F2.5 A7
 B.00076 ◇ B50 F2.5 A7

PHI-T PHI-F PHI-A MACH
 .000 .000 .000 .250
 .000 .000 .000 .250
 .000 .000 .000 .250

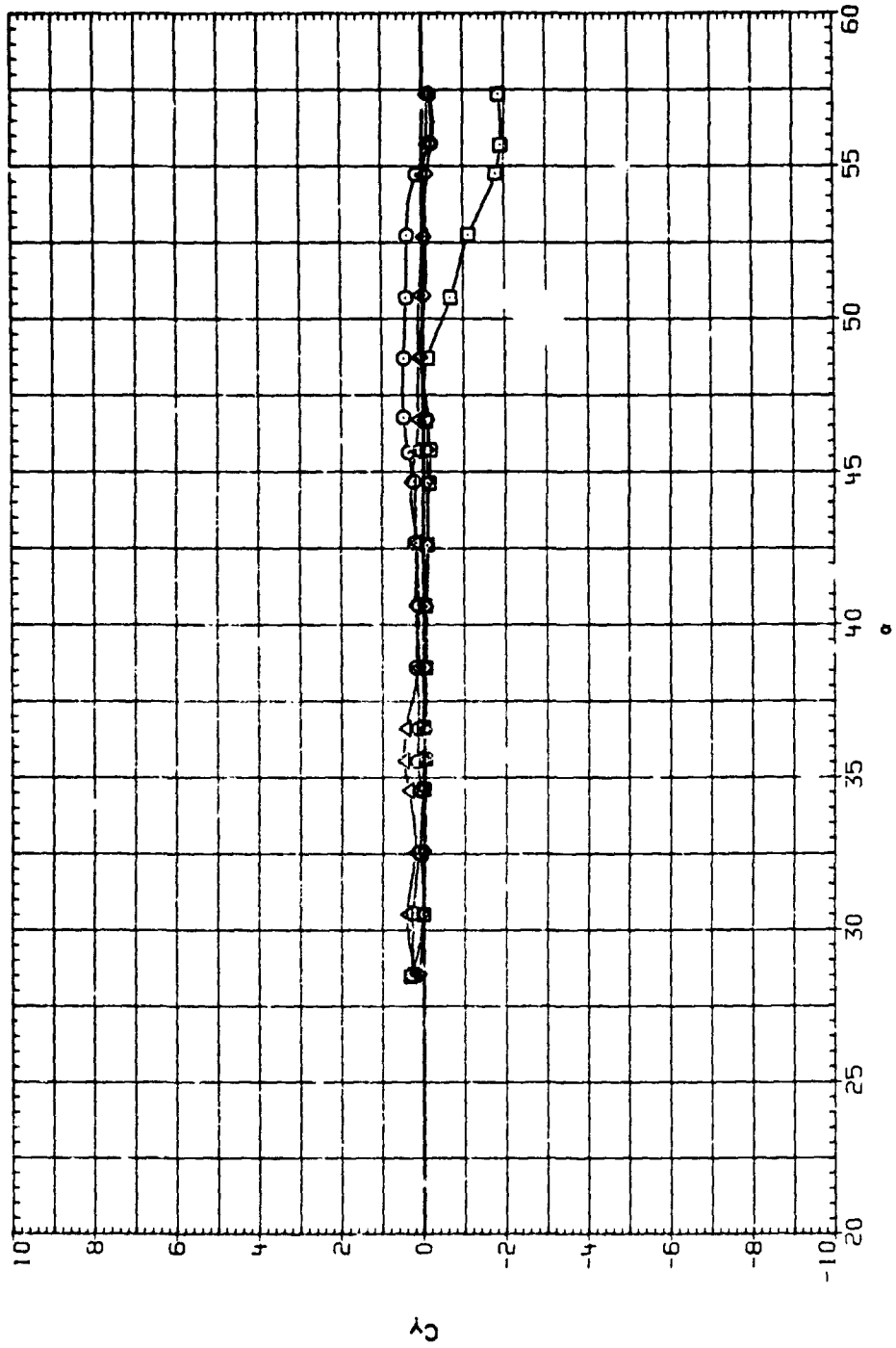


(b) C_l vs α .

Figure 27. Concluded.

DATA SET SYMBOL CONFIGURATION
 FJ0070 88 F2.5 A7
 FJ0071 88 F2.5 A7
 FJ0072 88 F2.5 A7
 FJ0073 88 F2.5 A7

PHI-T PHI-F PHI-A MACH
 .000 .000 .000 .250
 90.000 .000 .000 .250
 180.000 .000 .000 .250
 270.000 .000 .000 .250

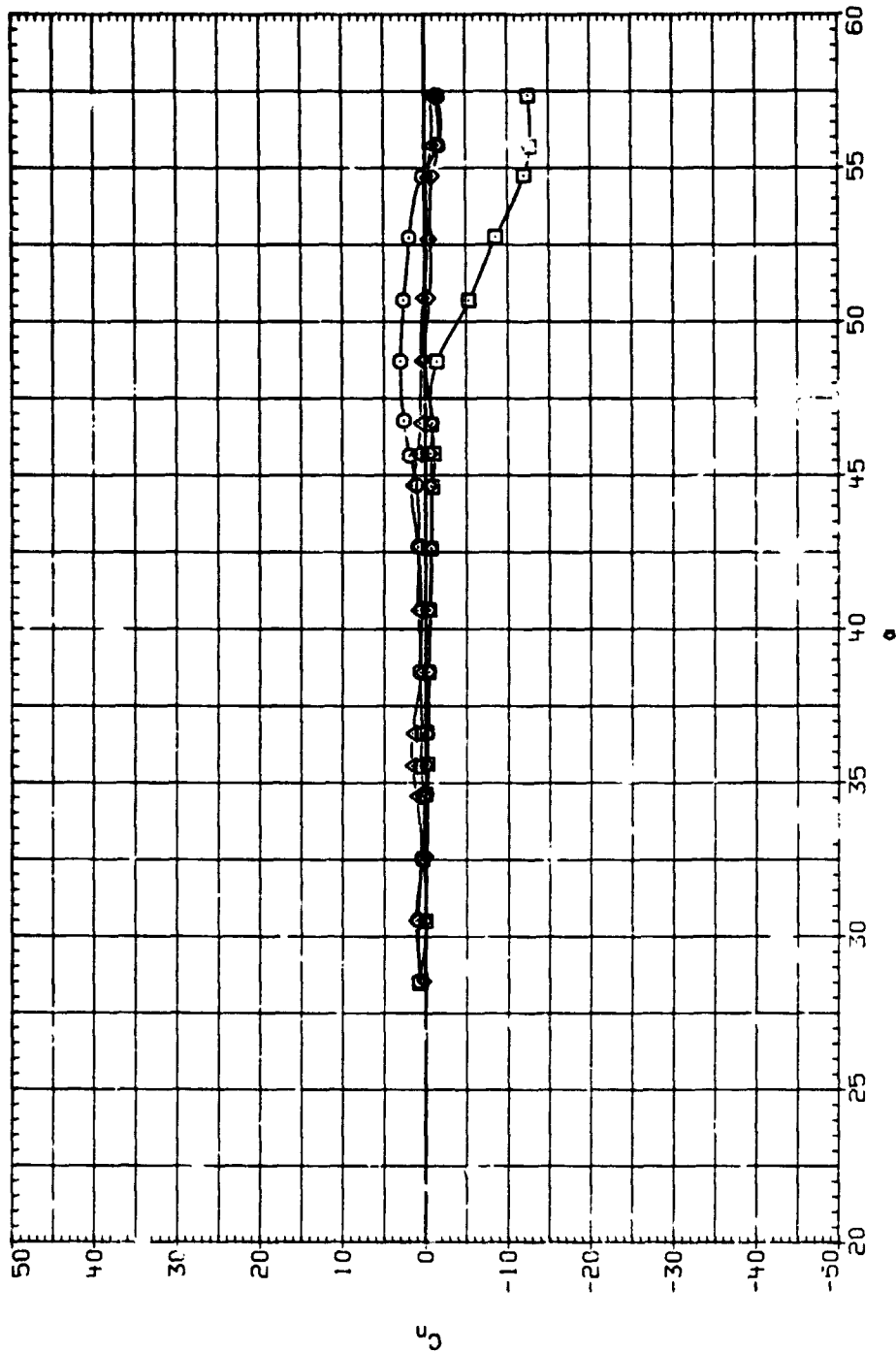


(a) C_y vs α .

Figure 28. — Effect of rotation of blunted tip, B8F2.5A7: forebody and afterbody fixed, Mach number = 0.25, $Re = 0.32 \times 10^6$.

DATA SET SYMBOL CONFIGURATION
 FJ0070 88 F2.5 A7
 FJ0071 88 F2.5 A7
 FJ0072 88 F2.5 A7
 FJ0073 88 F2.5 A7

PHI-T PHI-F PHI-A MACH
 .000 .000 .000 .250
 90.000 .000 .000 .250
 180.000 .000 .000 .250
 270.000 .000 .000 .250



(b) C_L vs α .

Figure 28. - Concluded.

END DATE

OCT, 23, 1979